

THESIS

Study of Optimization Problems
by Quantum Annealing

Tadashi Kadowaki

Department of Physics, Tokyo Institute of Technology

December, 1998

Acknowledgments

I would like to express my sincerest gratitude to Professor Hidetoshi Nishimori for his guidance, useful discussions and above all his encouragements.

I acknowledge useful discussions with Professor Seiji Miyashita, Dr. Naomichi Hatano, Dr. Yukiyasu Ozeki, Professor Kazuyuki Tanaka and Dr. Jun-ichi Inoue. I also thank all members of the Nishimori group and the condensed-matter theory group in the Physics Department of Tokyo Institute of Technology for stimulating discussions.

Numerical calculations were performed on the CRAY C916/12256 in the Computer Center, Tokyo Institute of Technology.

Most of the work on computers was performed by various free or open source softwares on Debian GNU/Linux system. I would like to thank people who support free or open source softwares and the community of Debian GNU/Linux.

Finally, I thank my family for spiritual and financial supports.

Preface

On the occasion to submit my thesis to the preprint server, I would like to refer to previous and recent studies which are not referred to in the original thesis.

In the early days of quantum annealing study, Amara et al. used the imaginary time Schrödinger equation to search the global minimum state of the classical system[1]. Finnila et al. introduced a controlled and scheduled quantum effect to the Monte Carlo Simulation[2].

Recently, thermal and quantum annealing in the disordered Ising magnet, $\text{LiHo}_{0.44}\text{Y}_{0.56}\text{F}_4$, with transverse magnetic field were compared[3,4]. Numerical studies of quantum annealing for the disordered Ising model and the protein folding problem were performed by a few different groups[5,6].

A quantum computer algorithm is also related with quantum annealing. The algorithm uses the adiabatic evolution of a time dependent Hamiltonian[7,8,9,10].

1 May 2002

TK

Bibliography

- [1] P. Amara, D. Hsu and J. E. Straub, *Global Energy Minimum Searches Using an Approximate Solution of the Imaginary Time Schrödinger Equation*, J. Phys. Chem. **97** (1993) 6715.
- [2] A. B. Finnila, M. A. Gomez, C. Sebenik, C. Stenson and J. D. Doll,

- Quantum Annealing: A New Method for Minimising Multidimensional Functions*, Chem. Phys. Lett. **219** (1994) 343, chem-ph/9404003 (1994).
- [3] J. Brooke, D. Bitko, T. F. Rosenbaum and G. Aeppli, *Quantum Annealing of a Disordered Magnet*, Science **284** (1999) 779, cond-mat/0105238 (2001).
- [4] J. Brooke, T. F. Rosenbaum and G. Aeppli, *Tunable Quantum Tunneling of Magnetic Domain Walls*, Nature **413** (2001) 610, cond-mat/0202361 (2002).
- [5] Y. H. Lee and B. J. Berne, *Global Optimization: Quantum Thermal Annealing with Path Integral Monte Carlo*, J. Phys. Chem. A **104** (2000) 86.
- [6] G. E. Santoro, R. Martoňák, E. Tosatti and R. Car, *Theory of Quantum Annealing of an Ising Spin Glass*, Science **295** (2002) 2427.
- [7] E. Farhi, J. Goldstone, S. Gutmann and M. Sipser, *Quantum Computation by Adiabatic Evolution*, quant-ph/0001106 (2000).
- [8] E. Farhi, J. Goldstone, S. Gutmann, J. Lapan, A. Lundgren and D. Preda, *A Quantum Adiabatic Evolution Algorithm Applied to Random Instance of an NP-Complete Problem*, science **292** (2001) 472, quant-ph/0104129 (2001).
- [9] A. M. Childs, E. Farhi and J. Preskill, *Robustness of adiabatic quantum computation*, Rhys. Rev. A **65** (2002) 012322, quant-ph/0108048 (2001).
- [10] E. Farhi, J. Goldstone and S. Gutmann, *Quantum Adiabatic Evolution Algorithms versus Simulated Annealing*, quant-ph/0201031 (2002).

Abstract

We introduce quantum fluctuations into the simulated annealing process of optimization problems, aiming at faster convergence to the optimal state. Quantum fluctuations cause transitions between states and thus play the same role as thermal fluctuations in the conventional approach. The idea is tested by the two models, the transverse Ising model and the traveling salesman problem.

Adding the transverse field to the Ising model is a simple way to introduce quantum fluctuations. The strength of the transverse field is controlled as a function of time similarly to the temperature in the conventional method. The goal is to find the ground state of the diagonal part of the Hamiltonian with high accuracy as quickly as possible. We also consider the traveling salesman problem. This model can be described by the Ising spin, so that we also apply the same technique to the transverse Ising model.

We solve the time-dependent Schrödinger equation numerically for small size systems with various types of exchange interactions of the Ising model. Comparison with the results of the corresponding classical (thermal) method reveals that the quantum method leads to the ground state with much larger probability in almost all cases if we use the same annealing schedule of the control parameters. We check the case of large-size systems by using the quantum Monte Carlo method. The simulation supports the results of the small-size systems, while the dynamics of the Schrödinger equation and the quantum Monte Carlo method are not the same. We find that the simulated annealing by quantum fluctuations has a better performance than the conventional method for the ground state search of the Ising-spin systems.

The calculation of the traveling salesman problem is also performed as

an application to the general optimization problems. We obtain the same feature of the fast convergence to the optimal state as the transverse Ising model by using the quantum fluctuations.

We also find that the relaxation time is quite short for quantum systems by numerical simulations. We consider this is one of the reasons why the annealing in quantum systems have a better performance of finding the optimal state in comparison with classical systems.

List of Papers

1. T. Kadowaki and H. Nishimori, “Quantum annealing in the transverse Ising model”, Phys. Rev. E **58** (1998) 5355.
2. T. Kadowaki and H. Nishimori, “Monte Carlo study of quantum annealing”, in preparation.

List of Papers Added for Reference

1. T. Kadowaki, Y. Nonomura and H. Nishimori, “Exact Ground-State Energy of the Ising Spin Glass on Strips”, J. Phys. Soc Jpn. **65** (1996) 1609.
2. M. Yamana, H. Nishimori, T. Kadowaki and D. Sherrington, “High-Temperature Dynamics of Spin Glasses”, J. Phys. Soc Jpn. **66** (1997) 1962.

Contents

Preface	ii
Abstract	iv
1 Introduction	1
1.1 The Combinatorial Optimization Problem	1
1.2 The <i>NP</i> -hard and The <i>NP</i> -complete Problems	2
1.3 Spin Glass Models and Optimization	7
1.4 Simulated Annealing	10
1.5 Quantum Annealing	13
2 Analysis by Differential Equations	18
2.1 The Transverse Ising Model	19
2.2 Numerical results	21
2.2.1 Ferromagnetic Model	21
2.2.2 Frustrated Model	22
2.2.3 Random Interaction Model	26
2.3 Solution of the single-spin problem	27
2.4 Summary	30
3 Monte Carlo Analysis	33
3.1 Monte Carlo Method	34
3.2 Quantum Monte Carlo Method	35
3.3 Path-Integral Monte Carlo	37
3.4 Applying Monte Carlo to Annealing Process	40
3.5 Results of the Monte Carlo simulation	47

<i>CONTENTS</i>	viii
3.5.1 Dependence on the temperature	48
3.5.2 Dependence on the number of Trotter slices	49
3.5.3 Results of large size system for the EA model	50
3.5.4 Difference between the annealing and the quenching processes	55
3.6 Summary	56
4 Application to TSP	61
4.1 The Traveling Salesman Problem	61
4.2 Simulated Annealing on TSP	62
4.3 Quantum Annealing on TSP	63
4.4 Results of Monte Carlo Simulations	67
4.5 Summary	74
5 Summary	78
A Single-spin problem	82
Appendix	82
A.1 Case of $\Gamma(t) = -ct$ (Landau-Zener model)	82
A.2 Case of $\Gamma(t) = c/t$	83
A.3 Case of $\Gamma(t) = c/\sqrt{t}$	85
A.4 Final value dependence on initial condition	86
Bibliography	88

Chapter 1

Introduction

1.1 The Combinatorial Optimization Problem

The combinatorial optimization problem is to find a minimum or maximum value of a function of very many independent variables, where the variables take discrete values. This function, usually called the cost function or objective function, represents a quantitative measure of the “goodness” of some complex systems. A famous example is the traveling salesman problem [1, 2] to find the shortest or lowest-cost route to visit given cities. The techniques to find the shortest route have been studied for a long time, because such a problem actually happens in various situations, and people have to obtain the solution. One of the most important application of the optimization problems today is the circuit design of the computer systems. The cost function is the wiring length in this case. Long wiring makes delays in electric circuit, and the speed of computer slows down.

The algorithm to find the shortest tour of the traveling salesman problem or the wiring length of the circuit design in polynomial time of N , where N is the size of the problem, is not found yet. When N increases, the complexity of the calculation increases exponentially and goes over the limit of the computational power. This kind of problems are called the “Nondeterministic Polynomial-time solvable hard or complete (NP -hard or NP -complete)” problems. (Details of the definitions are explained in the next section.) Any

algorithm of solving an NP -hard or NP -complete problem in polynomial time is not found so far and people consider that there does not exist such an algorithm. Therefore we consider approximate algorithms by which we can obtain an approximate solution or an exact solution with some probability in polynomial time. In this thesis we focus on how to solve the NP -hard or NP -complete problems approximately as fast as possible.

1.2 The NP -hard and The NP -complete Problems

In this section we explain several levels of difficulty of optimization problems. The NP -hard and NP -complete problems belong to the class quite hard to solve. The difference between the classes NP -hard and NP -complete is not in the degree of difficulty but the way to answer the questions; “yes or no” for NP -complete and in general statements for NP -hard.

First, let us consider the class NP before the definition of the classes NP -hard and NP -complete. The class NP is a subclass of the solvable class of decision problems whose answer is expressed by either “yes” or “no”. For instance, the Hamilton circuit problem is the problem to check the existence of the Hamilton circuit which is the closed loop constructed by edges and all the vertexes in a given graph. An example of the Hamilton circuit problem and its Hamilton circuit are shown in Fig. 1.1.

Roughly speaking, the NP problem is the problem which can be verified in polynomial time by the people who know the evidence to prove the existence of the solution. For instance, one can answer “yes” for the Hamilton circuit problem shown in Fig. 1.1, when the Hamilton circuit (the evidence in this case) is given as a bold line in Fig. 1.1. The verification time of the evidence, checking the closed loop which contains all the vertexes, is proportional to N . To be precise, the NP problem is defined as a problem which can be solved by the nondeterministic Turing machine in polynomial time of N . However, the definition of the nondeterministic Turing machine is complicated, and the reader who is not interested in the detail can skip the following two paragraphs.

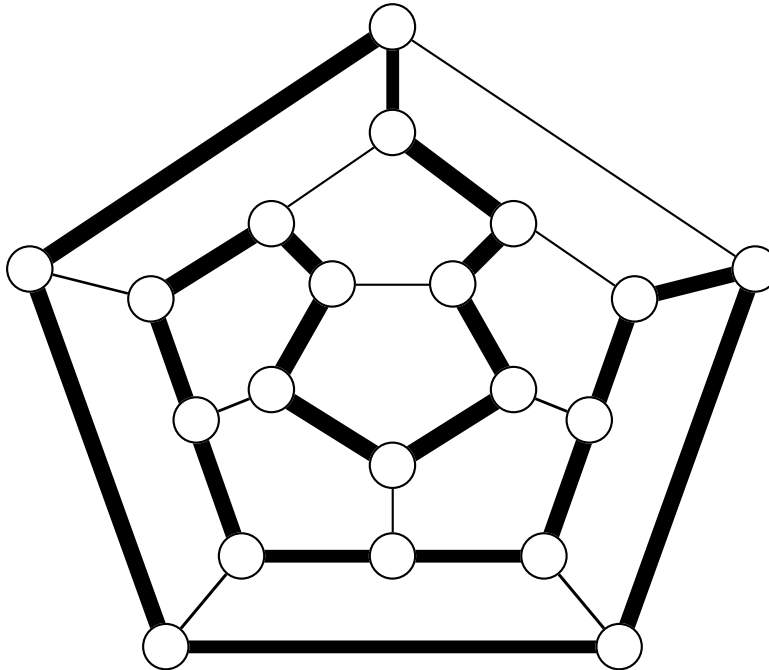


Figure 1.1: The Hamilton graph is the graph which has a Hamilton circuit. The bold line is the Hamilton circuit.

Before presenting the definition of the nondeterministic Turing machine, we explain the definition of the usual (deterministic) Turing machine. The nondeterministic Turing machine is the extended model of the Turing machine. The definition of the Turing machine is constructed with

- the tape which includes alphabets (as commands and data).
- the state of the machine.
- the transition function of the state by using the alphabet read from the tape.

The Turing machine is a simple model of actual computers. For the deterministic Turing machine, the transition function is single-valued. Turing machine reads an alphabet from the tape and modifies its configuration (the state and alphabets on the tape) from the previous configuration according to the given alphabet. A unique modified state is given by this transition.

On the other hand, the transition function of the nondeterministic Turing machine is multi-valued. The feature of the nondeterministic Turing machine quite differs from conventional computers. The configuration of the nondeterministic Turing machine becomes multiple configurations. This can be understood loosely in a way that the nondeterministic Turing machine makes replicas of possible configurations by a single step and the number of replicas increases exponentially as a function of the step. This feature is quite useful to solve complicated problems. For finding the ground-state energy of Ising-spin systems, for example, we have to enumerate all possible spin configurations, if the ground state is nontrivial. These configurations are illustrated by the tree structure in Fig. 1.2. The direction of spins is assigned at each branching point and the level corresponds to the location of the spin. Each path means the configuration. The nondeterministic Turing machine can check all paths in parallel. At the first step, the machine makes a replica and the number of machines is two. Each machine makes a replica at each step so that the number of machines is 2^N at the N th step. The calculations in the same level of the tree are performed at a time. By this procedure, we can enumerate 2^N configurations in N steps.

All NP problems can be verified in polynomial time even on a deterministic Turing machine, but the difficulty of solving the problems is not the same. The problems are divided into some subclasses — the subclasses P for easy problems and NP -complete for difficult problems. The problem which has the algorithm to be solved in polynomial time by the deterministic Turing machine belongs to the class of Polynomial-time solvable (P). Obviously NP contains P , because the nondeterministic Turing machine includes the deterministic Turing machine in its definition.

For an example of the P problem, we explain the Hamilton circuit problem for the graph whose maximum degree of the edge in a vertex is limited to two belongs to P . The typical graphs are shown in Fig. 1.3. The answers of the left and the right problems are “yes” and “no” respectively. One can check the existence of the Hamilton circuit by the following way:

1. Start from a vertex and jump to the neighbor vertex connected by an edge. (One can not jump to the neighbor which has already been

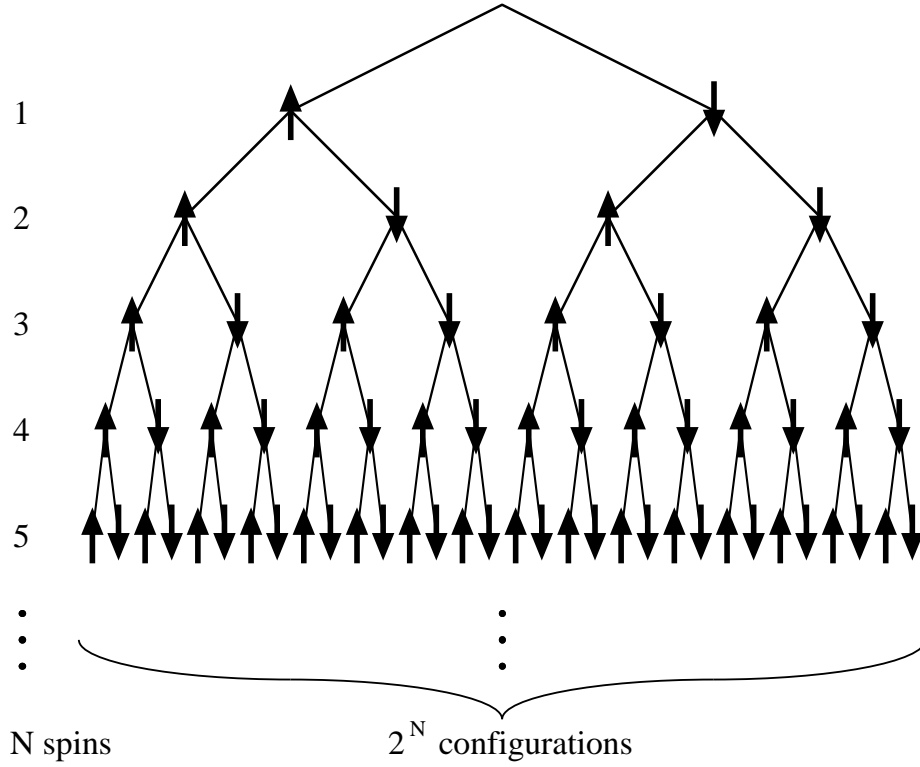


Figure 1.2: The path means the spin configuration. The number of the leaves (the bottom ends of the tree) equals to the number of configurations as 2^N .

- visited once.)
- 2. Repeat 1 until no vertex to jump is left.
- 3. If the last vertex is connected to the starting vertex and all the vertexes have been visited, the answer is “yes”. The answer is “no” other wise.

This procedure needs polynomial time. If the maximum degree of the edge in a vertex is not limited to two, this procedure does not work.

Let us consider the difficult classes *NP*-hard and *NP*-complete. If any problems in *NP* can be solved by using a particular algorithm of the problem repeatedly polynomial times at most, the problem is called “*NP*-hard”. In other wards, we can solve any *NP*-problems by calling the subroutine for a particular *NP*-hard problem (maybe once except for other *NP*-hard problems). The *NP*-hard problem is more difficult than any *NP* problems or as

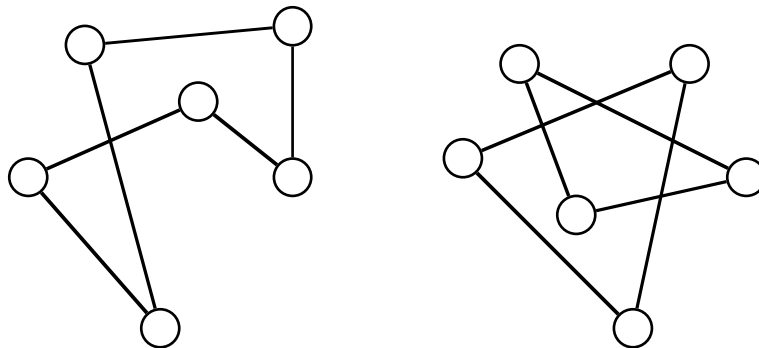


Figure 1.3: The Hamilton circuit problems with the answer “yes” and “no”. The left graph is the single loop (the Hamilton circuit) and right one is not the single loop.

difficult as the other NP -hard problems in polynomial order. The algorithm of the NP -hard problem is the most general algorithm in NP class. The NP -hard problems by definition are not limited to belong to the class NP . For instance, the traveling salesman problem is not an NP problem but an NP -hard problem because the answer is not “yes or no” but the tour length and route. The subclass “ NP -complete” is the set of the NP -hard problems which belong to the class NP . The NP -complete problems are more difficult than any other NP problems and as difficult as the NP -hard problems. The Hamilton circuit problem is known as an NP -complete problem [3].

The difficulty of the problems can be expressed symbolically as $P \leq (NP - P - NP\text{-complete}) \leq NP\text{-complete} \approx NP\text{-hard}$. It is a trivial consequence of their definition that if one of the NP -complete problems can be solved in polynomial time, then all the problems of the NP class are also polynomial. In this case one would have $P = NP$. So far no polynomial algorithm has been found for an NP -complete problem, and the question of whether P is equal to NP is still open, although the general belief is that NP -complete problems are not polynomial. The most probable situation is sketched in Fig. 1.4. The NP problems can be divided into three subclasses, NP -complete, P and the subclass which does not belong to the previous two subclasses. The class NP -hard is separated into two subclasses, NP -complete and the other part by whether the problem is the

decision problem or not. Empirically the time it takes to solve an NP -hard and an NP -complete problems tends to scale exponentially with the size N . All the problems can be solved by the enumeration method by which all the configurational space of the problem are enumerated and this calculation needs the time proportional to e^N .

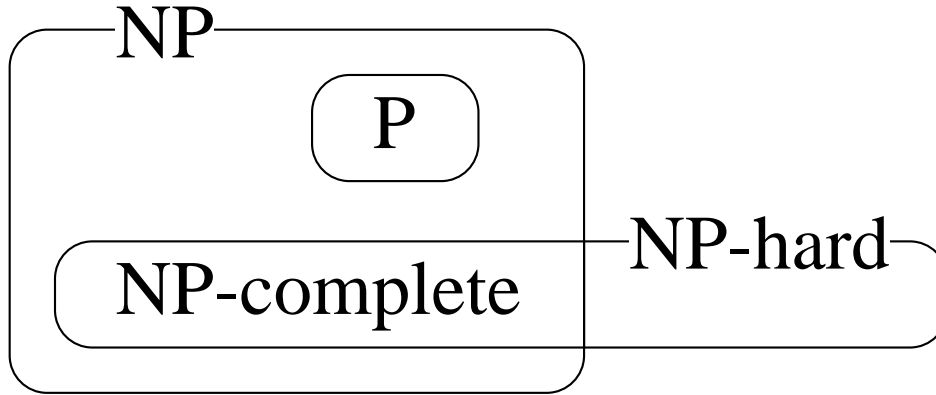


Figure 1.4: The class of NP problems assuming that $P \neq NP$. Under this assumption it can be shown that there are NP problems that are neither NP -complete nor P .

1.3 Spin Glass Models and Their Relation to Optimization

Combinatorial optimization problems appear in various disciplines. In statistical mechanics, the energy is equivalent to the cost function of the optimization problem. Until the 1970s, almost all the systems to be studied were homogeneous so that the energy landscape has a simple structure and the optimal solution (the ground state) is trivial. Although such a system has many variables, the degrees of freedom can be reduced to small numbers. For instance, spins turn to the same direction in the ground state of the ferromagnetic model and the spin variables are reduced to single-spin variable. This reduction comes from the homogeneous interactions. In the 1970s the study of the spin glass started. The spin glass system is a non-homogeneous system and the ground state is nontrivial. The background of the physics

of spin glasses and its relation to the combinatorial optimization problem is explained in this section.

The study of spin glasses started in 1972 when Cannella and Mydosh [4] investigated the AC susceptibility of a dilute magnetic alloy Au-Fe and found out that the AC susceptibility has a nontrivial sharp cusp. In the alloy, the interaction J_{ij} between two spins of Fe atoms is expressed as the RKKY interaction [5, 6, 7]

$$J_{ij} \propto \frac{1}{r_{ij}^3} \cos(2k_F r_{ij}) , \quad (1.1)$$

where r_{ij} is the distance between two spins and k_F is the Fermi wave number. From this interaction and a random distribution of Fe atoms in space, it is possible that the interaction is a positive or a negative random variable.

Edwards and Anderson proposed the so-called Edwards-Anderson (EA) model [8] to introduce the effect of the RKKY interaction in a diluted magnetic alloy. The EA model has nearest-neighbor interactions J_{ij} . The value of the interaction distributes as

$$P(J_{ij}) = \left(\frac{z}{2\pi J^2} \right)^{1/2} \exp \left[-\frac{z}{2J^2} \left(J_{ij} - \frac{J_0}{z} \right)^2 \right] , \quad (1.2)$$

where z is the number of nearest neighbors. The average of the distribution is J_0/z , and the standard deviation is J/\sqrt{z} . The Hamiltonian is given by

$$\mathcal{H} = - \sum_{\text{n.n.}} J_{ij} S_i S_j . \quad (1.3)$$

The EA solution is not solved exactly. Sherrington and Kirkpatrick [9] investigated an infinite-range model, the so-called SK model. The Hamiltonian is given by

$$\mathcal{H} = - \sum_{\langle ij \rangle} J_{ij} S_i S_j - h \sum_i S_i , \quad (1.4)$$

where $\langle ij \rangle$ denotes a summation over all spin pairs. This is the reason of the name of the infinite-range model. The summation is different from that in the EA model. If the average of distribution of interactions is equal

to zero and the external field is vanishing, a second order phase transition at a finite temperature $T_c (= J/k_B)$ occurs, and the spin glass phase realizes below T_c .

The statistical property as the SK model was almost solved by further studies [10, 11, 12, 13, 14, 15, 16, 17, 18], but it is difficult to analyze the EA model by the same approaches. The EA model is often studied by computer simulations, the Monte Carlo simulations or other methods. The great interest of the EA model or the $\pm J$ model whose interactions are distributed binary (at J and $-J$) is whether the same picture of the SK model — the picture of the ultrametricity and the structure of the $P(q)$ [13, 18] — exists or not. One can check this picture from the calculation of the distribution function $P(q)$ where the overlap q is calculated from the pure states which are the equilibrium states separated by high energy barriers and can be obtained by the Monte Carlo simulation. If the simulation starts from a random configuration which is equivalent to the configuration at high temperature, the system is stuck in a metastable state and it takes long time to escape from the metastable state because the basins of the pure states and the metastable states are separated by high energy barriers. To avoid this difficulty of the simulation, one can start the simulation from the ground state, which is close to the pure state at low temperature. However, finding the ground state is also difficult. The reason is the following: Spins on the some plaquettes in the EA model do not satisfy all the bonds illustrated in Fig.1.5. This situation occurs, when the product of all the bonds in the plaquette has a minus sign. The frustrated plaquettes are located at random so that we have to consider the global structure of the configuration which pays as small penalty of the energy as possible. Therefore the ground state is not the trivial configuration. The difficulties in studying the EA model are the slow relaxation and the non-trivial configuration of the ground state. The latter problem is a typical example of the combinatorial optimization problem.

The SK model is connected with the bipartition problem directly. We divide the group into two parts. “Likes and dislikes” between the members is expressed as the numerical value. The task is to find the best partition of the members. The case of $N = 6$ is illustrated in Fig. 1.6. The members are

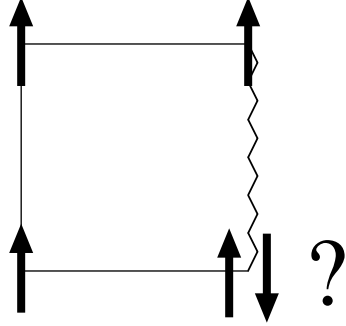


Figure 1.5: The frustrated plaquette. The solid and the zigzag lines are the ferromagnetic and antiferromagnetic bonds.

divided into open and closed circles, and the black and the gray lines mean “likes” and “dislikes” between the members. Assigning $+1$ to the members in one part and -1 to the members in the other part, we can regard that the members are expressed by Ising spins $\{\sigma_i\}$. The cost function of the “likes and dislikes” between two members i and j can be obtained as $J_{ij} \frac{\sigma_i \sigma_j + 1}{2}$. If the two members i and j are in the same part, “likes and dislikes” is counted as J_{ij} . If the two members are in the different parts, the value is zero. We can calculate the total cost of “likes and dislikes” by summing up all the pairs as:

$$\begin{aligned} \text{Total Cost} &= \sum_{(ij)} J_{ij} \frac{\sigma_i \sigma_j + 1}{2} \\ &= \frac{1}{2} \sum_{(ij)} J_{ij} \sigma_i \sigma_j + \text{const.} \end{aligned} \quad (1.5)$$

This cost function is exactly the same as the Hamiltonian of the SK model. The bipartition problem and the finding the ground state of the SK model are known as the NP -hard problems [19, 20].

1.4 Simulated Annealing

As shown in the previous section, large computational time is needed to solve an NP -complete or an NP -hard problem exactly. The technique of simulated annealing (SA) was first proposed by Kirkpatrick *et al.* [21] as a general

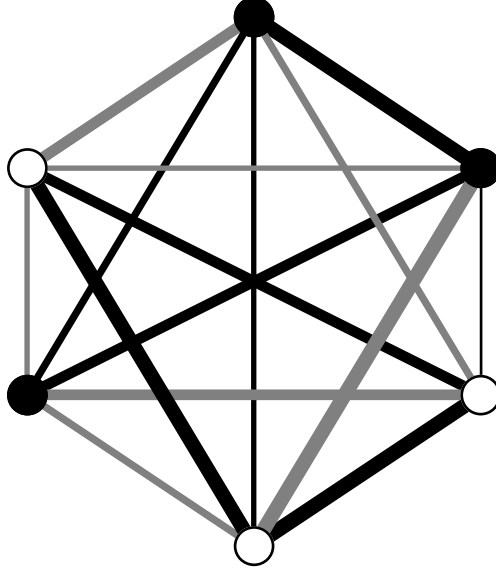


Figure 1.6: The bipartition problems with $N = 6$. The open and closed circles are the divided members of the group. The black and the gray lines mean “likes” and “dislikes” between the members.

method to solve optimization problems. This method is an approximate algorithm to find the optimal solution in finite time, but the solution converges to the optimal state in the infinite-time limit. The probability to find the ground state increase with time and converges to one in the infinite-time limit. For practical applications, it is important to find a sufficiently good solution, where “good” means that the cost function is close to the optimal value.

The idea is to use thermal fluctuations to allow the system to escape from local minima of the cost function so that the system reaches the global minimum under an appropriate annealing schedule (the rate of decrease of temperature). Let us consider a simple example of a system described by Ising spins $\{\sigma_i \pm 1\}$, binary variables. Spins interact each other as $-J\sigma_i\sigma_j$ and the total energy (cost function) of this system is $\mathcal{H} = -\sum_{ij} J\sigma_i\sigma_j$, where ij runs over all possible pairs of sites which interact with each other. If the two spins σ_i, σ_j take the same value, the energy becomes lower. This system is the simplest model of a ferromagnet. In the optimal configuration, all spins

align in the same direction, up or down.

Once we define the energy of the system, we can consider statistical mechanics of this system. The spin configuration $\{\sigma_i\}$ is modified by thermal noise. The probability with which the configuration $\{\sigma_i\}$ appears is proportional to the Boltzmann factor $\exp(-E(\{\sigma_i\})/k_B T)$, where T is the temperature and k_B is the Boltzmann constant. The probability has to be normalized and the normalization factor is $1/Z$. The inverse of the factor, the so-called partition function, is expressed as:

$$Z = \sum_{\{\sigma_i=\pm 1\}} \exp(-E(\{\sigma_i\})/k_B T) \quad (1.6)$$

The lower the temperature becomes, the larger the probability of the spin configuration of the lowest energy becomes. The system freezes to the ground state as the temperature goes to zero. However, the system does not always freeze to the ground state in rapid cooling. As illustrated in Fig. 1.7, the system may be trapped in a local minimum. Therefore, the temperature should be cooled attentively. At high temperature, the system changes the configuration almost randomly and searches the global structure of the energy landscape. The system seeks the area in which the valley of the global minimum is included when the temperature is decreased. Finally, the system is stuck at the valley of the global minimum at zero or sufficiently low temperature (lower than the energy gap of the ground state and the first excited state). The idea of this cooling is illustrated in Fig. 1.8

By the way, how can we cool the system slowly enough? Geman and Geman proved a theorem on the annealing schedule for combinatorial optimization problems [22]. They showed that any system reaches the global minimum of the cost function asymptotically if the temperature is decreased as $T = c/\log t$ or slower, where c is a constant determined by the system size and other structures of the cost function. When the product of the temperature and the Boltzmann constant $k_B T$ become less than the energy gap between the ground state and the first excited state, the system jumps to the excited state rarely by thermal fluctuation. Writing such a temperature as T_0 , we obtain the time to find the ground state as $t \sim \exp(c/k_B T_0)$. This

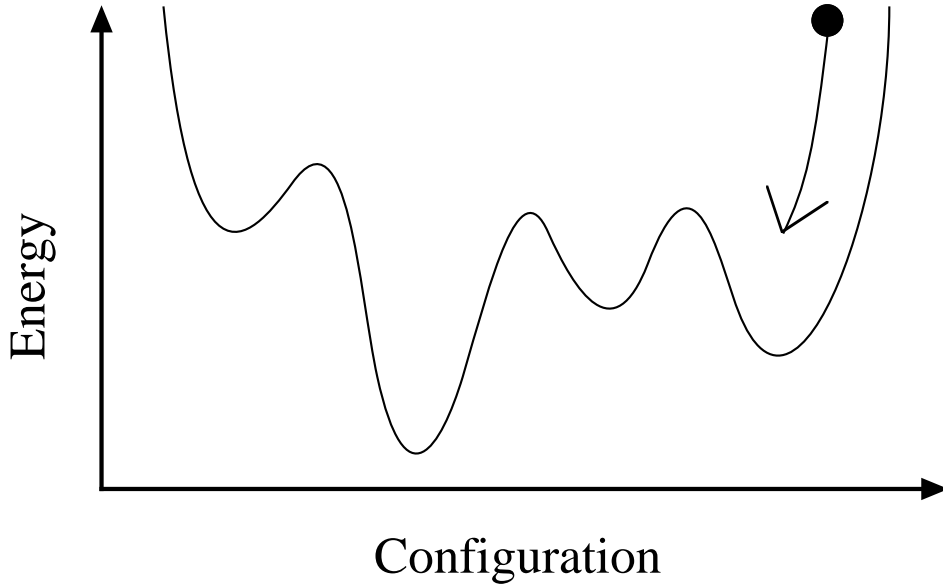


Figure 1.7: Cooling from high temperature to low temperature. If the cooling rate is too fast, the system may be trapped in a local minimum.

bound on the annealing schedule may be the optimal one under generic conditions although faster decrease of the temperature often gives satisfactory results in practical applications for many systems.

1.5 Quantum Annealing

In SA thermal fluctuations are introduced in the optimization problem so that transitions between states take place in the process of search for the global minimum among many states. Thus there seems to be no reasons to avoid use of other mechanisms for state transitions if these mechanisms may lead to better convergence properties. One such possibility is the generalized transition probability of Tsallis [23], which is a generalization of the conventional Boltzmann-type transition probability appearing in the master equation and thus used in Monte Carlo simulations. In this method, the system converges to the optimal state under power-law decrease of the tem-

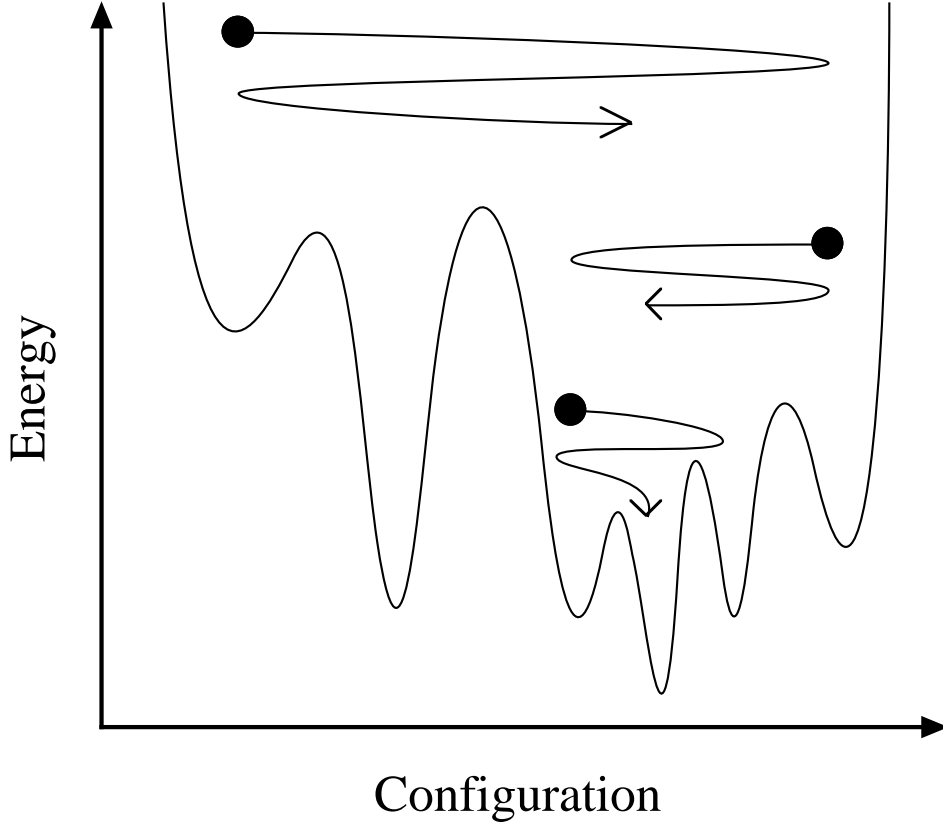


Figure 1.8: The system seek the various levels of the energy-landscape structure corresponding to the temperature. The system searches the global (local) structure at high (low) temperatures.

perature [23, 24, 25, 26]. This schedule is faster than the log schedule of the conventional SA. However, the generalized transition probability does not satisfy the condition of the detailed balance, the sufficient condition for convergence to the equilibrium state, and the physical meanings of the system is not trivial.

We seek another possibility of making use of quantum tunneling processes for state transitions, which we call quantum annealing (QA). In particular we would like to learn how effectively quantum tunneling processes possibly lead to the global minimum in comparison to temperature-driven processes

used in the conventional method of SA.

In the virtual absence of previous studies along such a line of consideration, it seems better to focus our attention on a specific model system, rather than to develop a general argument, to gain an insight into the role of quantum fluctuations in the situation of optimization problem. Quantum effects have been found to play a very similar role to thermal fluctuations in the Hopfield model and the image restoration problem in a transverse field in thermal equilibrium [27, 28]. This observation motivates us to investigate dynamical properties of the Ising model under quantum fluctuations in the form of a transverse field. We therefore start the study of the QA by the transverse Ising model with a variety of exchange interactions. The transverse field controls the rate of transition between states and thus plays the same role as the temperature does in SA. We assume that the system has no thermal fluctuations in the QA context and the term “ground state” refers to the lowest-energy state of the Hamiltonian without the transverse field term.

Static properties of the transverse Ising model have been investigated quite extensively for many years [29, 30, 31]. There have however been very few studies on the dynamical behavior of the Ising model with a transverse field. We refer to the work by Sato *et al.* who carried out quantum Monte Carlo simulations of the two dimensional EA model in an infinitesimal transverse field, showing a reasonably fast approach to the ground state [32]. We present a new point of view by comparing the efficiency of QA directly with that of classical SA in reaching the ground state.

In the next chapter, we consider the time-dependent Schrödinger equation for QA and the classical master equation for SA numerically for small-size systems with the same exchange interactions under the same annealing schedules. We explain the model and define the measure of closeness of the system in QA to the desired ground state. This measure is compared with the corresponding classical probability that the system is in the ground state. Calculations of probabilities that the system is in the ground state at each time for both classical and quantum cases give important implications on the relative efficiency of the two approaches. The numerical results for QA

and SA suggest that QA generally gives a larger probability to find to the ground state than SA under the same conditions on the annealing schedule and interactions. We also calculate the analytical solutions for the one-spin case which turns out to be quite non-trivial. Explicit solutions yield very useful information to clarify several subtle aspects of the problem.

In Chapter 3, we extend our method by using the Monte Carlo method to calculate large-size problems. We adopt the master equation as the time-evolution equation of SA in contrast to the Schrödinger equation of QA. The original definition of SA is expressed in terms of the Monte Carlo method, which is equivalent to the master equation. It is natural to consider the applicability of Monte Carlo method to QA. The time-evolution of the wave function is expressed as:

$$|\Psi(t)\rangle = \mathsf{T}e^{-i \int_0^t dt \mathcal{H}(t)} |\Psi(0)\rangle, \quad (1.7)$$

where the symbol T is the time ordering operator. There are two approaches to take into account the quantum effects or the time evolution gradually. The first one is to divide the Hamiltonian into some parts which are easy to diagonalize (for instance, into three terms which include σ^x , σ^y , σ^z , respectively) as

$$e^{\mathcal{H}} = \lim_{m \rightarrow \infty} (e^{\mathcal{H}_0/m} e^{\mathcal{H}_1/m} \dots)^m. \quad (1.8)$$

This division is the Suzuki-Trotter decomposition. By inserting the complete set $\sum_i |i\rangle\langle i| (= 1)$, the system is mapped to a $(d+1)$ -dimensional classical system. Once the system is expressed as a classical system, we can perform the Monte Carlo method, the so-called quantum Monte Carlo method. The second one is the division of the short-time evolution as

$$e^{-i \int_0^t dt \mathcal{H}(t)} = \lim_{\Delta t \rightarrow 0} e^{-i \Delta t \mathcal{H}(t)} \dots e^{-i \Delta t \mathcal{H}(0)}, \quad (1.9)$$

the path integral Monte Carlo method. The dynamics of the two approaches are not exactly the same as the dynamics of the Schrödinger equation. The performances of the two approaches are the same or better in comparison with the dynamics of the Schrödinger equation in some sense (a detailed discussion

is shown later). We finally adopt the quantum Monte Carlo method for the calculation of QA, because this method is similar to the original SA and we can find the optimal state precisely by the time evolution. The results of the simulations show that QA performs in finding the optimal state better than SA in spite of the disadvantage in the calculation of the quantum effect (the calculation on $(d + 1)$ -dimensional systems is larger than d -dimensional system). We also calculate the difference between the quenched system and annealed system. The calculation of the quenched system is almost the same as the study by Sato *et al.* [32]. In general, quenched systems tend to be stuck in local minima. We find that the classical quenched system is stuck more often than the quantum quenched system. We consider this is one of the reasons why QA works better than SA.

So far, the systems are physical models. The problems of the ground state finding of physical models occupy the small area of the combinatorial problems and we have to check applicability to the general problems. One of the well-known problems is the TSP. We apply QA to the traveling salesman problem (TSP) in Chapter 4. TSP can be mapped to the Ising spin system so that we can use the same framework of QA. The modification of the configuration of TSP in SA is not the same as the modification of the usual one-spin dynamics of SA. Four spins are changed at a time in TSP. The quantum-effect term of the Hamiltonian (the cost function) has to be changed to the product of the four spin operators to fit the dynamics of SA. However, we adopt the same quantum-effect term, the transverse field, because of the difficulty of the calculation. In spite of this, QA also works and improves in comparison to SA. This fact suggests that QA can be applied to various problems in which we can not define the quantum effect exactly.

Chapter 2

Analysis of Small-size Systems by Differential Equations

In this chapter, we introduce the quantum annealing (QA) for small-size systems by using the Schrödinger equation and compare the results of QA and the simulated annealing (SA). The models (problems) we deal with here are the models in statistical physics, precisely the Ising model. The transverse field is introduced as the quantum effect and scheduled as a decreasing function of the time. This field flips single spin at a time so that the transition is quite similar to the usual single-spin-flip dynamics of SA.

The analysis is performed numerically and analytically for SA and QA. The system size of the numerical calculation is up to eight. The calculation limit of the size is around fourteen by the middle-class supercomputer today. (for a fourteen-spin system, calculation needs the storage about 2G Byte!) The models we use as test-bed are ferromagnetic, frustrated and random-interaction models. We also study for the single-spin quantum system with longitudinal and transverse field. The exact solutions are obtained for some schedules. The single-spin system is too small to discuss the property of QA, but the result provides some information for the results of the numerical calculations.

2.1 The Transverse Ising Model

Let us consider the following Ising model with longitudinal and transverse fields:

$$\mathcal{H}(t) = - \sum_{ij} J_{ij} \sigma_i^z \sigma_j^z - h \sum_i \sigma_i^z - \Gamma(t) \sum_i \sigma_i^x \quad (2.1)$$

$$\equiv \mathcal{H}_0 - \Gamma(t) \sum_i \sigma_i^x, \quad (2.2)$$

where the type of interactions will be specified later. The term of longitudinal field was introduced to remove the trivial degeneracy in the exchange interaction term coming from the overall up-down symmetry that effectively reduces the available phase space by half. The $\Gamma(t)$ -term causes quantum tunneling between various classical states (the eigenstates of the classical part \mathcal{H}_0). By decreasing the amplitude $\Gamma(t)$ of the transverse field from a very large value to zero, we hopefully drive the system into the optimal state, the ground state of \mathcal{H}_0 .

The natural dynamics of the present system is provided by the Schrödinger equation

$$i \frac{\partial |\psi(t)\rangle}{\partial t} = \mathcal{H}(t) |\psi(t)\rangle. \quad (2.3)$$

We solve this time-dependent Schrödinger equation numerically for small-size systems. The representation to diagonalize \mathcal{H}_0 (the z -representation) will be used hereafter.

The corresponding classical SA process is described by the master equation

$$\frac{dP_i(t)}{dt} = \sum_j \mathcal{L}_{ij} P_j(t), \quad (2.4)$$

where $P_i(t)$ represents the probability that the system is in the i th state. We consider single-spin flip processes with the transition matrix elements given as

$$\mathcal{L}_{ij} = \begin{cases} \frac{\exp(-E_i/T(t))}{\exp(-E_i/T(t)) + \exp(-E_j/T(t))} & \text{(single-spin difference)} \\ -\sum_{k \neq i} \mathcal{L}_{ki} & (i = j) \\ 0 & \text{(otherwise)} \end{cases}. \quad (2.5)$$

In SA, the temperature $T(t)$ is first set to a very large value and then is gradually decreased to zero. The corresponding process in QA should be to change $\Gamma(t)$ from a very large value to zero. The reason is that the high-temperature state in SA is a mixture of all possible states with almost equal probabilities, and the corresponding state in QA is the linear combination of all states with equal amplitude in the z -representation, which is the lowest eigenstate of the Hamiltonian (2.1) for very large Γ . The low-temperature state after a successful SA is the ground state of \mathcal{H}_0 , which should also be the eigenstate of $\mathcal{H}(t)$ as $\Gamma(t)$ is reduced to zero sufficiently slowly in QA. Another justification of identification of Γ and T comes from the fact that the $T = 0$ phase diagram of the Hopfield model in a transverse field has almost the same structure as the equilibrium phase diagram of the conventional Hopfield model at finite temperature if we identify the temperature axis of the latter phase diagram with the Γ axis in the former [27]. We therefore change $\Gamma(t)$ in QA and $T(t)$ in SA from infinity to zero with the same functional forms $\Gamma(t) = T(t) = c/t, c/\sqrt{t}, c/\log(t+1)$ ($t : 0 \rightarrow \infty$) or $-ct$ ($t : -\infty \rightarrow 0$). The reason for choosing these functional forms are that either they allow for analytical solutions in the single-spin case as shown in Sec. 2.3 or for comparison with the Geman-Geman bound mentioned in the previous chapter.

To compare the performance of the two methods QA and SA, we calculate the probabilities $P_{\text{QA}}(t) = |\langle g|\psi(t)\rangle|^2$ for QA and $P_{\text{SA}}(t) = P_g(t)$ for SA, where $P_g(t)$ is the probability to find the system in the ground state at time t in SA and $|g\rangle$ is the ground-state wave function of \mathcal{H}_0 . Note that we treat only small-size systems (the number of spins $N = 8$) and thus the ground state can be picked out explicitly. In the ideal situation $P_{\text{QA}}(t)$ and $P_{\text{SA}}(t)$ will be very small initially and increase towards 1 as $t \rightarrow \infty$.

It is useful to introduce another set of quantities $P_{\text{SA}}^{\text{st}}(T)$ and $P_{\text{QA}}^{\text{st}}(\Gamma)$. The former is the Boltzmann factor of the ground state of \mathcal{H}_0 at temperature T while the latter is defined as $|\langle g|\psi_\Gamma\rangle|^2$, where the wave function ψ_Γ is the lowest-energy stationary state of the full Hamiltonian (2.1) for a given fixed value of Γ . In the quasi-static limit, the system follows equilibrium in SA and thus $P_{\text{SA}}(t) = P_{\text{SA}}^{\text{st}}(T(t))$. Correspondingly for QA, $P_{\text{QA}}(t) = P_{\text{QA}}^{\text{st}}(\Gamma(t))$ when $\Gamma(t)$ changes sufficiently slowly. Thus the differences between both

sides of these two equations give measures how closely the system follows quasi-static states during dynamical process of annealing.

2.2 Numerical results

We now present numerical results on P_{SA} and P_{QA} for various types of exchange interactions and transverse fields. All calculations were performed with a constant longitudinal field $h = 0.1$ to remove trivial degeneracy.

2.2.1 Ferromagnetic Model

Let us first discuss the ferromagnetic Ising model with $J = \text{const}$ for all pairs of spins. Figure 2.1 shows the overlaps for the case of $\Gamma(t) = T(t) = 3/\log(t+1)$. It is seen that both QA and SA follow stationary (equilibrium) states during dynamical processes rather accurately. In SA the theorem of Geman and Geman [22] guarantees that the annealing schedule $T(t) = c/\log(1+t)$ assures convergence to the ground state ($P_{\text{SA}} \rightarrow 1$ in our notation) if c is adjusted appropriately. Our choice $c = 3$ is somewhat arbitrary but the tendency is clear for $P_{\text{SA}} \rightarrow 1$ as $t \rightarrow \infty$, which is also clear from approximate satisfaction of the quasi-equilibrium condition $P_{\text{SA}}(t) = P_{\text{SA}}^{\text{st}}(T(t))$. Although there are no mathematically rigorous arguments for QA corresponding to the Geman-Geman bound, the numerical data indicate convergence to the ground state under the annealing schedule $\Gamma(t) = 3/\log(t+1)$ at least for the ferromagnetic system. It should be remembered that the unit of time is arbitrary since we have set $\hbar = 1$ in the Schrödinger equation (2.3) and the unit of time $\tau = 1$ in the master equation (2.4). Thus the fact that the curves for QA in Fig. 2.1 lie below those for SA at any given time does not have any positive significance.

If we decrease the transverse field and the temperature faster, $\Gamma(t) = T(t) = 3/\sqrt{t}$, there appears a qualitative difference between QA and SA as shown in Fig. 2.2. The quantum method clearly gives better convergence to the ground state while the classical counterpart gets stuck in a local minimum with a non-negligible probability. To see the rate of approach of P_{QA} to 1,

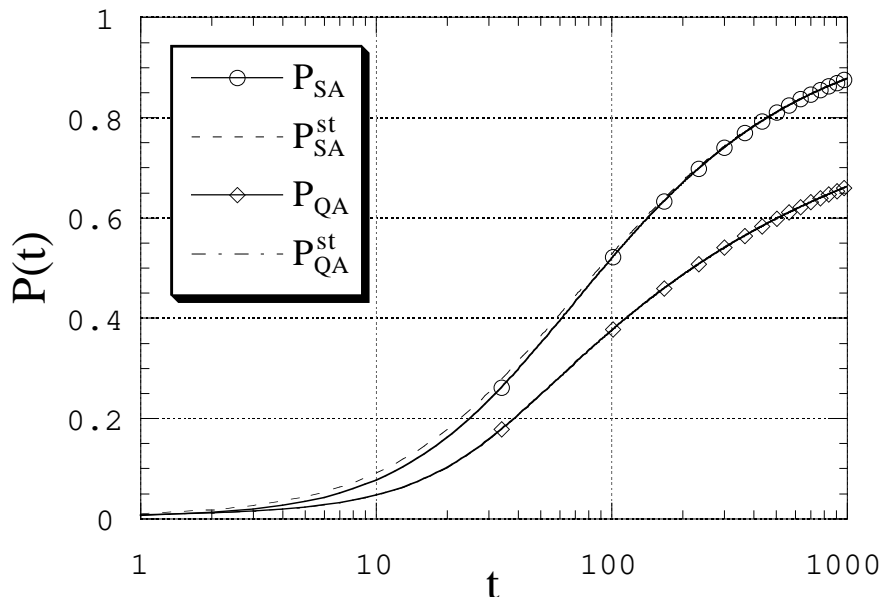


Figure 2.1: Time dependence of the overlaps $P_{SA}(t)$, $P_{QA}(t)$, $P_{SA}^{st}(T(t))$ and $P_{QA}^{st}(\Gamma(t))$ of the ferromagnetic model with $\Gamma(t) = T(t) = 3/\log(t+1)$.

we have plotted $1 - P_{QA}$ in a log-log scale in Fig. 2.3. It is seen that $1 - P_{QA}$ behaves as const/t in the time region between 100 and 1000.

By a still faster annealing schedule $\Gamma(t) = T(t) = 3/t$, the system becomes trapped in intermediate states both in QA and SA as seen in Fig. 2.4.

2.2.2 Frustrated Model

We next analyze the interesting case of a frustrated system shown in Fig. 2.5. The full lines indicate ferromagnetic interactions while the broken line is for an antiferromagnetic interaction with the same absolute value as the ferromagnetic ones. If the temperature is very high in the classical case, the spins 4 and 5 are changing their states very rapidly and hence the effective interaction between spins 3 and 6 via spins 4 and 5 will be negligibly small. Thus the direct antiferromagnetic interactions between spins 3 and 6 is expected to dominate the correlation of these spins, which is clearly observed in Fig. 2.6 as the negative value of the thermodynamic correlation function $\langle \sigma_3^z \sigma_6^z \rangle_c$ in the high-temperature side. At low temperatures, on the other hand, the spins

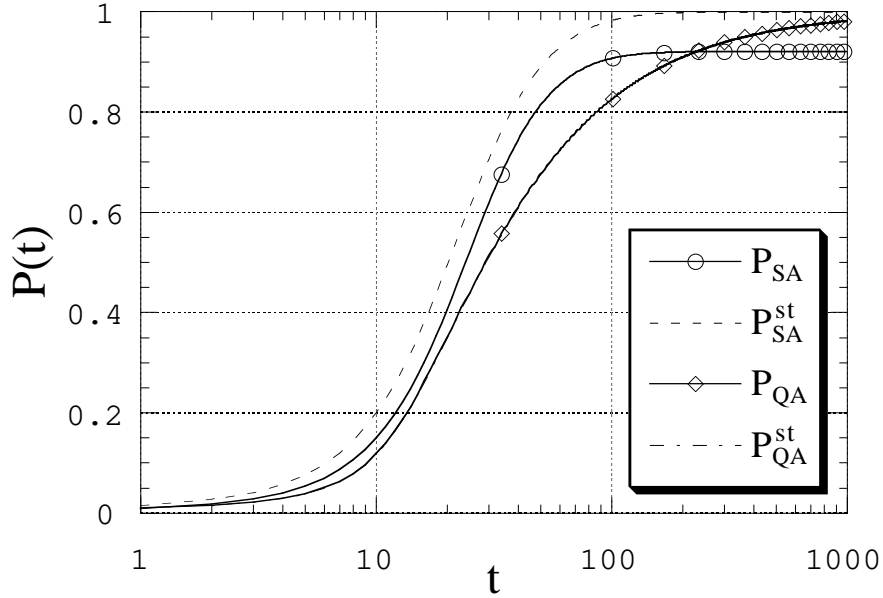


Figure 2.2: Time dependence of the overlaps of the ferromagnetic model with $\Gamma(t) = T(t) = 3/\sqrt{t}$.

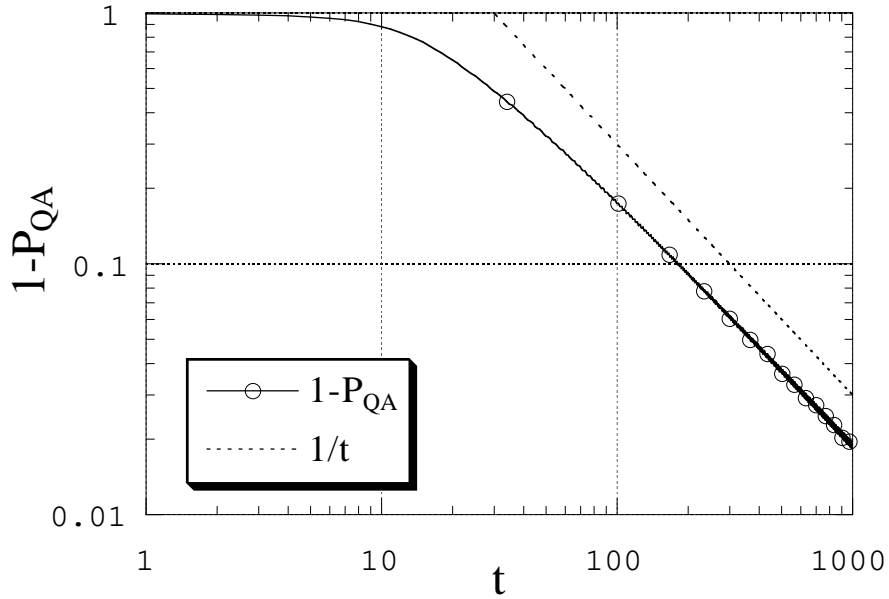


Figure 2.3: Time dependence of $1 - P_{QA}(t)$ of the ferromagnetic model with $\Gamma(t) = 3/\sqrt{t}$. The dotted line represents t^{-1} to guide the eye.

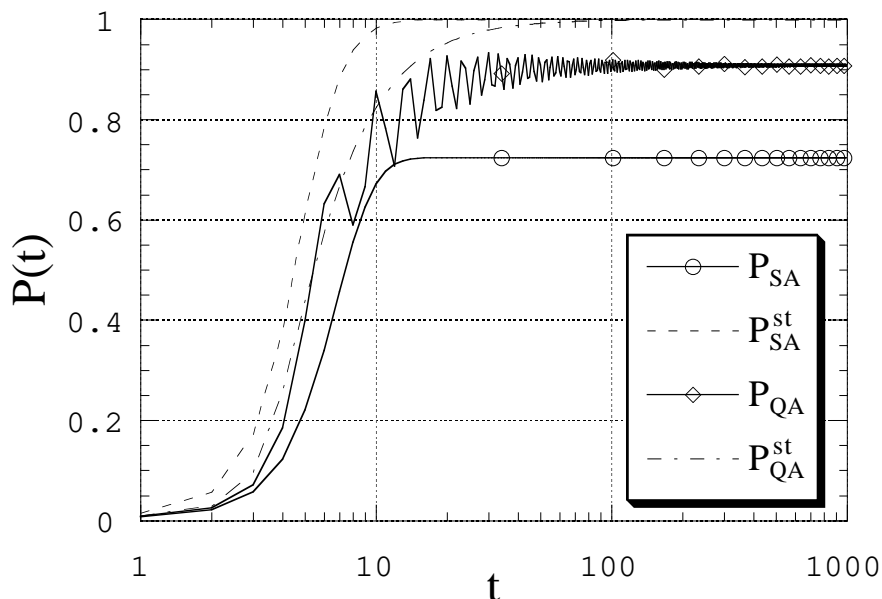


Figure 2.4: Time dependence of the overlaps of the ferromagnetic model with $\Gamma(t) = T(t) = 3/t$.

4 and 5 tend to be fixed in some definite direction and consequently the effective ferromagnetic interactions between spins 3 and 6 are roughly twice as large as the direct antiferromagnetic interaction. This argument is justified by the positive value of the correlation function at low temperatures in Fig. 2.6. Therefore the spins 3 and 6 must change their relative orientation at some intermediate temperature. This means that the free-energy landscape goes under significant restructuring as the temperature is decreased and therefore the annealing process should be performed with sufficient care.

If the transverse field in QA plays a similar role to the temperature in SA, we expect similar dependence of the correlation function $\langle \sigma_3^z \sigma_6^z \rangle_q$ on the transverse field Γ . Here the expectation value is evaluated by the stationary eigenfunction of the full Hamiltonian (2.1) with the lowest eigenvalue at a given Γ . The broken curve in Fig. 2.6 clearly supports this idea. We therefore expect that the frustrated system of Fig. 2.5 is a good test ground for comparison of QA and SA in the situation with a significant change of spin configurations in the dynamical process of annealing.

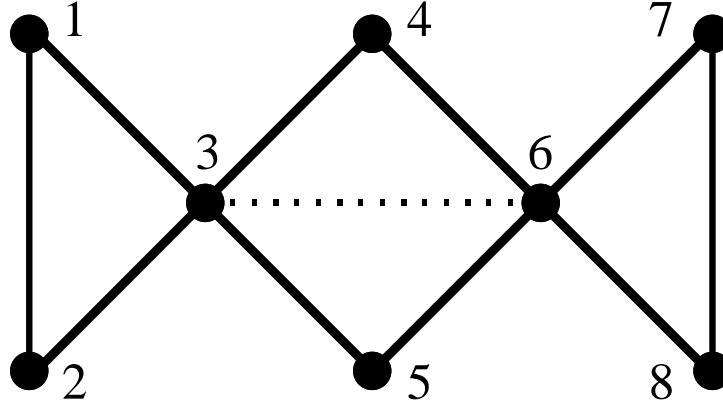


Figure 2.5: The frustrated model where the solid lines denote ferromagnetic interactions and the broken line is for an antiferromagnetic interaction.

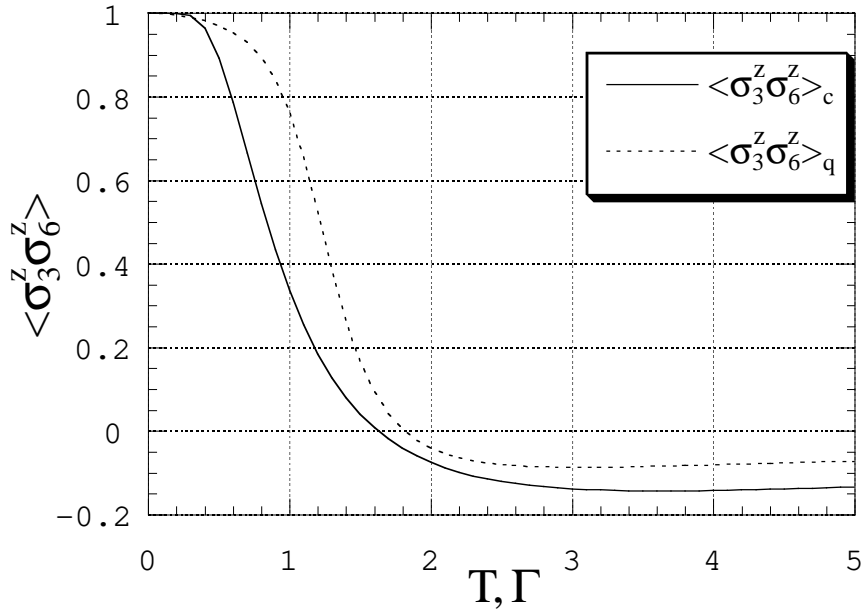


Figure 2.6: Correlation functions of spins 3 and 6 in Fig. 2.5 for the classical and quantum cases. In the classical model (full line) the correlation is shown as a function of temperature while the quantum case (dotted line) is regarded as a function of the transverse field.

The results are shown in Fig. 2.7 for the annealing schedule $\Gamma(t) = T(t) = 3/\sqrt{t}$. The time scale τ is normalized as $\tau = tT_c^2$ in SA and $\tau = t\Gamma_c^2$ in QA. The values, T_c and Γ_c , are the points where the correlation functions vanish in Fig. 2.6. Thus both classical and quantum correlation functions vanish at $\tau = 1$. The tendency is clear that QA is better suited for ground-state search in the present system.

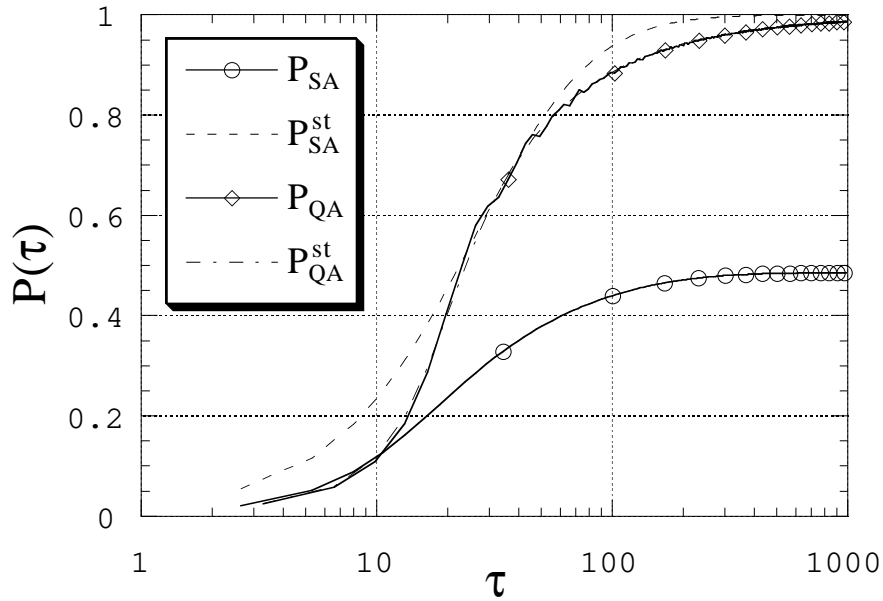


Figure 2.7: Time dependence of the overlaps of the frustrated model under $\Gamma(t) = T(t) = 3/\sqrt{t}$. Here the time scale τ is normalized by Γ_c and T_c (the points where the correlation functions vanish in Fig. 2.6.)

2.2.3 Random Interaction Model

The third and final example is the Sherrington-Kirkpatrick (SK) model of spin glasses [9]. Interactions exist between all pairs of spins and are chosen from a Gaussian distribution with vanishing mean and variance $1/N$ ($N = 8$ in our case). Figure 2.8 shows a typical result on the time evolution of the probabilities under the annealing schedule $\Gamma(t) = T(t) = 3/\sqrt{t}$. We have checked several realizations of exchange interactions under the same distribution function and have found that the results are qualitatively the

same. Figure 2.8 again suggests that QA is better suited than SA for the present optimization problem.

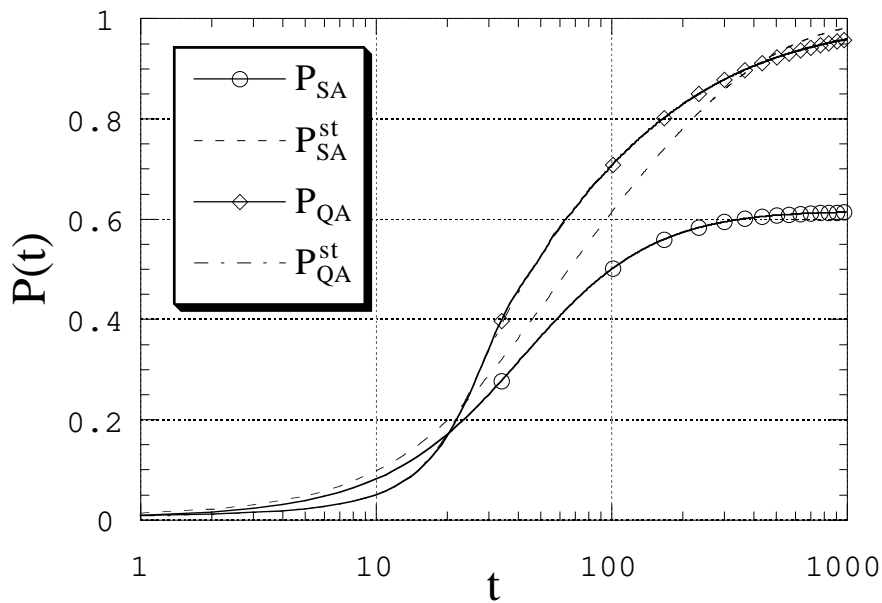


Figure 2.8: Time dependence of the overlaps for the SK model with $\Gamma(t) = T(t) = 3/\sqrt{t}$.

2.3 Solution of the single-spin problem

It is possible to solve the time-dependent Schrödinger equation explicitly when the problem involves only a single spin and the functional form of the transverse field is $\Gamma(t) = -ct, c/t$ or c/\sqrt{t} . We note that the single-spin problem is trivial in SA because there are only two states involved (up and down) and thus there are no local minima. This does not mean that the same single-spin problem is also trivial in the quantum mechanical version. In QA with a single spin, the transition between the two states is caused by a finite transverse field. The system goes through tunneling processes to reach the other state, and an appropriate annealing schedule is essential to reach the ground state. On the other hand, in SA, the transition from the higher state to the lower state takes place even at $T = 0$ and thus the system always reaches the ground state.

Let us first discuss the case of $\Gamma(t) = -ct$ with t changing from $-\infty$ to 0. This is the well-known Landau-Zener model and the explicit solution of the time-dependent Schrödinger equation is available in the literature [33, 34, 35, 36, 37]. With the notation $a(t) = \langle +|\psi(t)\rangle$ and $b(t) = \langle -|\psi(t)\rangle$ and the initial condition $a(-\infty) = b(-\infty) = 1/\sqrt{2}$ (the lowest eigenstate), the solution for $b(t)$ is found to be (see Appendix)

$$b(t) = \frac{he^{-\pi h^2/8c}}{2\sqrt{c}} \left\{ -\frac{2ct+h}{h} D_{-\lambda-1}(-iz) - \frac{ih^2+2c}{\sqrt{2ch}} e^{3/4\pi i} D_{-\lambda-2}(-iz) \right\}, \quad (2.6)$$

where $D_{-\lambda-1}, D_{-\lambda-2}$ represent the parabolic cylinder function (or Weber function) and z and λ are given as

$$z = \sqrt{2c} e^{-\pi i/4} t, \quad (2.7)$$

$$\lambda = \frac{ih^2}{2c}. \quad (2.8)$$

The final value of $b(t)$ at $t = 0$ is

$$b(0) = -\frac{h\sqrt{\pi}2^{-ih^2/4c}e^{-\pi h^2/8c}}{2\sqrt{2c}} \times \left\{ \frac{1}{\Gamma(1+ih^2/4c)} + \frac{\sqrt{c}e^{3/4\pi i}(1+ih^2/2c)}{h\Gamma(3/2+ih^2/4c)} \right\}. \quad (2.9)$$

The probability to find the system in the ground state at $t = 0$ is, when $h^2/c \gg 1$,

$$P_{QA}(0) = |a(0)|^2 = 1 - |b(0)|^2 \sim 1 - \frac{c^2}{16h^4}. \quad (2.10)$$

Thus the probability $P_{QA}(t)$ does not approach 1 for finite c .

We next present the solution for $\Gamma(t) = c/t$ with t changing from 0 to ∞ under the initial condition $a = b = 1/\sqrt{2}$ (see Appendix):

$$b(t) = \frac{1}{\sqrt{2}} e^{iht+ic} F(1+ic, 1+2ic; -2iht), \quad (2.11)$$

where F is the confluent hypergeometric function. The asymptotic form of $b(t)$ as $t \rightarrow \infty$ is

$$b(t) \sim \frac{\sqrt{2}(2h)^{-ic}\Gamma(2ic)}{\Gamma(ic)} \times \{e^{-iht-\pi c/2} + ce^{iht+\pi c/2}(2ht)^{-1}\}. \quad (2.12)$$

The probability to find the system in the target ground state behaves asymptotically as

$$P_{\text{QA}}(t) = |a(t)|^2 \quad (2.13)$$

$$= 1 - |b(t)|^2 \quad (2.14)$$

$$\begin{aligned} &\sim 1 - \frac{\sinh(\pi c)}{\sinh(2\pi c)} \\ &\quad \times \left\{ e^{-\pi c} + \frac{c \cos(2ht)}{ht} + \frac{c^2 e^{\pi c}}{4h^2 t^2} \right\} \end{aligned} \quad (2.15)$$

$$\sim 1 - e^{-2\pi c}, \quad (2.16)$$

the last approximation being valid for $c \gg 1$ after $t \rightarrow \infty$. The system does not reach the ground state as $t \rightarrow \infty$ as long as c is finite. Larger c gives more accurate approach to the ground state, which is reasonable because it takes longer time to reach a given value of $\Gamma(= c/t)$ for larger c , implying slower annealing.

The final example of the solvable model concerns the annealing schedule $\Gamma(t) = c/\sqrt{t}$. The solution for $b(t)$ is derived in Appendix under the initial condition $a = b = 1/\sqrt{2}$ as

$$\begin{aligned} b(t) &= \frac{1}{\sqrt{2}} e^{iht} F\left(\frac{1}{2} - i\gamma, \frac{1}{2}; -2iht\right) \\ &\quad + \frac{c}{\sqrt{h}} e^{(3/4)\pi i} e^{iht} (-2iht)^{1/2} F\left(1 - i\gamma, \frac{3}{2}; -2iht\right), \end{aligned} \quad (2.17)$$

where $\gamma = c^2/2h$. The large- t behavior is found to be

$$\begin{aligned} b(t) &\sim \sqrt{\pi} e^{-\pi c^2/4h} \left[e^{-iht} (2ht)^{-i\gamma} \left\{ \frac{1}{\sqrt{2}\Gamma(\frac{1}{2} - i\gamma)} + \frac{\sqrt{h} e^{(5/4)\pi i}}{c\Gamma(-i\gamma)} \right\} \right. \\ &\quad \left. + e^{iht} (2ht)^{-1/2+i\gamma} \left\{ \frac{e^{-(1/4)\pi i}}{\sqrt{2}\Gamma(i\gamma)} + \frac{c}{2\sqrt{h}\Gamma(\frac{1}{2} + i\gamma)} \right\} \right], \end{aligned} \quad (2.18)$$

and the probability $P_{\text{QA}}(\infty)$ for $c^2/h \gg 1$ is obtained as

$$P_{\text{QA}}(\infty) = 1 - |b(\infty)|^2 \sim 1 - \frac{h^2}{64c^4}. \quad (2.19)$$

This equation indicates that the single-spin system does not reach the ground state under the present annealing schedule $\Gamma(t) = c/\sqrt{t}$ for which the numerical data in the previous section suggested an accurate approach. We therefore conclude that the asymptotic value of $P_{\text{QA}}(t)$ in the previous section may not be exactly equal to 1 for $\Gamma(t) = 3/\sqrt{t}$ although it is very close to 1.

The annealing schedule $\Gamma(t) = c/\sqrt{t}$ has a feature which distinguishes this function from the other ones $-ct$ and c/t . As we saw in the previous discussion, the final asymptotic value of $P_{\text{QA}}(t)$ is not 1 if the initial condition corresponds to the ground state for $\Gamma \rightarrow \infty$, $a = b = 1/\sqrt{2}$. However, as shown in Appendix, by an appropriate choice of the initial condition, it is possible to drive the system to the ground state if $\Gamma(t) = c/\sqrt{t}$. This is not possible for any initial conditions in the case of $\Gamma(t) = -ct$ or c/t .

2.4 Summary

In this chapter we have started the study of quantum annealing (QA) from the transverse Ising model obeying the time-dependent Schrödinger equation. The transverse field term was controlled so that the system approaches the ground state. The numerical results on the probability to find the system in the ground state were compared with the corresponding probability derived from the numerical solution of the master equation representing the SA processes. We have found that QA shows convergence to the optimal (ground) state with larger probability than SA in all cases if the same annealing schedule is used. The system approaches the ground state rather accurately in QA for the annealing schedule $\Gamma = c/\sqrt{t}$ but not for faster decrease of the transverse field.

We have also solved the single-spin model exactly for QA in the cases of $\Gamma(t) = -ct, c/t$ and c/\sqrt{t} . The results showed that the ground state is not reached perfectly for all these annealing schedules. Therefore the asymptotic values of $P_{\text{QA}}(t)$ in numerical calculations are probably not exactly 1 although they seem to be quite close to the optimal value 1.

The rate of approach to the asymptotic value close to 1, $1 - P_{\text{QA}}(t)$,

was found to be proportional to $1/\bar{t}$ in Fig. 2.3 for the ferromagnetic model. On the other hand, the single-spin solution shows the existence of a term proportional to $1/\sqrt{\bar{t}}$, see Eq. (2.18). Probably the coefficient of the $1/\sqrt{\bar{t}}$ -term is very small in the situation of Fig. 2.3 and the next-order contribution dominates in the time region shown in Fig. 2.3.

A simple argument using perturbation theory yields useful information about the asymptotic form of the probability function if we assume that the system follows quasi-static states during dynamical processes. The probability to find the system in the ground state is expressed using the perturbation in terms of $\Gamma(\ll 1)$ as

$$P_{\text{QA}}(\Gamma) \sim 1 - \Gamma^2 \sum_{i \neq 0} \frac{1}{(E_0^{(0)} - E_i^{(0)})^2}, \quad (2.20)$$

where $E_i^{(0)}$ is the energy of the i th state of the non-perturbed (classical) system and $E_0^{(0)}$ is the ground-state energy. If we set $\Gamma = c/\sqrt{\bar{t}}$, we have

$$P_{\text{QA}}(\Gamma) \sim 1 - \frac{1}{\bar{t}} \sum_{i \neq 0} \left(\frac{c}{E_0^{(0)} - E_i^{(0)}} \right)^2. \quad (2.21)$$

Thus the approach to the asymptotic value is proportional to $1/\bar{t}$ as long as the system stays in quasi-static states. The corresponding probability for SA is

$$P_{\text{SA}}(T) \sim \frac{e^{-E_0/T}}{\sum_i e^{-E_i/T}} \sim 1 - \sum_{i \neq 0} e^{-(E_i - E_0)/T}, \quad (2.22)$$

which shows absence of universal ($1/\bar{t}$ -like) dependence on time.

The present method of QA bears some similarity to the approach by the generalized transition probability in which the dynamics is described by the master equation but the transition probability has power-law dependence on the temperature in contrast to the usual exponential form of the Boltzmann factor [23]. This power-law dependence on the temperature allows the system to search for a wider region in the phase space because of larger probabilities of transition to higher-energy states at a given $T(t)$, which may be the reason of faster convergence to the optimal states [23, 26]. The transverse field term

Γ in our QA represents the rate of transition between states which is larger than the transition rate in SA (see (2.5)) at a given small value of the control parameter $\Gamma(t) = T(t)$. This larger transition probability may lead to a more active search in wider regions of the phase space, leading to better convergence similarly to the case of the generalized transition probability.

We have solved the Schrödinger equation and the master equation directly by numerical methods for the purpose of comparison of QA and SA. This method faces difficulties for larger N because the number of states increases exponentially as 2^N . The classical SA solves this problem by exploiting stochastic processes, Monte Carlo simulations, which have the computational complexity growing as a power of N . The corresponding reduction of the computational complexity is lacking in QA, because the Schrödinger equation is not replaced directly by the stochastic processes. While the quantum Monte Carlo is not equivalent to the Schrödinger equation, we will conduct QA in the quantum Monte Carlo framework in the next chapter. Another problem is to devise implementations of QA in other optimization problems such as the traveling salesman problem or the Hamilton problem. The implementation of QA to the traveling salesman problem is explained as an example in Chapter 4.

Chapter 3

Monte Carlo Analysis of Larger Systems

We will apply the Monte Carlo method to QA in this chapter. Two possible ways to solve QA are considered. Comparison between SA and QA by the Monte Carlo method is also performed.

We desire to solve SA and QA by another method, because the calculations of the master equation for SA and the Schrödinger equation for QA become difficult for large-size systems. As shown in the previous chapter, when we search the ground state by SA and QA, the operation of 2^N -dimensional matrices is needed to solve the differential equations in the Ising-spin systems. For example, real and complex 1024×1024 matrixes are needed for SA and QA with ten spins, respectively. To avoid such a difficulty of solving the master equation, the calculation is performed by the Monte Carlo method in the original definition of SA. Solving SA by the master equation is the equivalent to the Monte Carlo method. From the relation of the master equation and the Monte Carlo method in SA, we consider QA by the Monte Carlo method.

Another motivation of considering the Monte Carlo method is the following: In the actual procedure of QA, all the elements of the Hamiltonian matrix are calculated to solve the Schrödinger equation. If the matrix is expressed in the z -representation, the diagonal elements are the classical-term energy of each configuration. This implies that there is no advantage to the enumeration method (to enumerate all the possible configurations), because

we already calculated all the energy of possible configurations. Therefore, we have to solve QA by another method which requires less calculations than to solve the differential equation, like the Monte Carlo method.

We consider the two methods, the path-integral Monte Carlo and the quantum Monte Carlo methods, for QA. The results of the two methods are not the same as the result of the Schrödinger equation, but the ground state can be found by both of the methods. We adopt the quantum Monte Carlo method for QA and compare the results of SA and QA by the Monte Carlo simulation.

3.1 Monte Carlo Method

The Monte Carlo method is powerful to analyze various problems of statistical mechanics. In classical statistical mechanics, we obtain the expectation value of a quantity A as a function of the temperature $T = 1/\beta$ in the following form:

$$\langle A \rangle = \frac{\sum A e^{-\beta E}}{\sum e^{-\beta E}}, \quad (3.1)$$

where the summation runs over all the possible configurations of the system and E corresponds to the energy of each configuration. The number of all possible configurations is S^N , if the system includes N sites and each site takes S states independently. The number of the terms in the summation increases exponentially as a function of the system size N . It is difficult to calculate the whole summation for large-size systems.

We consider replacing the summation with the weighted sampling. Equation (3.1) is rewritten as

$$\langle A \rangle = \sum_i P_i A_i, \quad (3.2)$$

where $P_i = e^{-\beta E_i} / \sum_j e^{-\beta E_j}$. P_i is the Gibbs distribution, the probability of the configuration i . The sampling configurations are generated to obey the Gibbs distribution.

The expression of the expectation values by the weighted sampling is given by

$$\langle A \rangle_{\text{sampling}} = \frac{1}{M} \sum_{i=1}^M A(i), \quad (3.3)$$

where the summation runs over the sampled configurations. In the large M limit, $\langle A \rangle_{\text{sampling}}$ converges to $\langle A \rangle$.

The configuration obeying the Gibbs distribution can be obtained from the Markov chain which comes from the master equation as

$$\frac{d\mathbf{P}(t)}{dt} = \mathcal{L}\mathbf{P}(t), \quad (3.4)$$

where \mathcal{L} is the transition matrix defined in the previous chapter. The matrix element which is the transition probability from i th state to j th state has a non-zero value, when the configurations of i th and j th states differ only by one spin. Therefore, the i th state can be modified to N states. We create a new configuration from the i th state by the following steps: Choose a site randomly and determine the direction of the spin on the site by the transition ratio from the configuration before flip to the configuration after flip. Next, repeat this procedure N times. These N trials of the spin flip are called “one Monte Carlo step”. The Markov chain is obtained from the calculation of this Monte Carlo steps. In principle, every configuration can change to any configuration in one Monte Carlo step, because all spins can flip once. However, the distance between two configurations is close, if one configuration is obtained from the other configuration by one Monte Carlo step. For the precise calculation, the interval of the sampling has to be long enough.

3.2 Quantum Monte Carlo Method

In quantum systems, the definition of the expectation value is not the same as in the classical systems. The expectation value of a quantity A is given by

$$\langle A \rangle = \frac{\text{Tr} A e^{-\beta \mathcal{H}}}{\text{Tr} e^{-\beta \mathcal{H}}}, \quad (3.5)$$

where \mathcal{H} is the Hamiltonian. To calculate the operator $e^{-\beta\mathcal{H}}$ is difficult for large-size systems because of non-diagonal terms of the Hamiltonian \mathcal{H} . The same procedure as in the classical Monte Carlo method can not be applied to quantum systems, if we can not diagonalize the Hamiltonian.

The following procedure avoids the above difficulty. Now we consider the the Ising system with transverse field Γ as a quantum system,

$$\mathcal{H} = - \sum_{ij} J_{ij} \sigma_i^z \sigma_j^z - \Gamma \sum_i \sigma_i^x. \quad (3.6)$$

This Hamiltonian is not diagonal in the z -representation. By the Trotter formula, the operator $e^{-\beta\mathcal{H}}$ can be described as a product of many operators diagonalized in z - or x -representation:

$$e^{-\beta\mathcal{H}} = \lim_{M \rightarrow \infty} (e^{A/M} e^{B/M})^M, \quad (3.7)$$

where $A = \sum_{ij} K_{ij} \sigma_i^z \sigma_j^z$ ($K_{ij} = \beta J_{ij}$) and $B = \gamma \sum_i \sigma_i^x$ ($\gamma = \beta\Gamma$). This decomposition is called the Suzuki-Trotter decomposition [38, 39]. Using this decomposition, we obtain the partition function of the M th decomposition Z_M as

$$\begin{aligned} Z_M &= \text{Tr}(e^{A/M} e^{B/M})^M \\ &= \sum_{\{\sigma_{jk}=\pm 1\}} \langle \{\sigma_{j1}\} | e^{A/M} | \{\sigma'_{j1}\} \rangle \langle \{\sigma'_{j1}\} | e^{B/M} | \{\sigma_{j2}\} \rangle \\ &\quad \times \langle \{\sigma_{j2}\} | e^{A/M} | \{\sigma'_{j2}\} \rangle \langle \{\sigma'_{j2}\} | e^{B/M} | \{\sigma_{j3}\} \rangle \\ &\quad \times \dots \times \langle \{\sigma_{jM}\} | e^{A/M} | \{\sigma'_{jM}\} \rangle \langle \{\sigma'_{jM}\} | e^{B/M} | \{\sigma_{j1}\} \rangle, \end{aligned} \quad (3.8)$$

where $|\{\sigma_{jk}\}\rangle$ is the M th direct product of eigenstates $\{\sigma_j\}$ defined as

$$|\{\sigma_{jk}\}\rangle = |\sigma_{j1}\rangle \otimes |\sigma_{j2}\rangle \otimes \dots \otimes |\sigma_{jM}\rangle. \quad (3.10)$$

From this decomposition, the partition function is expressed as a trace of products of diagonalized matrices. Each part of the product is rewritten as follows:

$$\langle \{\sigma_{jk}\} | e^{A/M} | \{\sigma'_{jk}\} \rangle = \exp \left(\frac{1}{M} \sum_{ij} K_{ij} \sigma_{ik} \sigma_{jk} \right) \prod_j^N \delta(\sigma_{jk}, \sigma'_{jk}). \quad (3.11)$$

$$\langle \{\sigma_{jk}\} | e^{B/M} | \{\sigma_{j,k+1}\} \rangle = a_M^N \exp \left(\gamma_M \sum_{j=1}^N \sigma_{jk} \sigma_{j,k+1} \right), \quad (3.12)$$

where

$$a_M = \left\{ \frac{1}{2} \sinh \left(\frac{2\gamma}{M} \right) \right\}^{1/2}, \quad \gamma_M = \frac{1}{2} \ln \coth \left(\frac{\gamma}{M} \right).$$

The partition function Z is represented as

$$\begin{aligned} Z &= \lim_{M \rightarrow \infty} a_M^{NM} \sum_{\{\sigma_{jk}=\pm 1\}} \\ &\quad \exp \left\{ \sum_{k=1}^M \left(\frac{1}{M} \sum_{ij} K_{ij} \sigma_{ik} \sigma_{jk} + \gamma_M \sum_{j=1}^M \sigma_{jk} \sigma_{j,k+1} \right) \right\} \\ &= \lim_{M \rightarrow \infty} a_M^{NM} \sum_{\{\sigma_{jk}=\pm 1\}} \\ &\quad \exp \left\{ \beta_{\text{eff}} \sum_{k=1}^M \left(\sum_{ij} J_{ij} \sigma_{ik} \sigma_{jk} + \Gamma_M \sum_{j=1}^N \sigma_{jk} \sigma_{j,k+1} \right) \right\} \end{aligned} \quad (3.13)$$

where $\beta_{\text{eff}} = \beta/M$ and $\Gamma_M = \gamma_M/\beta_{\text{eff}}$. This is the partition function of a $(d+1)$ -dimensional classical spin system at the effective inverse temperature β_{eff} . The quantum d -dimensional partition function is mapped to a $(d+1)$ -dimensional classical partition function. The representation of the classical $(d+1)$ -dimension system thus can be obtained by the usual Monte Carlo method (see Fig. 3.1).

The framework does not change, when the longitudinal field is applied. It produces the term $-h \sum_i \sigma_i^z$ in the Hamiltonian. We can deal with this term similarly to the term $-\sum_{ij} J_{ij} \sigma_i^z \sigma_j^z$.

3.3 Path-Integral Monte Carlo

The time development of the wave function in quantum systems is given as

$$|\Psi(T)\rangle = \text{T}e^{-i \int_0^T dt \mathcal{H}(t)} |\Psi(0)\rangle, \quad (3.14)$$

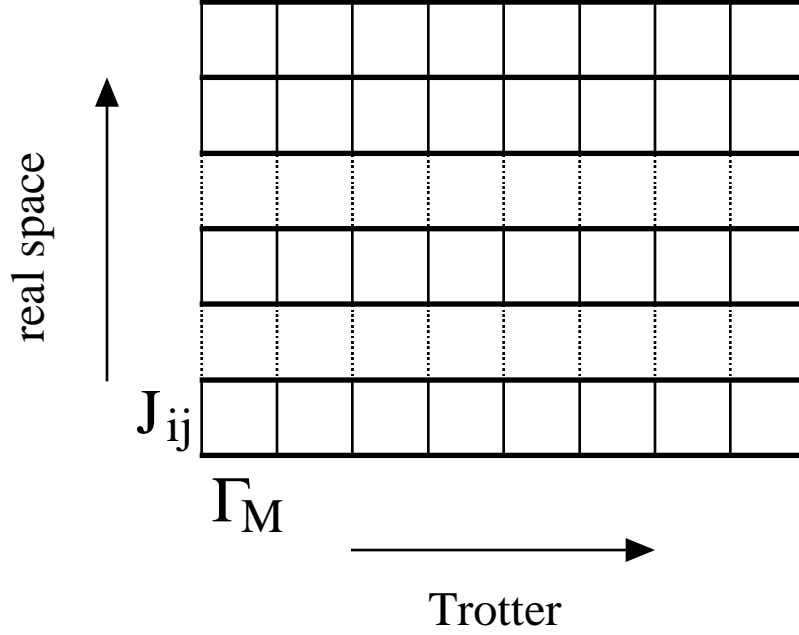


Figure 3.1: The d -dimensional quantum system is mapped to a $(d + 1)$ -dimensional classical system at the inverse temperature β_{eff} . The original d -dimensional space is expressed as the “real space” and the additional space is expressed as the “Trotter”. Copies of the original system without the quantum term are placed in the Trotter direction. The real space interactions J_{ij} are random variables in the real space direction but uniform in the Trotter direction. The interactions between the Trotter slices, Γ_M , are uniform and depend on the amplitude of the transverse field Γ .

where the symbol T means that the operator acts on the ket vectors with time ordering. Decomposing the product of the short time ($\delta t = T/M$) operators, we have

$$|\Psi(T)\rangle = \lim_{M \rightarrow \infty} e^{-i\frac{T\mathcal{H}_{M-1}}{M}} e^{-i\frac{T\mathcal{H}_{M-2}}{M}} \dots e^{-i\frac{T\mathcal{H}_1}{M}} e^{-i\frac{T\mathcal{H}_0}{M}} |\Psi(0)\rangle, \quad (3.15)$$

where $\mathcal{H}_j = \mathcal{H}(Tj/M)$. By replacing the time with the imaginary time ($iT \rightarrow \beta$), we obtain

$$|\Psi(-i\beta)\rangle = \lim_{M \rightarrow \infty} e^{-\frac{\beta\mathcal{H}_{M-1}}{M}} \dots e^{-\frac{\beta\mathcal{H}_0}{M}} |\Psi(0)\rangle. \quad (3.16)$$

The expectation value of A is obtained as,

$$\langle A(T) \rangle = \langle A(-i\beta) \rangle \quad (3.17)$$

$$= \langle \Psi(-i\beta) | A | \Psi(-i\beta) \rangle \quad (3.18)$$

$$= \lim_{M \rightarrow \infty} \langle \Psi(0) | e^{-\beta/M \mathcal{H}_0} \dots e^{-\beta/M \mathcal{H}_{M-1}} A \\ \times e^{-\beta/M \mathcal{H}_{M-1}} \dots e^{-\beta/M \mathcal{H}_0} | \Psi(0) \rangle. \quad (3.19)$$

If the imaginary time β is a real number, this formulation is similar to the quantum Monte Carlo method. Dividing the Hamiltonian into two parts, the terms including σ^z or σ^x , and inserting the complete sets between each product, we can map the equation (3.19) to the weighted sampling of the Monte Carlo simulation. One configuration in the Monte Carlo simulation corresponds to one possible path of the imaginary time dynamics in the original system. The summation of the samplings is the discrete version of the imaginary time path integral. The system simulated in the Monte Carlo is shown in Fig. 3.2. The initial state $|\Psi(0)\rangle$ is located at the right and the left sides. The evolved state $|\Psi(\beta)\rangle$ locates at the center. A path of the sampling is obtained from the snapshot of the thermal equilibrium state of a $(d + 1)$ -dimensional space. The horizontal interaction comes from the transverse field. If the field is scheduled (decreases as a function of time), the interaction changes stronger toward the center. The same systems are located in the horizontal direction. These are similar to the Trotter slices in the quantum Monte Carlo method.

3.4 Applying Monte Carlo Method to Annealing Process

In statistical mechanics, Monte Carlo simulation and the master equation of the classical system give the same result except for statistical errors. The results in the dynamics are also the same. (For the dynamics of the SK model, see [40, 41, 42, 43]) From this equivalence, we regard the Monte Carlo step as the time of the master equation. Figure 3.3 shows the probability to find the ground state of the SK model with $N = 8$ for the master equation and

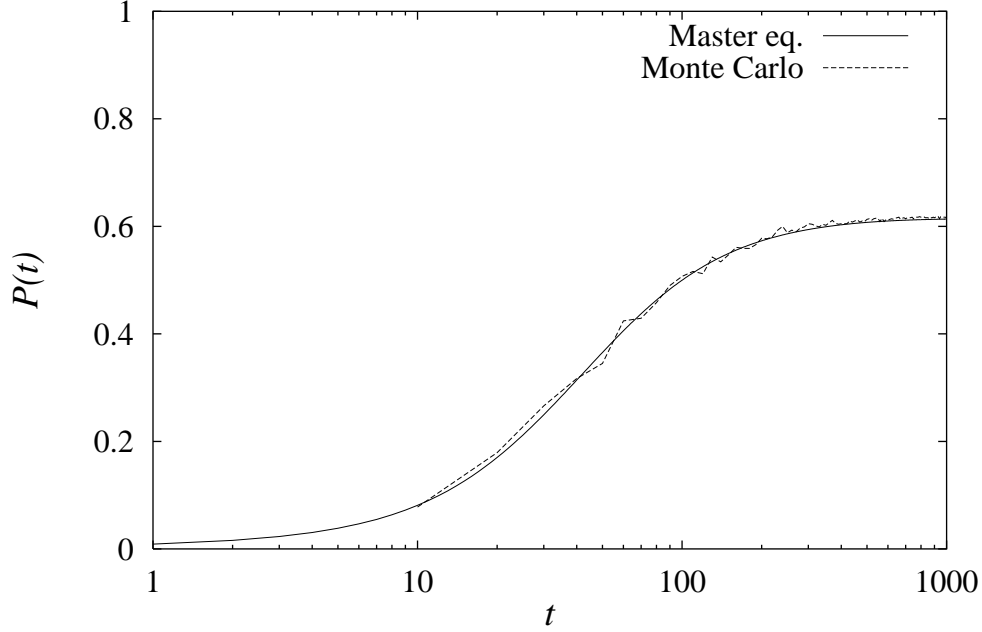


Figure 3.3: The results of the master equation and the Monte Carlo simulation. Two curves show good agreement.

the Monte Carlo simulation. The probability for the Monte Carlo simulation is obtained from the ratio of the number of the ground state configurations for each time in one hundred independent runs. The temperature schedule of both cases is $T = 3/\sqrt{t}$. Two curves show good agreement.

On the other hand, there is no reason that the quantum Monte Carlo simulation is equivalent to the solution of the Schrödinger equation. However, we regard that the Monte Carlo step in the quantum Monte Carlo simulation is also equivalent or similar to the time in the Schrödinger equation. How different between the two results is shown later.

Besides the above approach, the path-integral Monte Carlo also describes the dynamics of the quantum system. The imaginary time path integral of the quantum system and the partition function at the temperature $1/\beta$, where β is the imaginary time, have the same expression. The time developing operator $e^{-\beta\mathcal{H}}$ can be decomposed like the Suzuki-Trotter decomposition in the quantum Monte Carlo method. Therefore, the imaginary time path

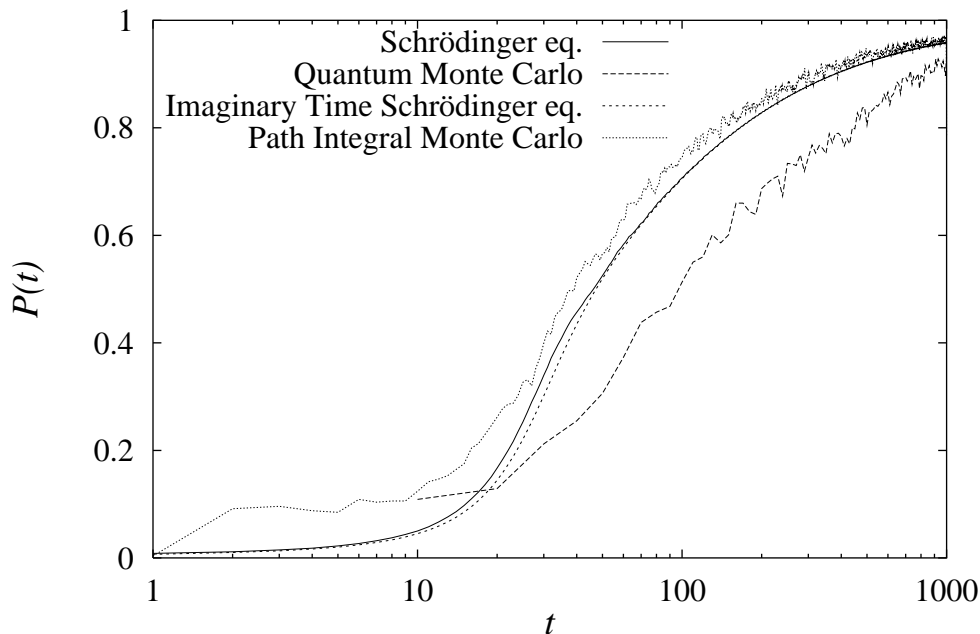


Figure 3.4: The results for the Schrödinger equation, the quantum Monte Carlo method, the imaginary time Schrödinger equation and the path-integral Monte Carlo method. Imaginary time Schrödinger equation means the results of imaginary time dynamics of the Schrödinger equation. The schedule of $\Gamma(t)$ is $3/\sqrt{t}$.

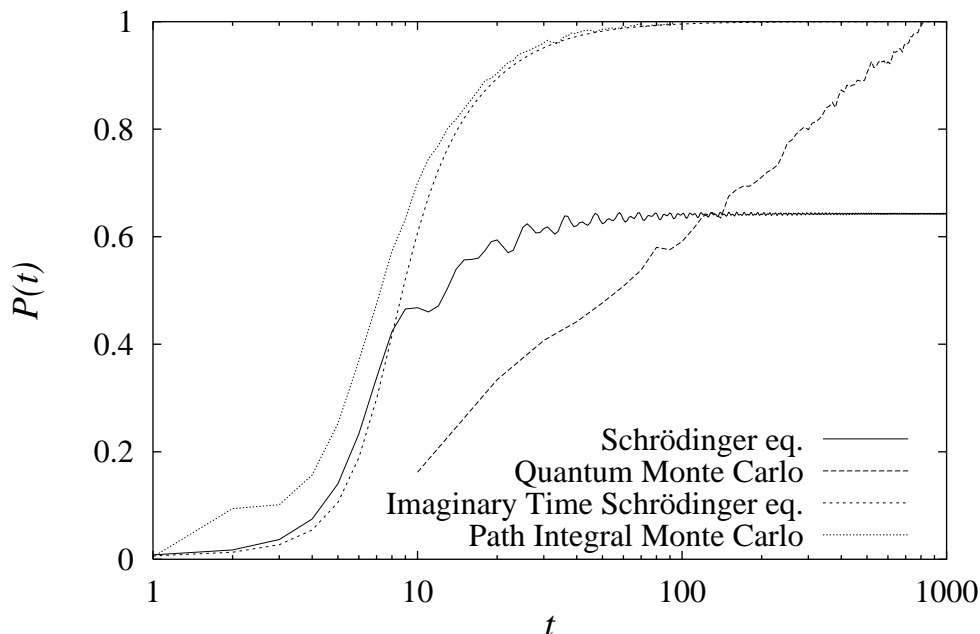


Figure 3.5: The results for the Schrödinger equation, the quantum Monte Carlo method, the imaginary time Schrödinger equation and the path-integral Monte Carlo method. The schedule of $\Gamma(t)$ is $3/t$. Except for the result for the Schrödinger equation, the probabilities converge to one.

integral is evaluated numerically.

In this formulation, the path integral is replaced with the Monte Carlo simulation. However, we have three difficulties about this simulation. The Hamiltonian with the imaginary time $\mathcal{H}(-i\beta j/M)$ is no longer a Hermitian matrix, because the amplitude of the transverse field $\Gamma(t)$ is a function of the time and generally becomes a complex number when β is a real number. We can avoid this difficulty by changing the definition of the time in $\Gamma(t)$ as $t \rightarrow \sqrt{tt^*}$, where t^* is the complex conjugate of t , because $\sqrt{tt^*}$ is a real number for any complex number t . Secondly, the simulation is performed by replacing imaginary numbers with real numbers, so that we have to evaluate $A(T)$ from $A(\beta)$ by the process of analytic continuation. The analytic continuation for the function whose values are given as a numerical number is a great problem itself and needs large computational power like the simulated annealing. Finally, the computational time of the path-integral Monte Carlo method may be longer than the quantum Monte Carlo method. The imaginary time evolution is mapped to the spatial axis, so that we have to wait until the system becomes in equilibrium. We can decrease the transverse field in the quantum Monte Carlo method without care that the system is trapped at a local minimum or not. In the path-integral Monte Carlo, we care about that the system is trapped at a local minimum or not, because the expectation value is obtained from the average of various paths whose distribution obeys the Gibbs distribution of the $(d + 1)$ -dimensional system.

If we accept that the imaginary time expectation value $A(\beta)$ is regarded as a real time one $A(T)$, the final problem is still a difficult problem. It takes long time to wait until the system becomes in equilibrium, if the landscape of the system is complicated.

We compared the above two approaches, the quantum and the path-integral Monte Carlo methods, with the results of the direct solutions of the Schrödinger equation. The system is the SK model with $N = 8$ and the schedule is $\Gamma = 3/\sqrt{t}$. The probability to find the ground state is plotted in Fig. 3.4. The quantum Monte Carlo is performed with $M = 1000$. We wait 5000 Monte Carlo steps for the initial relaxation and take average over

the next 5000 steps in the path-integral Monte Carlo simulation. We put the inverse temperature $\beta = 1000$ for each calculation. The result of the imaginary time dynamics of the Schrödinger equation is also plotted.

In Fig. 3.5, we plot the solution whose schedule is $\Gamma = 3/t$. In this schedule, the solution of the Schrödinger equation does not converge to the ground state with probability one, but the others converge to one. The curve of the path-integral Monte Carlo agrees with the curve of the imaginary time Schrödinger equation.

From these results, we can conclude that the quantum Monte Carlo and the path-integral Monte Carlo simulations are not the same as the Schrödinger equation. We regard that the assumptions of the two Monte Carlo simulations are not correct. The assumptions are the following: For the quantum Monte Carlo simulation, we assume that the Monte Carlo step equals to the real time. For the path-integral Monte Carlo simulation, we assume that the imaginary time dynamics equals to the real time one.

However, the goal is to find the ground state as fast as possible. The two Monte Carlo methods find the ground state configuration with probability one, even if the schedule is too fast to solve for QA by the Schrödinger equation. For this purpose, we can adopt one of the Monte Carlo methods. We consider that the quantum Monte Carlo method has the advantage. The quantum Monte Carlo method is similar to SA, because the control parameter (T for SA and Γ for QA) decreases as a function of the Monte Carlo step. Thus, the longer we perform the simulation, the larger the probability to find the ground state becomes. On the other hand, a long simulation makes the statistical errors small for the path-integral Monte Carlo method, but the probability does not increase. For these reasons hereafter we adopt the quantum Monte Carlo method for QA of the large-size systems.

We compared the probabilities to find the ground state in the Monte Carlo version of SA and QA for the SK model with $N = 51$ and $T = \Gamma = 3/\sqrt{t}$ in Fig. 3.6. In this calculation, we perform 100 independent runs of long-time ($t = 100000$) SA with the sufficiently slow schedule $T = 3/\ln(t + 1)$ and determine the ground state energy beforehand. Using this ground state energy, we can calculate the probability to find the ground state. The

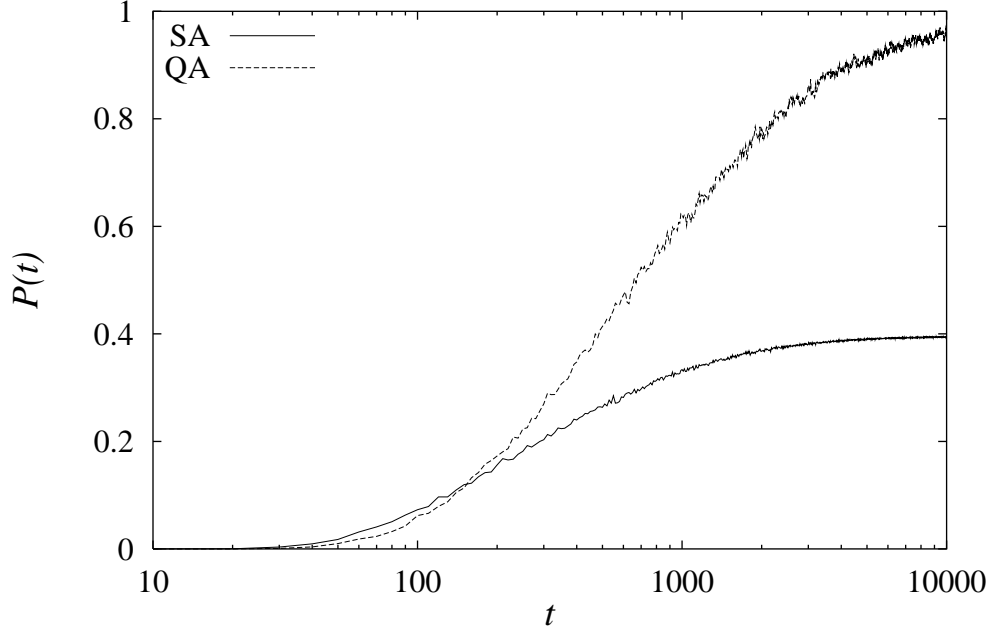


Figure 3.6: Overlaps with the ground state are plotted. The system is the SK model with $N = 51$ and $3/\sqrt{t}$ schedule.

probability to find the ground state is the ratio of the number of the ground state configurations for each time in ten thousand independent runs of SA and Trotter slices of QA. The probability in QA is larger than SA. This result means that the QA in the quantum Monte Carlo method also improves the performance in finding ground state. The quantity $1 - P(t)$ is plotted in Fig. 3.7 under the log-log scale. The curve converges to zero asymptotically as $1/t$. This implies that the system almost follows the stationary state and the annealing schedule is sufficiently slow. Moreover, we apply fast schedule to the same system and the probability converges to one asymptotically as $1/t^2$. In this fast schedule, system also follow the stationary state.

We also plot the average energy of SA and QA under the same condition in Fig. 3.9. As we need the ground state of the classical term of the Hamiltonian, we neglect the contribution of the transverse field term in the calculation of the energy. We take the average energy which does not contain the interactions between the Trotter slices for each snapshot of the Trotter

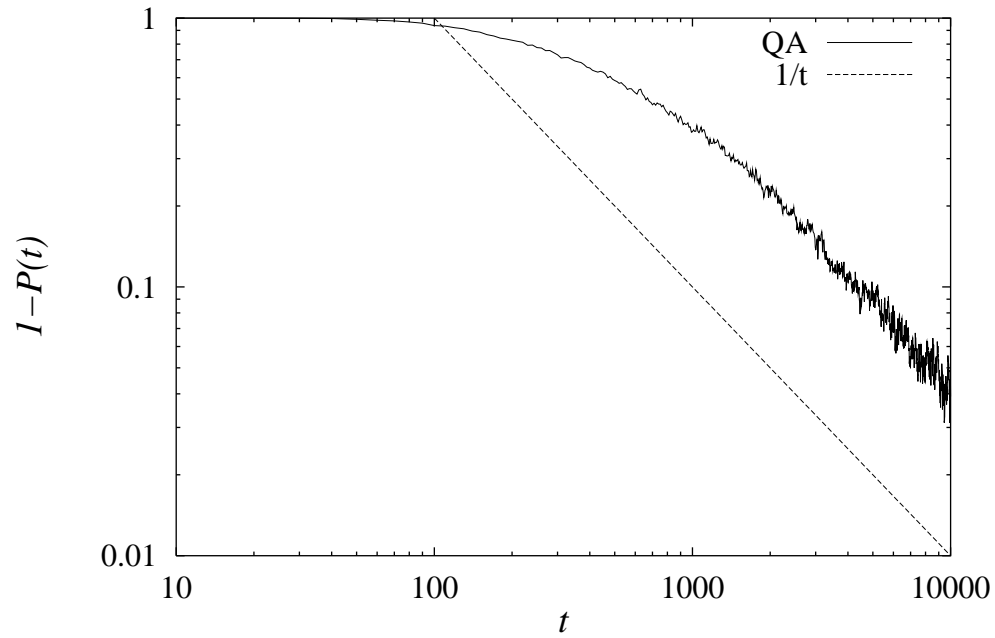


Figure 3.7: The quantity $1 - P(t)$ is plotted. The conditions are the same as in Fig. 3.6.

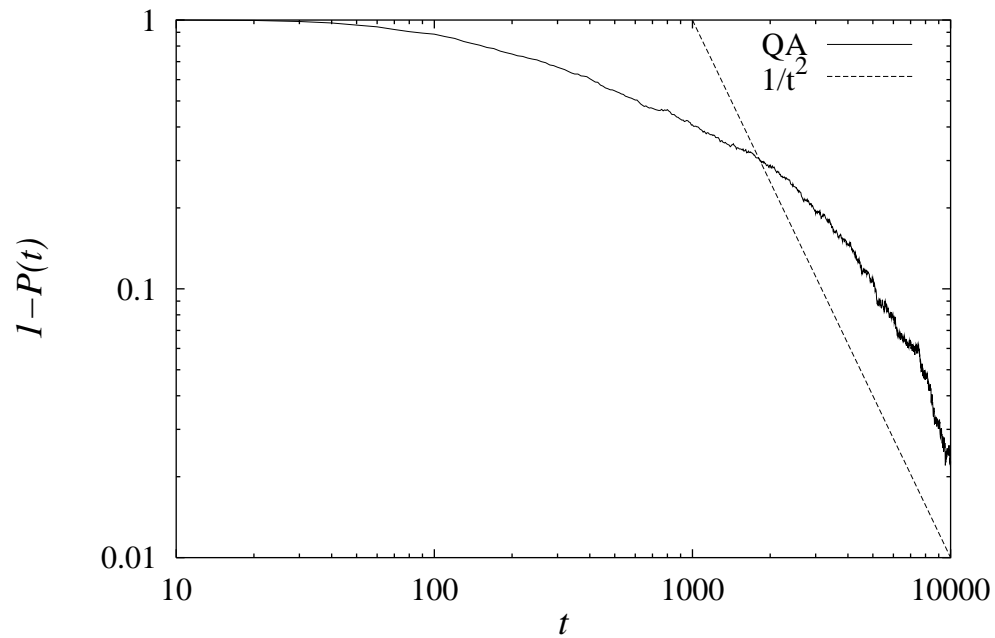


Figure 3.8: The quantity $1 - P(t)$ is plotted. The schedule is $\Gamma = 3/t$.

slices in QA. The average of the energy per spin is calculated by M independent runs for SA and M Trotter slices for QA, respectively. In spite of the large difference between SA and QA in $P(t)$, the energy of QA is lower than SA, but the difference is not so large. This can be understood that if the system is trapped in a local minimum, the trapped system also lowers the average energy but does not count in $P(t)$.

Calculating the probability to find the ground state is a useful index to check which method has a good performance. However it is too difficult to perform this calculation for large-size systems, because the calculation needs the ground state configuration, but we do not know it. In this case, we regard that the method whose average energy is lower has a better performance. If the average energy of QA is lower than SA, QA may find the ground state more efficiently than SA.

On the other hand, another index can be considered. That is the lowest energy in the M independent runs of SA or in M Trotter slices of QA. However, comparing the performance by the average energy gives more precise conclusion than by the lowest energy, because the lowest energy depends on the initial state more than the average energy. If the initial state is in the basin of the ground state, the system goes to the ground state with large probability. We will calculate SA and QA by the Monte Carlo method for the large-size systems up to $N = 10000$ and compare their performance by the average energy.

3.5 Results of the Monte Carlo simulation

Two additional parameters which do not appear in the Schrödinger equation are needed, when the calculation of QA is performed by the quantum Monte Carlo simulation. The first one is the (inverse) temperature $T(= 1/\beta)$, and second one is the Trotter number M . The original dynamics, the Schrödinger equation, does not contain thermal fluctuations, so that we have to take the limit $\beta \rightarrow \infty$. The Trotter number M should also be infinity to take into account the quantum effect correctly.

Each Trotter slice is the classical system with the effective inverse tem-

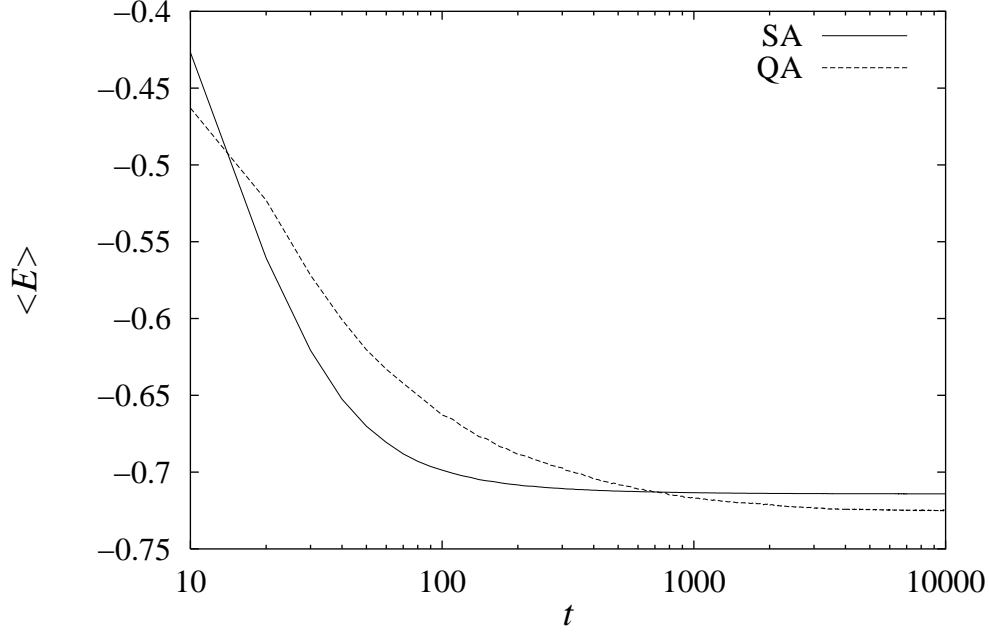


Figure 3.9: The average energy is plotted for SA and QA. The system is the SK model with $N = 51$ and $3/\sqrt{t}$ schedule.

perature $\beta_{\text{eff}} (= \beta/M)$ except for the interactions between Trotter slices. We consider the parameters β_{eff} and M instead of the parameters β and M , because it is natural to regard that we simulate the classical $(d+1)$ -dimensional system at the effective inverse temperature. The infinity limit of the Trotter number also means the infinity limit of the inverse temperature, because the ratio β/M is fixed.

3.5.1 Dependence on the temperature

First, we consider the effective inverse temperature β_{eff} . At the initial time, the strength of the interaction between Trotter slices is small and each slice is almost an independent classical system. At the end, the strength goes to infinity. The M spins in the Trotter direction take the same value because of the interactions of the infinite strength and the freedom of this direction vanishes. The $(d+1)$ -dimensional system which is equivalent to the d -dimensional quantum system reduced to the d -dimensional classical system. This can

be understood naturally, because the transverse field $\Gamma(t)$ vanishes and the Hamiltonian goes to the classical Hamiltonian.

The spins in the Trotter direction take same value when the interactions between the Trotter slices is stronger than the thermal fluctuation. If the temperature is high, we need long time until the interaction becomes large enough. From this, the temperature should be low to save the time for the calculation. On the other hand, the temperature is required to be high enough for searching the configuration space widely at the initial time. If the temperature is low, the system can not visit various configurations and trapped at a local minimum.

To satisfy the above two conflicting conditions, we have to choose moderate values of temperature. The system can seek all possible configurations when the temperature is above the critical temperature of the order-disorder transition of the classical system. Thus, we choose $\beta_{\text{eff}} = 1$ for the SK model.

The dependence of the probability on β_{eff} is shown in Fig. 3.10. The condition is $\beta_{\text{eff}} = 1/2, 1, 2, 5$, $N = 8$ and $M = 1000$ for the SK model in the $3/\sqrt{t}$ schedule. The simulation with $\beta_{\text{eff}} = 1$ has a best performance among the four.

3.5.2 Dependence on the number of Trotter slices

Secondly, we consider the Trotter number M . A simulation with large number of Trotter slices gives precise results, but the computational power for the calculation becomes large. The computational time for the quantum Monte Carlo simulation is M times longer than the conventional simulated annealing. We have to estimate the reasonable Trotter number of the correct simulation.

We check the dependence of the simulation on the Trotter number. The probabilities to find the ground state versus the transverse field are plotted for the cases of $M = 10, 20, 50, 100, 200, 500, 1000$ in Fig. 3.11. The condition is $\Gamma = 2/\sqrt{t}$, $N = 625$ and $\beta_{\text{eff}} = 1$ for the two-dimensional Edward-Anderson model. We find that $M = 100$ is large enough.

From the above two results, we regard that the conditions of $\beta_{\text{eff}} = 1$ and

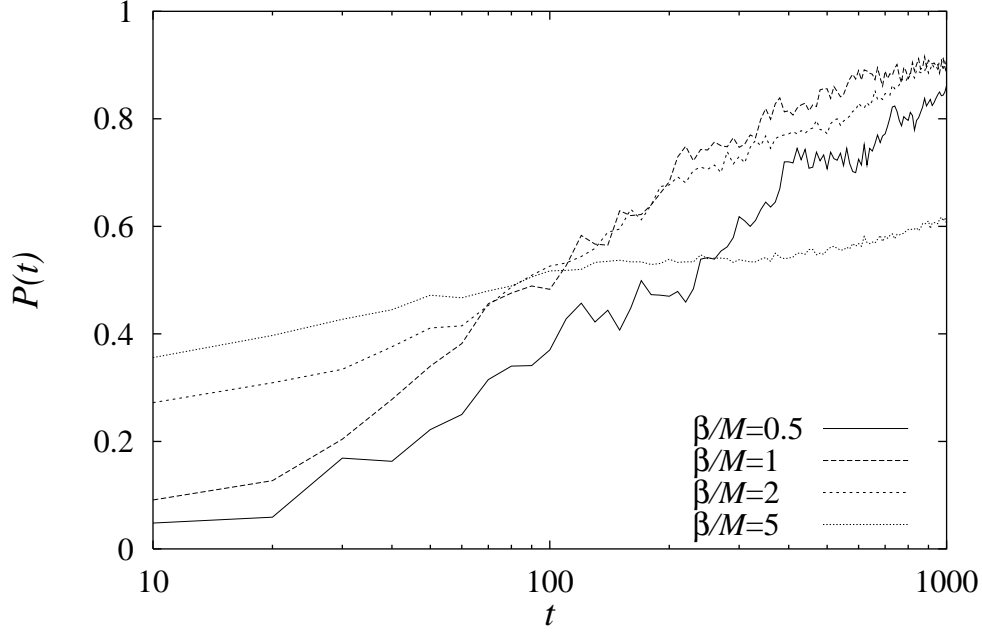


Figure 3.10: The probability dependence on the ratio β/M . The simulation with $\beta_{\text{eff}} = 1$ has a best performance among the four.

$M = 100$ give a reasonable solution. Hereafter we will use this condition.

3.5.3 Results of large size system for the EA model

Next, we consider systems of larger size than the previous calculations to demonstrate that our method can be applied to the actual problems. The model is the two-dimensional Edward-Anderson (EA) model. The calculation per Monte Carlo step for the EA model is less than the SK model. The spin flip is determined by the calculation of the energy gap of the spin flip. We have to sum up $N - 1$ interactions for the SK model, because all spins interact with each other in such an infinite range model. For the two-dimensional EA model on the square lattice the number of the interactions is four. Therefore, we can accelerate the summation in the EA model $(N - 1)/4$ times faster than the SK model. The acceleration affects both of the methods SA and QA.

We choose the standard condition of the calculation of this model as

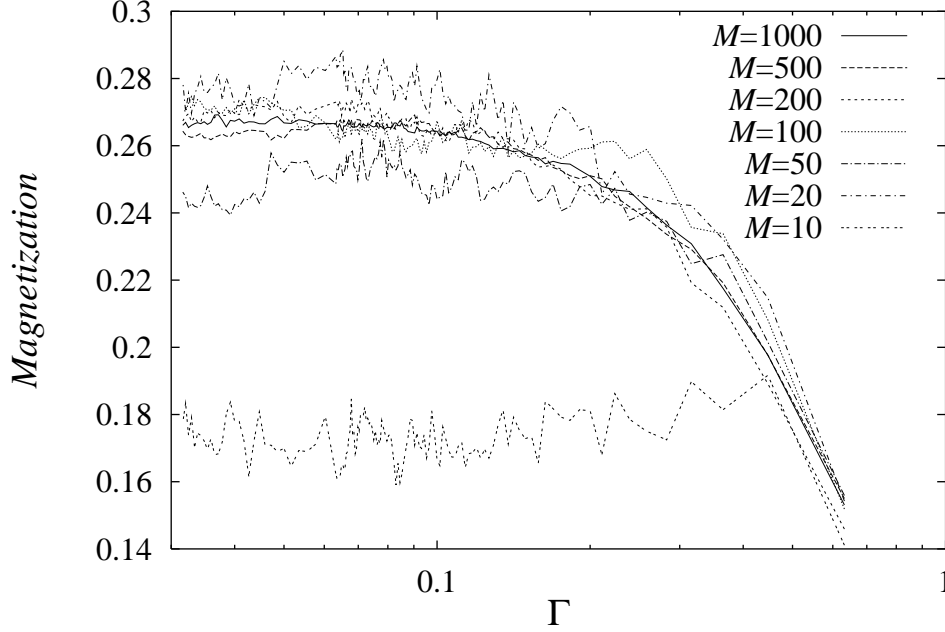


Figure 3.11: The magnetization dependence on the Trotter number M . Curves of over $M = 100$ are large enough.

follows; $N = 625(25^2)$ with periodic boundary conditions, $\beta_{\text{eff}} = 1$, $M = 100$ and the schedule $T = \Gamma = c/\sqrt{t}$. The critical temperature T_c is considered zero in this model. This is not the same value of the SK model. However, the zero temperature dynamics only seeks the configuration whose energy is lower than the present configuration and tends to be trapped at local minima, so that we use the same condition as $\beta_{\text{eff}} = 1$.

We check how the system follows the stationary (equilibrium) state which means equilibrium state at fixed T for SA and ground state at fixed Γ for QA. For small-size systems, we can calculate the probabilities to find the ground state $P_{\text{SA}}(t)$ and $P_{\text{QA}}(t)$ and compare with the probabilities in the stationary state $P_{\text{SA}}^{\text{st}}(T(t))$ and $P_{\text{QA}}^{\text{st}}(\Gamma(t))$. If the two curves, the results of the dynamics and the statics, are the same, the system follows the stationary state. For large-size systems we cannot calculate the probability to find the ground state, because the calculation of the probability needs the ground state configuration beforehand and that is difficult. Nevertheless, we can

check whether the system follows the stationary state or not by another quantity. In our case, a longitudinal magnetic field is applied to the system, and magnetic order grows as a consequence of this field. If the system is in the stationary state, the magnetization is characterized by the temperature for SA or the transverse field for QA and does not depend on the speed of the schedule. The functional form of the schedule is c/\sqrt{t} , thus the speed of our schedule is controlled by c (slow for large c and fast for small c). The system can not follow the stationary state for the rapid schedules, the cases of small c . We check the dependence of magnetization on c .

The magnetization versus the temperature for SA and the transverse field for QA is plotted in Figs. 3.12 and 3.13. For SA, the final value of the magnetization (the left end of the curves) depends on c . This means that the schedule is too fast to follow the stationary state. This result implies that the system tends to be trapped at local minima in this schedule up to $c = 50$. For QA, the final value of the magnetization does not depend on c beyond $c = 10$. Thus, we can regard that the schedule $\Gamma = c/\sqrt{t}$ with $c = 10$ is slow enough to search the ground state of the two-dimensional EA model. The conclusion of these two results for SA and QA is that SA does not follow the stationary state and QA does in the c/\sqrt{t} schedule. This is consistent with small-size analysis by differential equations (the master equation for SA and the Schrödinger equation for QA).

We average out the energy for SA with $M(= 100)$ independent runs and QA with M Trotter slices. The results on the average energy are plotted in Fig. 3.14. Only in the middle region of the time, the energy in QA is higher than in SA, but finally the energy in QA goes lower than in SA.

As shown in the previous chapter, the performance in finding the ground state is improved by the quantum effect. However, the quantum Monte Carlo uses the Suzuki-Trotter decomposition by definition. The calculation of the quantum Monte Carlo needs Trotter-number M times longer than the calculation of the classical system. Therefore, the comparison between SA and QA is still incomplete. The time scales of the two computations are not the same. One Monte Carlo step in QA takes about M times evaluations of spin flips than in SA. (To be precise, the calculation in QA is $M(z + 2)/z$

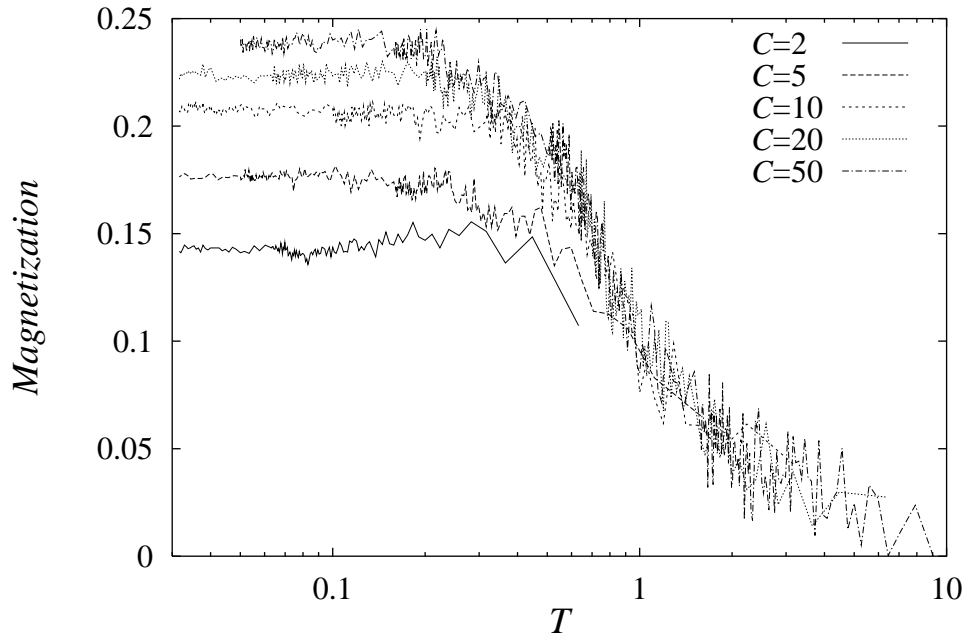


Figure 3.12: The dependence of magnetization on c for the conventional simulated annealing (SA)

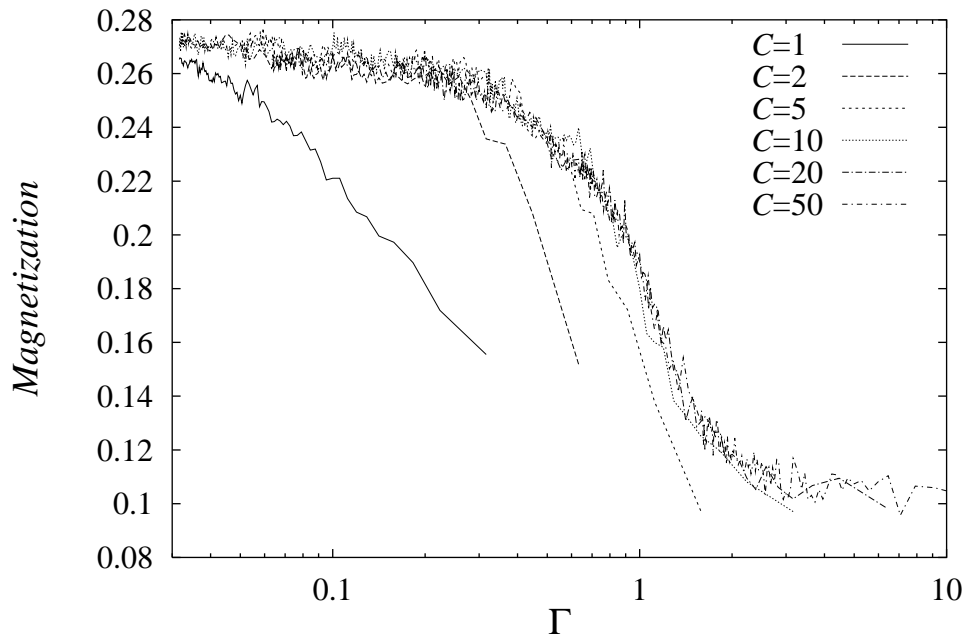


Figure 3.13: The dependence of magnetization on c for quantum annealing (QA)

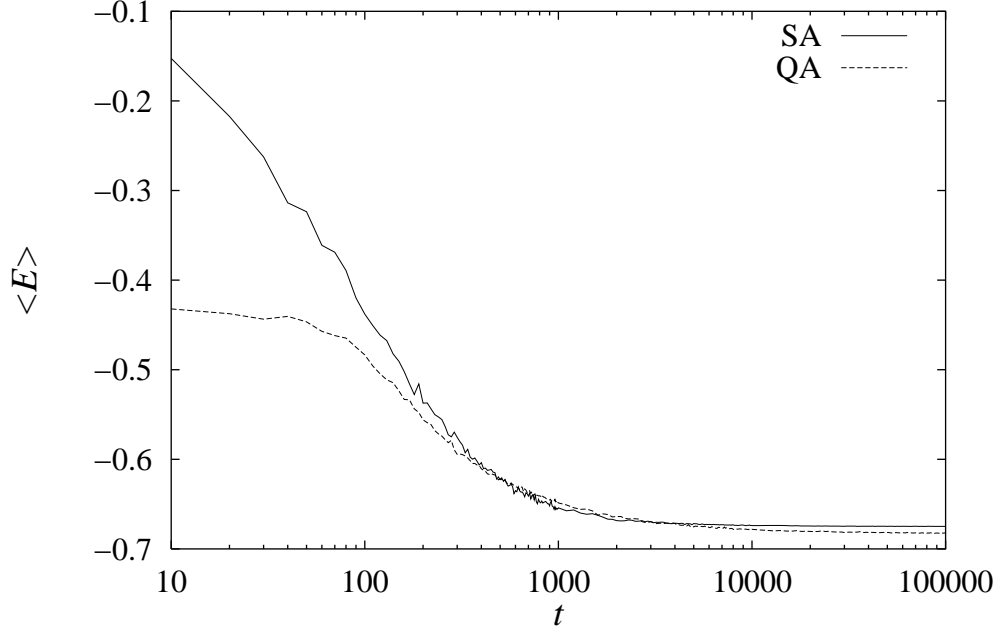


Figure 3.14: Average energy for SA and QA are plotted. The schedule is $T = \Gamma = 10/\sqrt{t}$ and the system size is $N = 625$.

times longer than the calculation in SA, where z is the number of nearest neighbors and “2” is the number of the interactions in the Trotter direction. It is exactly “ M times” for the infinite range model in the thermodynamic limit.) Taking into account this disadvantage gives a reasonable comparison between SA and QA. We provide a reasonable definition of the time t' of which the quantity is plotted and compared as a function as,

$$t' = t \quad (\text{for SA}) \quad t' = Mt \quad (\text{for QA}), \quad (3.20)$$

The Trotter number is 100 in our case, so that the time is $t' = 100t$ for QA.

The average energy for SA and QA is plotted in Fig. 3.15 under the condition of such a scaling of the time. QA improves the performance in finding the ground state. In the calculation, we adopt that the schedule in SA is 100 times slower than QA, because SA could not follow the stationary state in the c/\sqrt{t} schedule (see Fig. 3.12). The total Monte Carlo step of SA is 100 times longer than QA, because we have to use same amount of the computational power to compare the two methods (QA needs 100 times

calculations than SA). The values of the temperature and the transverse field at the end of the simulations are the same. We also plot the cases of various schedules for the temperature and the transverse field in Fig. 3.16 and Fig. 3.17. QA's performance is also good in the various schedules. For another system size, $N = 10000$, the average energy in QA is also lower than SA as seen in Fig. 3.18.

At the end of simulations, we cannot reach the zero temperature or zero transverse field. The values are quite small (~ 0.03) but not equal to zero. For example, the strength of the interaction between the Trotter slices is 1.73, when $\Gamma = 0.1/\sqrt{10}$. It is not so strong compared with the effective inverse temperature $\beta_{\text{eff}} = 1$. The thermal fluctuation still remains. To remove this fluctuation, we execute zero temperature dynamics after the annealing. Then, almost all the Trotter slices (more than 90% for the situation of the calculation for Fig. 3.15) converge to the same configuration in QA, while the independent runs in SA do not.

3.5.4 Difference between the annealing and the quenching processes

Let us take another approach to investigate the property of QA. How efficiently does the annealing process find the ground state in comparison with the quenching process? We calculate the average energy of the two processes, the annealing and the quenching, for SA and QA. The temperature and the transverse field are quenched at $T = \Gamma = 0.1/\sqrt{10} = 0.0316\dots$, and scheduled from infinity to zero by a function $10/\sqrt{t}$. The quenching process of the quantum system is almost equivalent to the case of the work by Sato *et al.* [32] They considered the dynamics of the quenched system with $\Gamma \rightarrow \infty$. The results are shown in Fig. 3.19. The temperature T and the transverse field Γ for annealed and quenched systems are the same at the end of the simulations. If the systems stay in the stationary state, the curves arrive at the same point at the end. The average values of energy of SA, QA and Γ -quenched systems converge to almost the same value, but the T -quenched system is trapped in a high-energy state. Of course the energy of the Γ -quenched system is

higher than that of QA (see Fig. 3.20. It is an enlargement of Fig. 3.19). The behavior of the two quenched systems are quite different, though both of the controlled parameters T and Γ are quenched. The quantum system relaxes faster than the classical system, when the transverse field takes the same value as the temperature of the classical system. This is consistent with the result that QA reaches the stationary state in magnetization, but SA does not when the coefficient c changes from 2 to 50.

3.6 Summary

We applied the Monte Carlo method to QA. There are two ideas to translate the time in the Schrödinger equation to the Monte Carlo method. One is the path-integral Monte Carlo which regards the Trotter direction as the time (more precise, the imaginary time). The other is the quantum Monte Carlo with “the Monte Carlo step”-dependent inter-Trotter interaction. We regard the Monte Carlo step as the time in the Schrödinger equation.

The path-integral Monte Carlo is performed in the imaginary time dynamics. This results in the different behavior from the solution of the Schrödinger equation. For the quantum Monte Carlo, the result also differs from the result of the Schrödinger equation. Two reasons are mentioned. The energy dissipation occurs in the Monte Carlo simulation, while it does not occur in the original Schrödinger equation. Beside this, the time in the path-integral and the quantum Monte Carlo methods are not same as the time in the Schrödinger equation. However, these methods have good performance and the ground state is found, even if the schedule is too fast to find the ground state for the Schrödinger equation.

We adopt the quantum Monte Carlo for large-size QA to reduce the computational time. We have to wait until the system is in equilibrium in the path-integral Monte Carlo and summing up sampling paths. This takes large computational time.

The Trotter number we adopt is $M = 100$, which is large enough for our calculations (two-dimensional EA model with $N = 625$). The results are compared with SA. We found that QA improves a performance in finding the

ground state even if we take into account that the QA need M times more calculations than SA. Moreover, almost all the configurations of the Trotter slices converge to the same configuration.

We also checked the difference between annealed and quenched systems. The relaxation time of the classical quenched system is quite long. On the other hand, the quantum quenched system does not so differ from the annealed system QA. This implies that the quantum effect accelerates relaxations. Moreover, it is remarkable that the average energy of the quantum quenched system is lower than SA. The short relaxation time makes the dependence on the schedule small. This can be seen in Figs. 3.12 and 3.13. A rapid decrease in the characteristic relaxation times for the random Ising magnet, $\text{LiHo}_{0.167}\text{Y}_{0.833}\text{F}_4$, with the transverse field is observed [44]. We consider that the results may come from the same mechanism.

From the application side, the optimal schedule is not known in general. If the dependence of the performance to find the ground state on the annealing speed is small, we can decrease the rate not to reach the ground state or the optimal configuration. This is an attractive property for the actual applications.

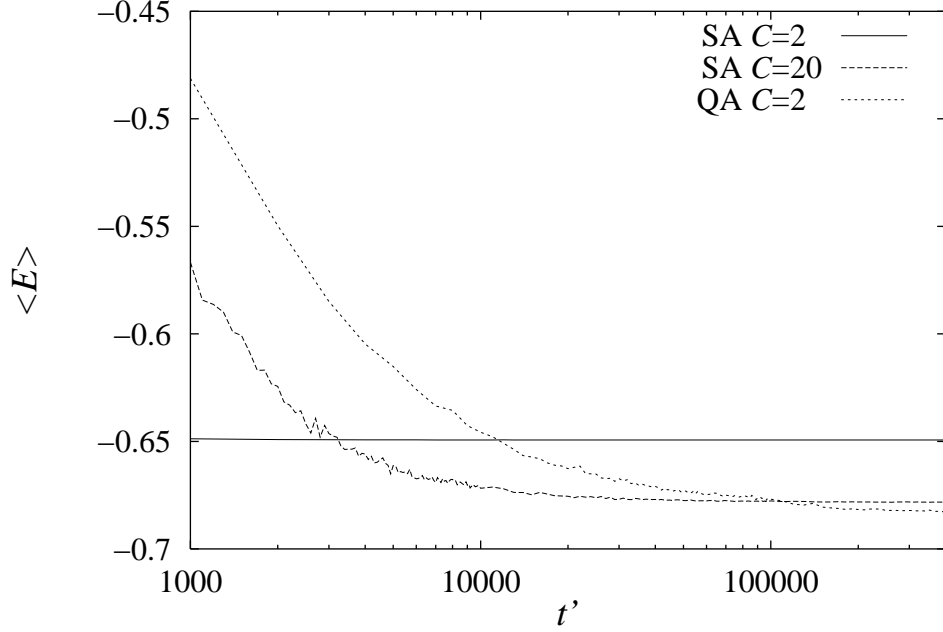


Figure 3.15: Time evolution of the average energy for QA and SA. The system size is $N = 625$. One hundred Trotter slices are averaged for QA and 10 runs are averaged for SA. For “SA $C = 2$ ” and “QA $C = 2$ ” the schedules of the temperature and the transverse field are the same function. “SA $C = 20$ ” and “QA $C = 2$ ” take the same value of the temperature and the transverse field $T = \Gamma = 0.1/\sqrt{10} = 0.0316\dots$ at the end of the simulations.

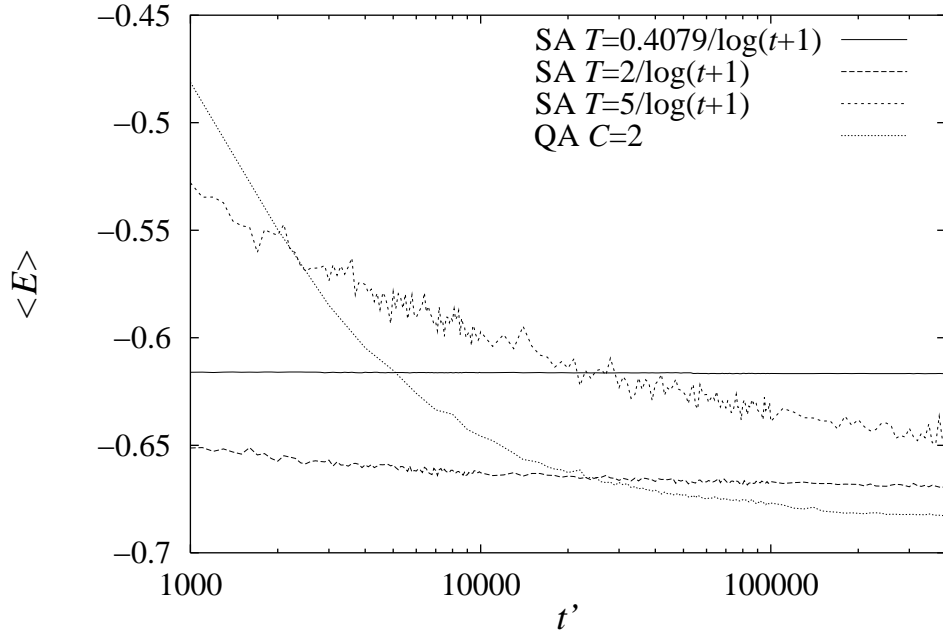


Figure 3.16: Time evolution of the average energy for QA and SA. The system size is $N = 625$. One hundred Trotter slices are averaged for QA and 10 runs are averaged for SA. “SA $T = 0.4079/\log(t+1)$ ” and “QA $C = 2$ ” take the

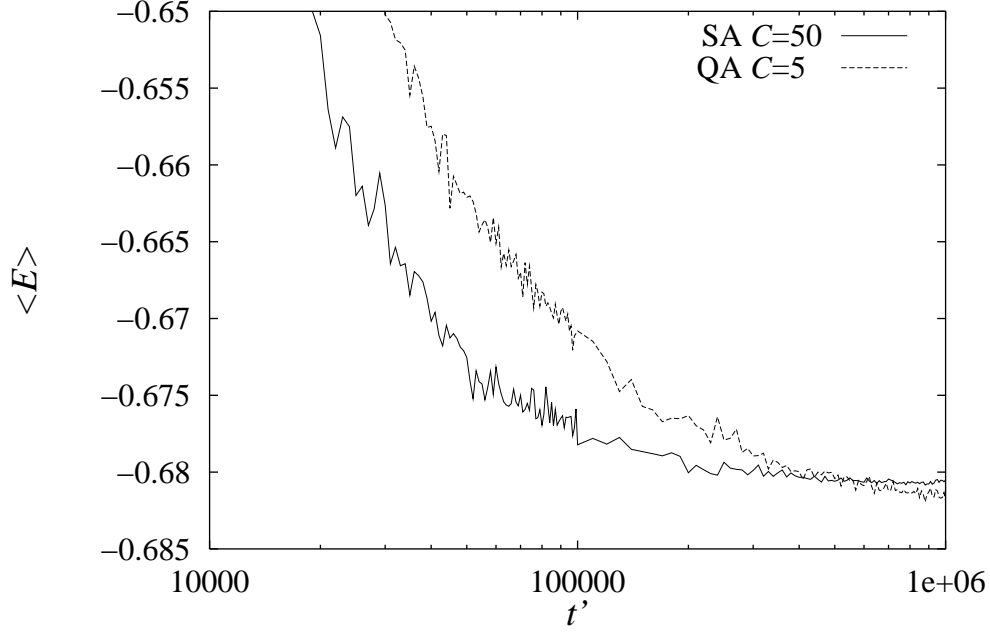


Figure 3.17: Time evolution of the average energy for QA and SA. The system size is $N = 625$ and the schedule is $T = 50/\sqrt{t}$ and $\Gamma = 5/\sqrt{t}$. One hundred Trotter slices are averaged for QA and 10 runs are averaged for SA. The temperature and the transverse field at the end of the simulations are the same value $T = \Gamma = 0.05$.

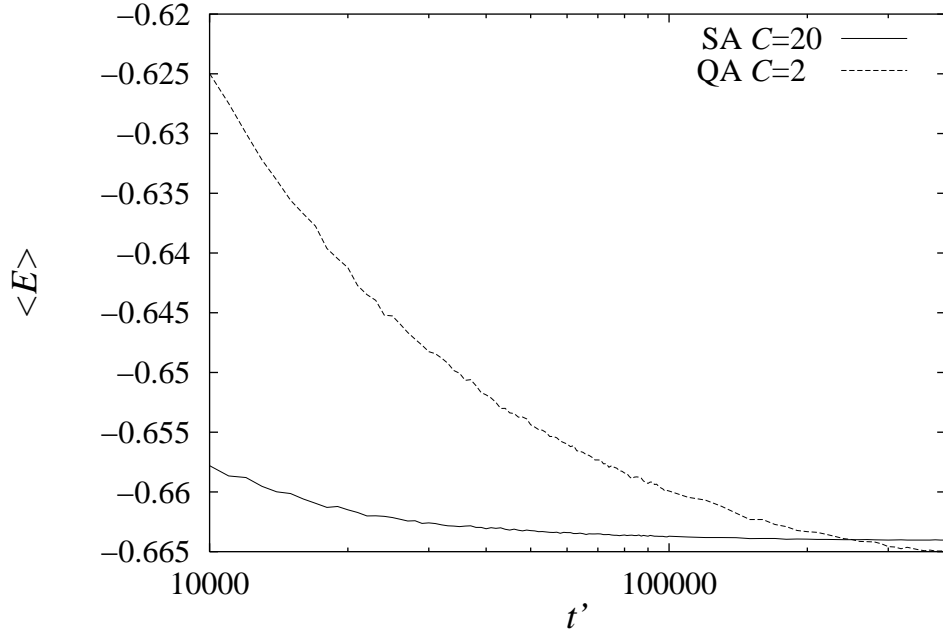


Figure 3.18: Time evolution of the average energy for QA and SA. The system size is $N = 10000$ and the schedule is $T = 20/\sqrt{t}$ and $\Gamma = 2/\sqrt{t}$. One hundred Trotter slices are averaged for QA and 10 runs are averaged for SA. The temperature and the transverse field at the end of the simulations are the same value $T = \Gamma = 0.1/\sqrt{10} = 0.0316$.

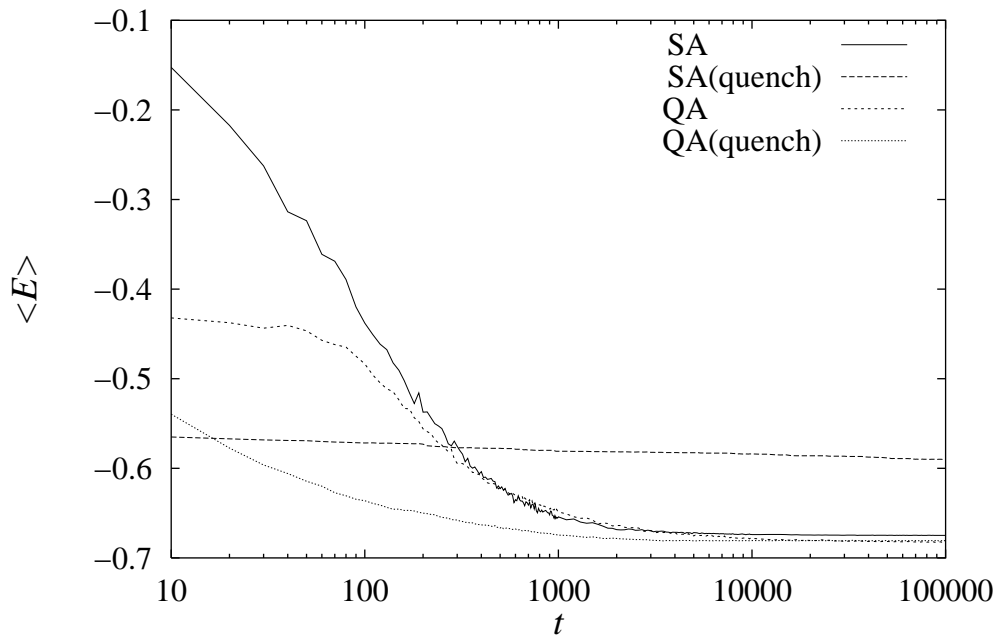


Figure 3.19: Solutions for annealing and quenching processes are plotted. The annealing schedule is $T = \Gamma = 10/\sqrt{t}$ and the quenched value is $T = \Gamma = 0.1/\sqrt{10} = 0.0316\dots$ which is the final value of the schedule.

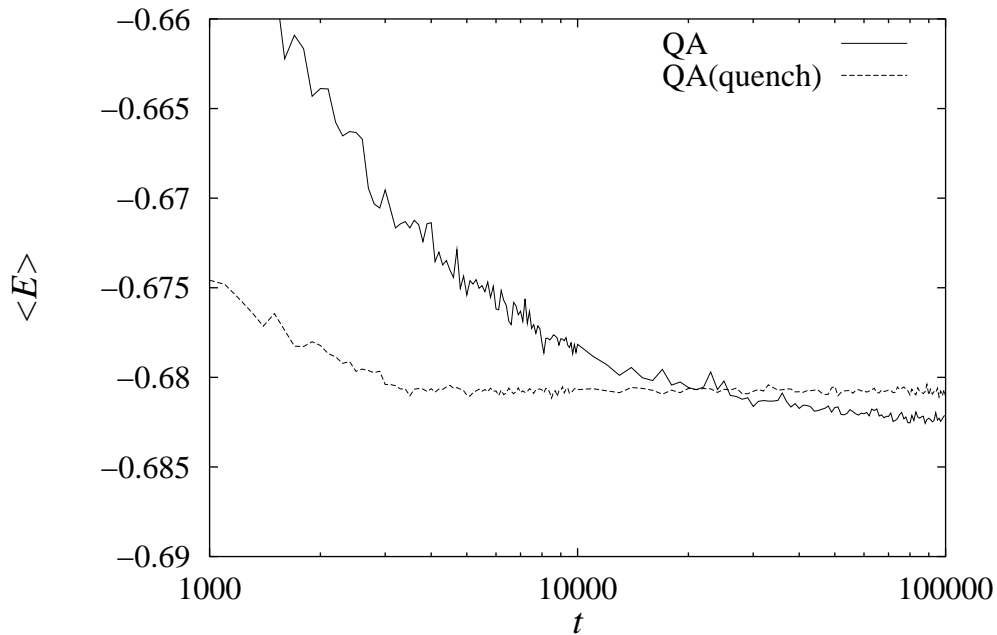


Figure 3.20: Solutions for annealing and quench process for QA are plotted. This is the enlargement of Fig. 3.19.

Chapter 4

Application to the Traveling Salesman Problem

All the problems we calculated up to the previous chapter were on the Ising-spin systems. However, the combinatorial optimization problem is not limited to the problems based on physics. One of the major problems is the traveling salesman problem (TSP) [1, 2]. We will apply our method to the TSP in this chapter. The TSP is a hard problem to solve by a computer, say an *NP*-hard problem. Therefore, comparison between SA and QA in the TSP may provide a good measure of their performances in the problems of other areas not limited to physics. In other words, we will check generality of QA for combinatorial problems.

4.1 The Traveling Salesman Problem

We have N points or cities in a space with distances d_{ij} between them. The task is to find the minimum-length closed tour that visits each city once and returns to its starting point. Figure 4.1 shows an example. Practical applications include scheduling of truck deliveries, airline crews, and the movements of an automatic drill-press or robot arm. In many applications the “distances” d_{ij} are abstract quantities not related to a Euclidean distance between points in a real space; they may not even satisfy the triangle inequality $d_{ij} \leq d_{ik} + d_{kj}$. For the example of truck deliveries, the cost to transport freight from city i to j is affected by many factors, amount of the

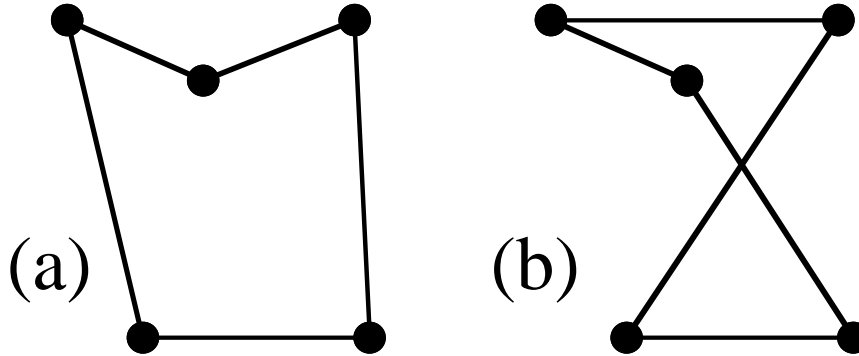


Figure 4.1: The traveling salesman problem, showing a good (a) and a bad (b) solution to the same problem.

freight to city j , labor, gas, highway charge, the weather, etc. The length of the tour is defined by

$$L = \sum_{m=1}^N d_{i(m),i(m+1)}, \quad (4.1)$$

where $i(m)$ means the city of the m th stop, the tour is closed as $i(N+1) = i(1)$ and N is the number of cities.

One can think of a simple approach, listing all possible tours of the problem to search the optimal tour. The number of all the possible tours is $(N-1)!/2$. This number increases rapidly and becomes over the limit of the computer power. Thus, a faster algorithm is needed to solve the actual problems. Some algorithms are optimized for TSP [1, 2] and others are general algorithms which can be applied to TSP [21]. The simulated annealing and the quantum annealing belong to the latter.

4.2 Simulated Annealing on TSP

The simulated annealing is based on the Monte Carlo simulation, so that we have to determine the dynamics, how to rearrange of the tour. We choose the simplest rearrangement of the tour like one-spin flip in the Ising-spin system. That is to exchange two stops of cities i and j , which is illustrated in Fig. 4.2.

This rearrangement of the tour is realized in the following way: (1) Choose two cities i and j . (2) Exchange stops of cities i and j with the probability

$$\omega_{A \rightarrow B} = \frac{\exp(-\beta L_B)}{\exp(-\beta L_A) + \exp(-\beta L_B)}, \quad (4.2)$$

where A is the route before exchange and B is the route after exchange.

One Monte Carlo step consists of $N(N-1)/2$ exchange trials of all pairs. We fix the starting point and reduce the trials to $(N-1)(N-2)/2$, because the tour is closed. The reversibility of the tour still remains in our calculation. The temperature T is scheduled in a form c/\sqrt{t} , where t is the Monte Carlo step.

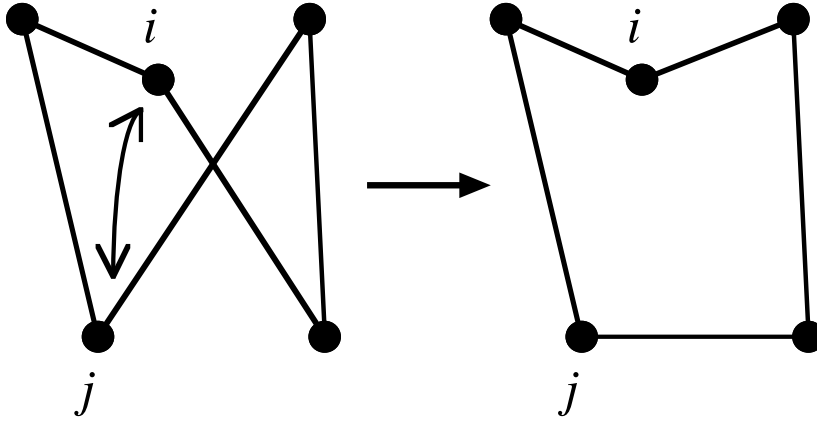


Figure 4.2: The simplest rearrangement of the tour. This rearrangement is expressed in four spin-flip dynamics.

4.3 Quantum Annealing on TSP

We have to introduce a quantum fluctuation to the TSP, but that is not trivial. The system is not the physical system. We cannot easily imagine how to introduce a quantum fluctuation. A straightforward way is that we express TSP as a binary system namely, the Ising system, so that we can introduce the quantum effect. The idea to express TSP as a binary system was proposed by Hopfield and Tank [45, 46].

We choose stochastic binary units n_{ia} to represent possible solutions: $n_{ia} = 1$ if and only if city i is the a th stop on the tour and $n_{ia} = 0$ for otherwise. There are N^2 units altogether. The spin representation can be obtained by the transformation $n_{ia} \rightarrow (\sigma_{ia} + 1)/2$. The total length of the tour is

$$L = \frac{1}{2} \sum_{ij,a} d_{ij} n_{ia} (n_{j,a+1} + n_{j,a-1}) \quad (4.3)$$

$$= \frac{1}{8} \sum_{ij,a} d_{ij} \sigma_{ia} (\sigma_{j,a+1} + \sigma_{j,a-1}) + \text{const.} , \quad (4.4)$$

and there are two constraints:

$$\sum_a n_{ia} = 1 \quad (\text{for every city } i), \quad (4.5)$$

$$\sum_i n_{ia} = 1 \quad (\text{for every stop } a). \quad (4.6)$$

The first constraint says that each city appears only once on the tour, while the second says that each stop on the tour is at just one city. The tour is expressed as a configuration of $N \times N$ units as illustrated in Fig. 4.3

The simplest rearrangement of the route of the traveling salesman is exchanging the stop of cities i and j . In the spin expression, four spins are flipped at a time. The salesman stops at cities i and j for the a th and the b th stops respectively. On-route spins take $\sigma_{ia} = \sigma_{jb} = 1$, and off-route spins take $\sigma_{ib} = \sigma_{ja} = -1$. One up spin and one down spin in the same row are flipped at a time, so that the summation which runs in the horizontal direction does not change. In the vertical direction, the same situation occurs. The constraints (4.5) and (4.6) are kept in the four-spin flip. The Monte Carlo simulation in the spin expression is performed by this procedure.

We fix $\sigma_{11} = 1$ which means that the tour starts from city 1. Possible exchanges with any two stops of cities are the combination number of choosing two from $N - 1$ as $(N - 1)(N - 2)/2$. One Monte Carlo step must contain $(N - 1)(N - 2)/2$ spin-flip trials. This number of trials is suitable that the system has N^2 spins and $\mathcal{O}(N^2)$ trials are performed in one Monte Carlo step like the usual one-spin flip procedure.

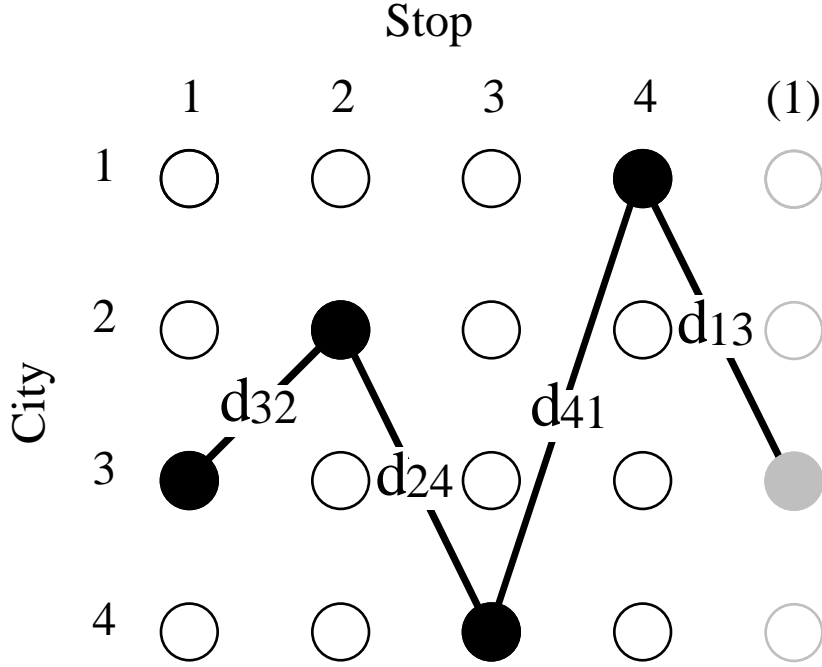


Figure 4.3: The illustrated tour is $3 \rightarrow 2 \rightarrow 4 \rightarrow 1$ with $N = 4$ TSP. Solid and open circles denote units that are “1” and “0” respectively. The condition is open boundary.

Let us consider to introduce quantum effects to the classical system. The dynamics of SA was described by one spin-flip procedure in the preceding chapters, and we chose the quantum effect which flips one spin at a time. That is the transverse field term, $-\Gamma \sum_i \sigma_i^x$. The linear combination of the off-diagonal operator σ_i^x has a non-zero value, when a bra state differ from a ket state only by one spin. If the two spin-flip dynamics is applied to SA, we have to choose the square term of σ_i^x as $-\Gamma \sum_{ij} \sigma_i^x \sigma_j^x$. As known in the Suzuki-Trotter decomposition of the XY or Heisenberg models, the two-spin interaction is mapped to the four-spin interaction in the classical Ising model of the $(d + 1)$ -dimensional system [47].

On the other hand, the traveling salesman problem mapped to the Ising system has to flip four spins at a time. The quantum fluctuation term should be the four-spin interaction term as $-\Gamma \sum_{ijkl} \sigma_i^x \sigma_j^x \sigma_k^x \sigma_l^x$. We have an eight-spin interaction term by the Suzuki-Trotter decomposition of the Hamilto-

nian with this term. Figure 4.4 shows the interactions in a decomposed classical system of one-, two- and four-spin interactions of the quantum system. Spins which contact through the gray domain in the figure interact with each other. The computational cost is expected to increase when the number of spins which interact each other increases. Moreover, various types of spin-flip dynamics have to be introduced to recover ergodicity for such a system.

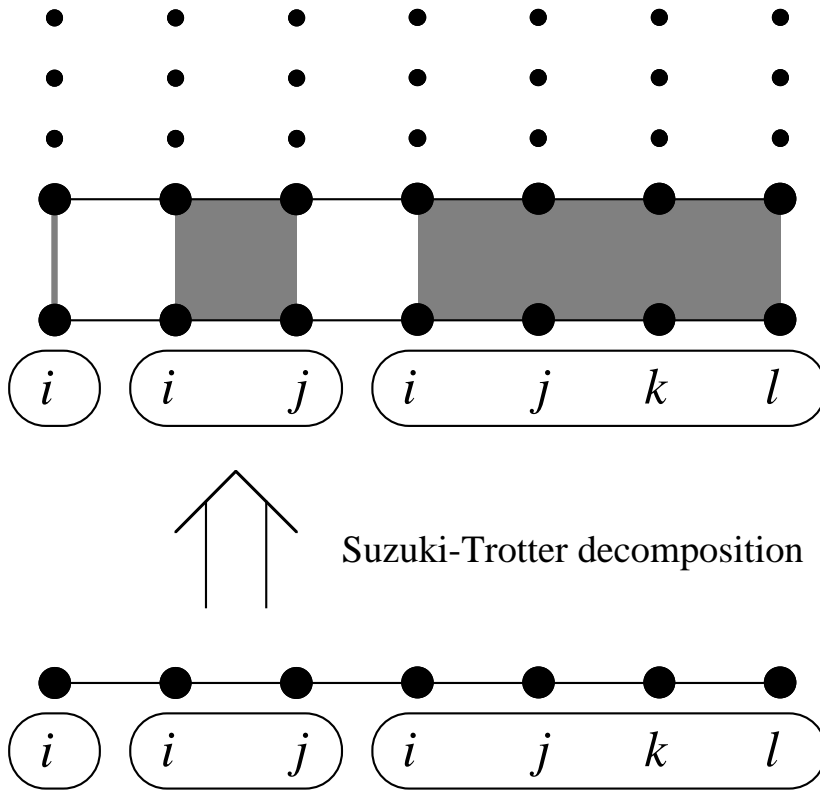


Figure 4.4: By the Suzuki-Trotter decomposition one-, two- and four-spin interactions transform to interactions which contain spins twice as many — two, four and eight spins.

To avoid such difficulties, we adopt the same quantum fluctuation we used before as $-\Gamma \sum_i \sigma_i^x$. The same approach as in the previous chapter can be applied. The system is mapped to a $(d + 1)$ -dimensional system by the Suzuki-Trotter decomposition. However, the spin-flip procedure of QA for

TSP differs from the procedure of QA in the previous chapter. The four spins in a Trotter slice are flipped at a time to keep the constraints, though one spin was flipped so far. The spins are flipped by obeying the transition probability which is obtained from the energy gap between the states before flip and after flip. We computed the energy gap from the classical energy term of the Hamiltonian (the tour length) and the interactions between the Trotter slices for the four spins. That is shown in Fig. 4.5. We can perform QA for the traveling salesman problem in this procedure.

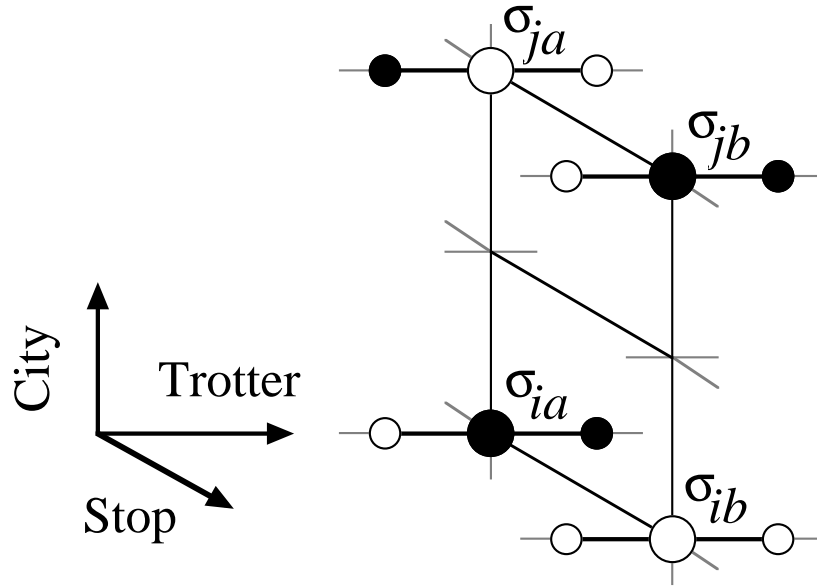


Figure 4.5: The four spins (big circles) are flipped at a time. The transition probability is computed from the length of the tour and the two-spin interactions of the nearest neighbors in the Trotter directions. (the interactions between big and small circles)

4.4 Results of Monte Carlo Simulations

We perform SA and QA for the four cases of TSP whose optimal tours are shown in Fig. 4.6. The first problem “random” is the case in which the cities are located at random. Cities are located at random but clumped with dense

and spares regions for the second problem “semi-random”. The optimal route of the third problem has an “H” shape. (we call this problem “H-character” hereafter.) The fourth problem is “ulysses16” of TSPLIB [48]. The number of cities is $N = 16$ for all the problems.

The cities are located on a square with the side length \sqrt{N} to make the length of the tour extensive for “random”, “semi-random” and “H-character”. For “ulysses16”, we re-scale d_{ij} and set the average to 2.2. The average, the dispersion and the ratio of the dispersion and the average are shown in Table 4.1.

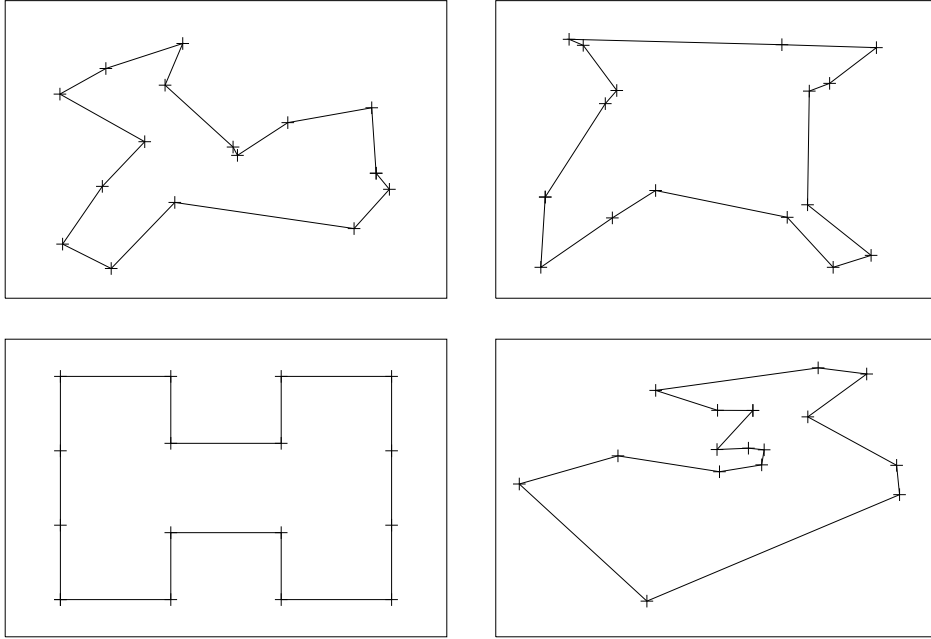


Figure 4.6: Optimal tours of the four problems.

Simulations are performed with 500 Trotter slices for QA and 100 independent runs for SA. We observe two quantities, the probability to find the minimum-length $P(t)$ and the average of length $\langle L \rangle$. The probability $P(t)$ is obtained from the ratio of the number of the ground state configurations for each time in 100 independent runs for SA and 500 Trotter slice for QA. The probabilities of SA and QA for the four problems with the $10/\sqrt{t}$ scheduling are plotted in Fig. 4.7 and the energy values are in Fig. 4.8. The plots are

	random	semi-random	H-character	ulysses16
average (a)	2.195	2.642	2.155	2.200
dispersion (b)	0.973	1.152	0.867	1.556
b/a	0.443	0.436	0.402	0.707

Table 4.1: The average, the dispersion and the ratio of the dispersion and the average for the four problems.

located in the same order as Fig. 4.6. In this schedule, QA has a better performance than SA for all the four problems. Moreover, we also calculated for the case of $5/\sqrt{t}$ and $2/\sqrt{t}$ schedules (see Fig. 4.9–4.12). Results show that QA is better than SA in both of the average length and the probability for all problems. The probabilities of SA for the “H-character” problem are obviously saturated and fall short of probability one, and the probability of QA almost reaches one. This is similar to the situation in the differential equations for small-size systems for SA and QA.

Next, we investigate the asymptotic property of finding the optimal state. The quantity $1 - P(t)$ is plotted in Fig. 4.13 under the log-log scale. The curve is proportional to $1/t$ in the asymptotic region. This implies that the system almost follows the stationary state and the annealing schedule is sufficiently slow. The reason is discussed in Sec. 2.4.

Lastly, we compare the annealed and quenched systems of SA and QA to make the effect of the annealing clear. Annealing is introduced to avoid slow relaxation in low or zero temperature in the system whose landscape is complicated. If the annealing works, the length for the annealed system is lower than the quenched system. The quenching parameter is the temperature T for SA and the transverse field Γ for QA. These values are quenched to $0.1/\sqrt{10} = 0.0316\dots$. In the annealed system, the temperature and the transverse field decrease from infinity to the same value as in the quenched system. We calculate for the two problems, “random” and “ulysses16”. The results of the probability and the average energy are shown in Fig. 4.14 and 4.15. We can list the four system in the order of the performance to find the ground state: (1) the quantum system with annealing “QA”, (2)

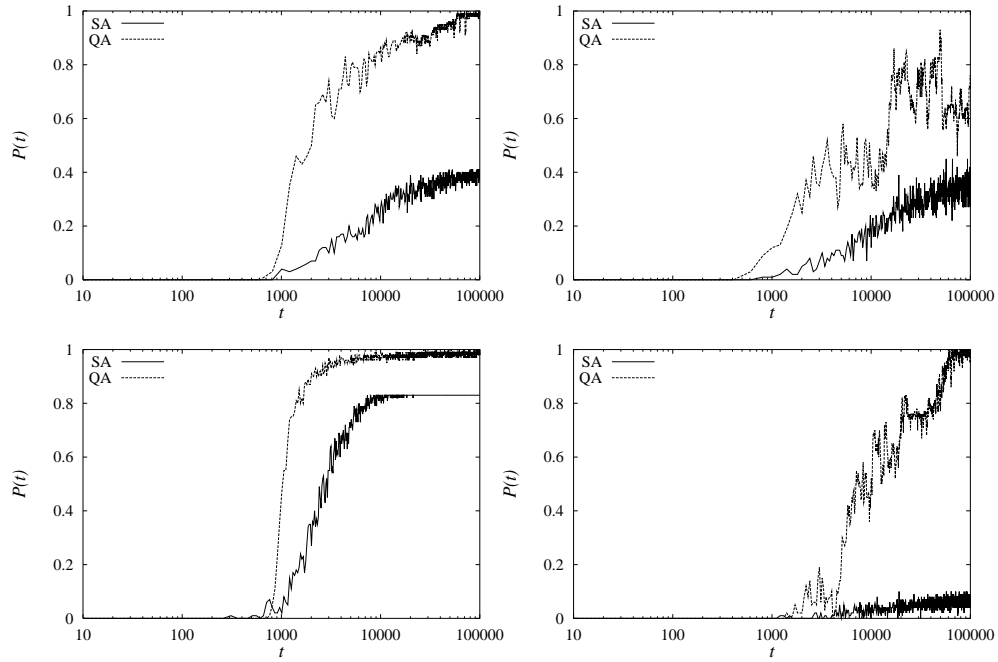


Figure 4.7: Probability to find the minimum-length. The scheduling is $10/\sqrt{t}$.

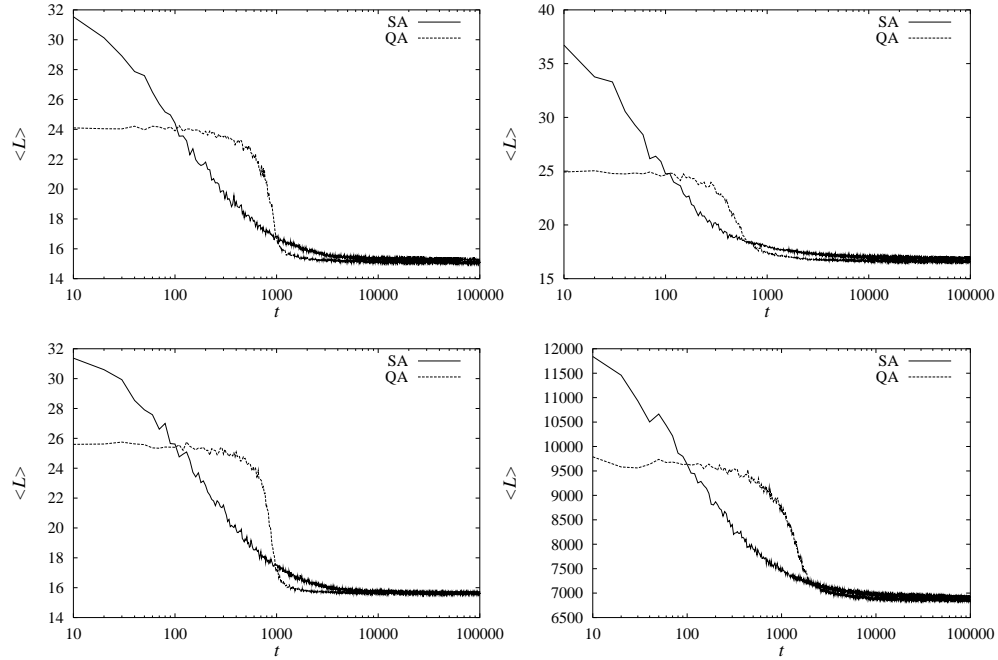


Figure 4.8: Average of the length. The scheduling is $10/\sqrt{t}$.

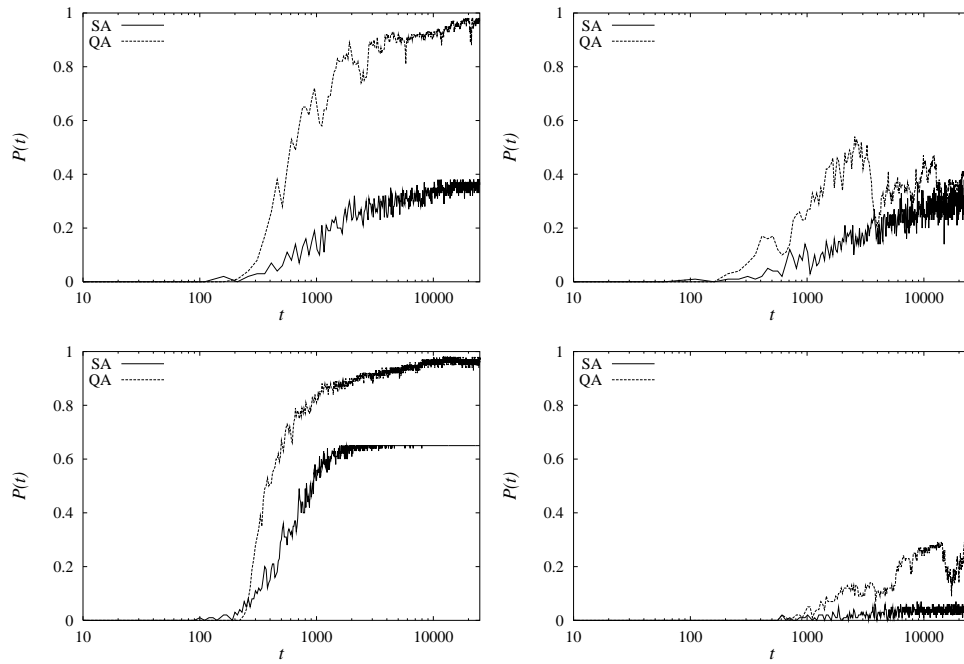


Figure 4.9: Probability to find the minimum-length. The scheduling is $5/\sqrt{t}$.

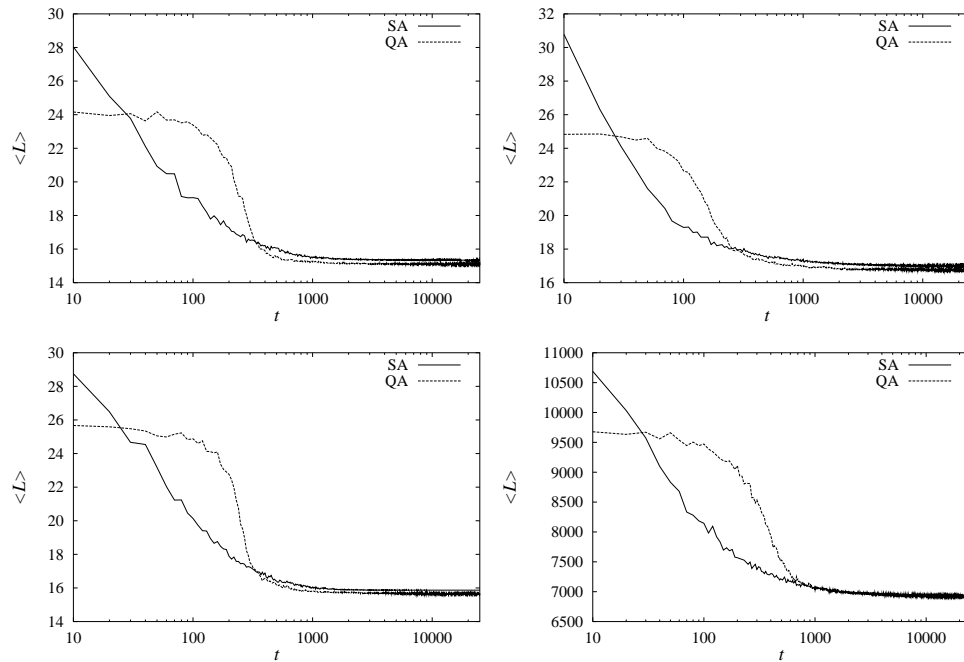


Figure 4.10: Average of the length. The scheduling is $5/\sqrt{t}$.

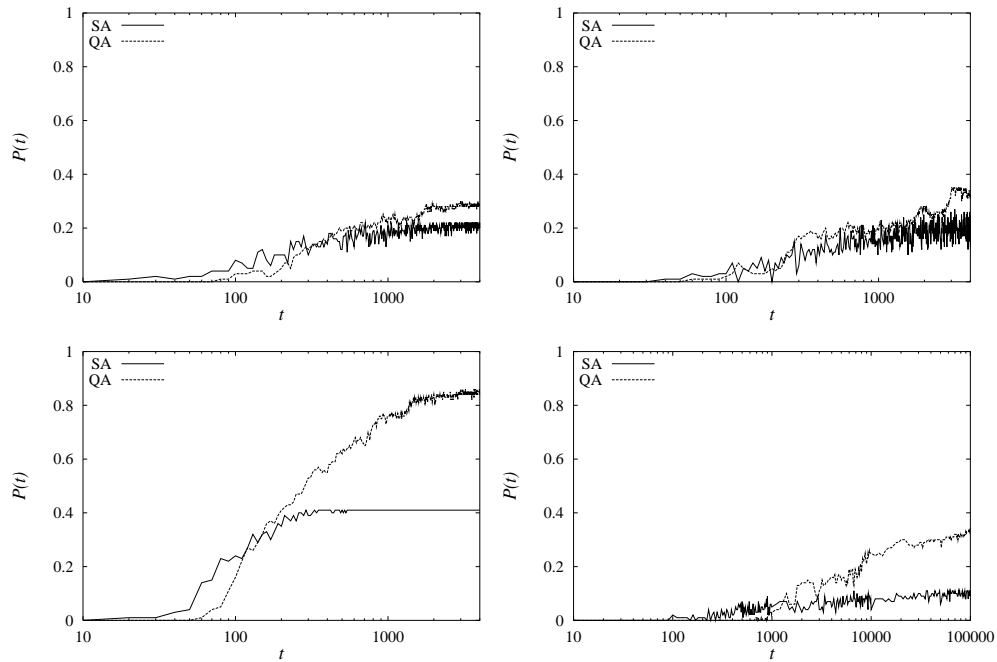


Figure 4.11: Probability to find the minimum-length. The scheduling is $2/\sqrt{t}$.

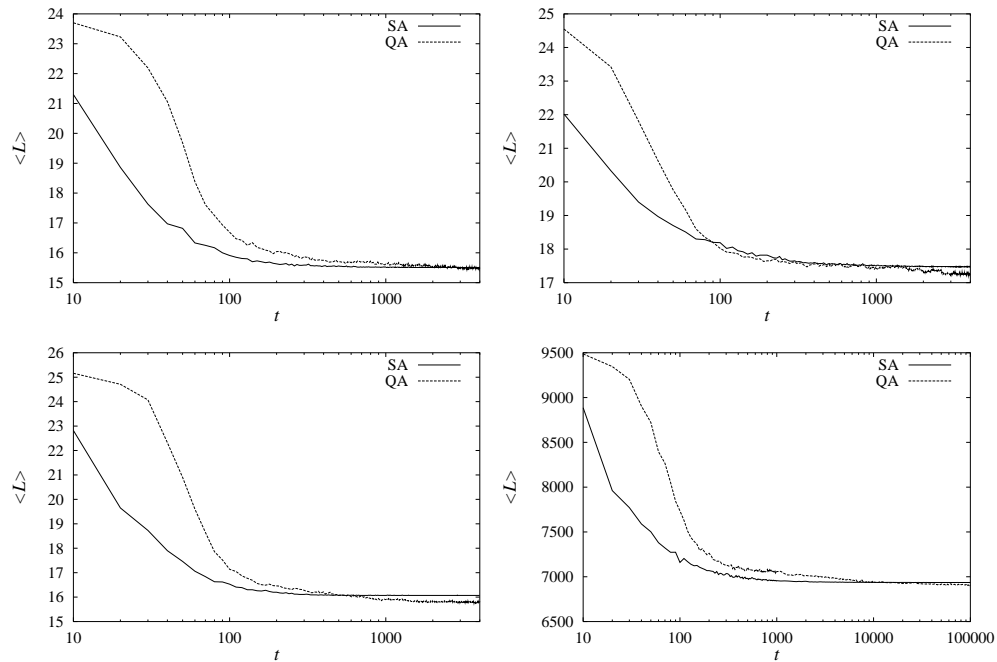


Figure 4.12: Average of the length. The scheduling is $2/\sqrt{t}$.

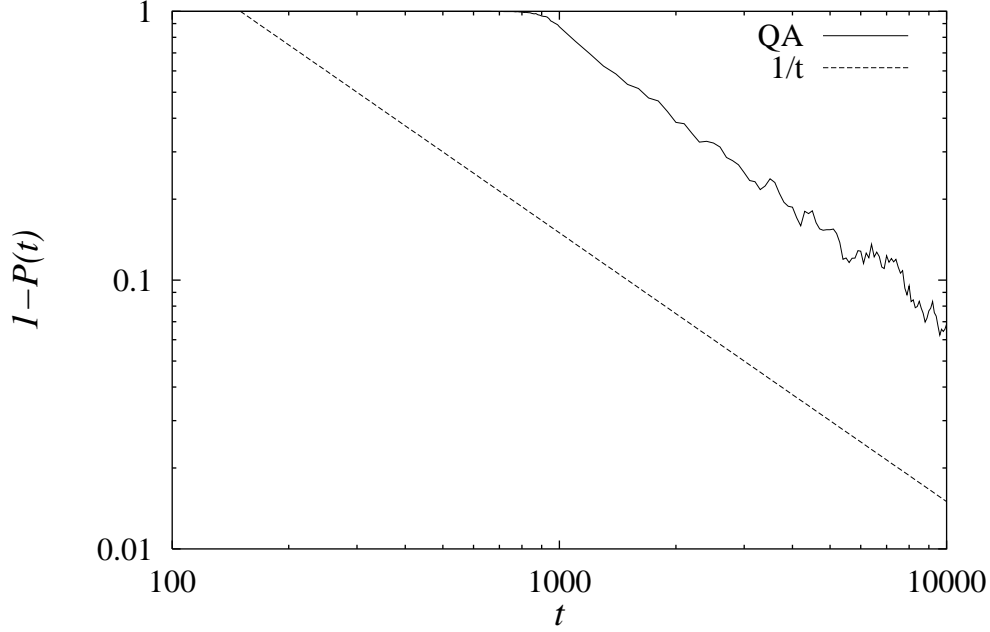


Figure 4.13: The quantity $1 - P(t)$ is plotted. The transverse field is scheduled as $\Gamma = 10/\sqrt{t}$.

the quantum system without annealing “QA(quench)”, (3) the classical system with annealing “SA” and (4) the classical system without annealing “SA(quench)”. We can find that both of the annealed systems show better performance than the quenched systems. It is notable that the probability for the quenched quantum system “QA(quench)” is larger than SA. In spite of annealing the temperature, SA finds the ground state less often than the quenched quantum system. From these results, we obtain the following conclusions. The relaxation of the quantum systems is faster than the classical systems whatever we control the parameters, annealing or quenching. The annealing process accelerate the relaxations for both of the quantum and the classical systems.

4.5 Summary

We have applied QA to TSP by mapping the problem to the Ising system. SA has a four-spin flip dynamics in the spin representation of the TSP. QA should contain the quantum effect which flips four spins at a time. Because of the difficulty of the calculation, we have adopted the one-spin dynamics by applying the transverse field.

Numerical results show that QA has better performance than SA in the probability to find the minimum-length of the closed tour and the average of the tour length and obeys the $1/t$ -law asymptotically. We only calculated the case in which the Trotter number is 500 for QA. The dependence on the Trotter number was not studied, and we did not estimate how many Trotter slices the quantum Monte Carlo simulation need. We also did not check the actual performance of QA. QA needs the computational power Trotter-number times as large as the calculation of SA, but we did not take into account this disadvantage. We only calculated the quantities as a function of the Monte Carlo steps, not the real computational time. In other words, we cannot conclude which methods find the minimum-length tour of TSP in small computer power, SA or QA, and only conclude so far that QA can be applied to TSP and QA improves in terms of the Monte Carlo step not the real computational time. These are the future problems. Another future problem is to study the effect of the four-spin interaction term as a quantum effect. It is not clear that the multi-spin interaction makes the system converge to the optimal state faster or not.

If QA for TSP accelerates the search for the optimal solution actually, QA may be applied to various problems which can be mapped to the Ising-spin systems. We should have used a four-spin transition term as a quantum effect in QA for TSP to have correspondence with the four-spin flip dynamics of SA, but we adopt a one-spin transition term $-\Gamma \sum_i \sigma_i^x$. The results show that QA finds the optimal solution and the one-spin transition term works. This term forces neighboring Trotter slices to be in the same configuration in the representation of Suzuki-Trotter decomposition. Assuming that this effect is the essence of QA, we can import such an effect to non-Ising systems.

For instance, it is possible to extend our method to the problems represented in terms of Potts spins.

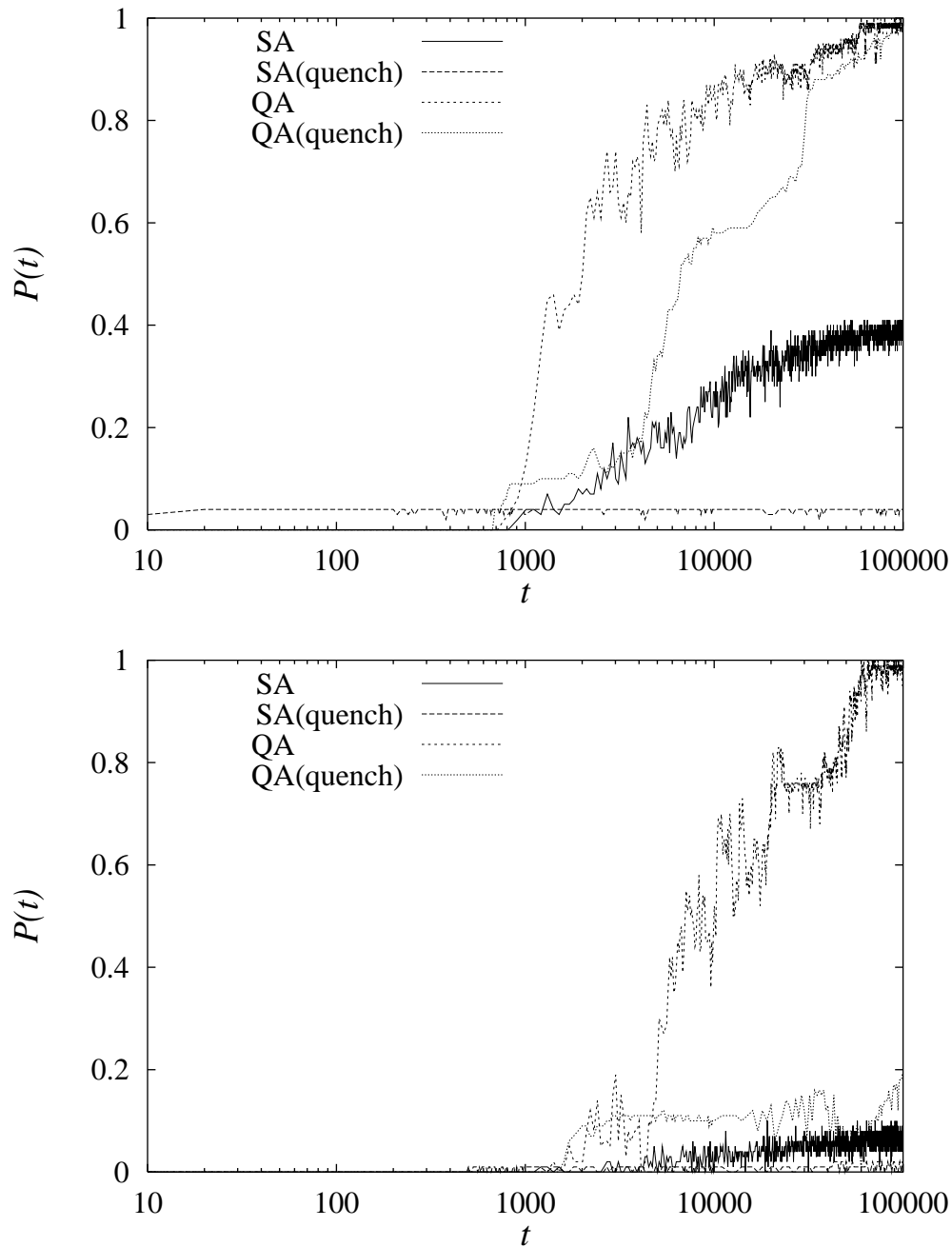


Figure 4.14: Difference in the probability between annealed and quenched systems. Top and bottom figures are the results of “random” and “ulysses16” respectively.

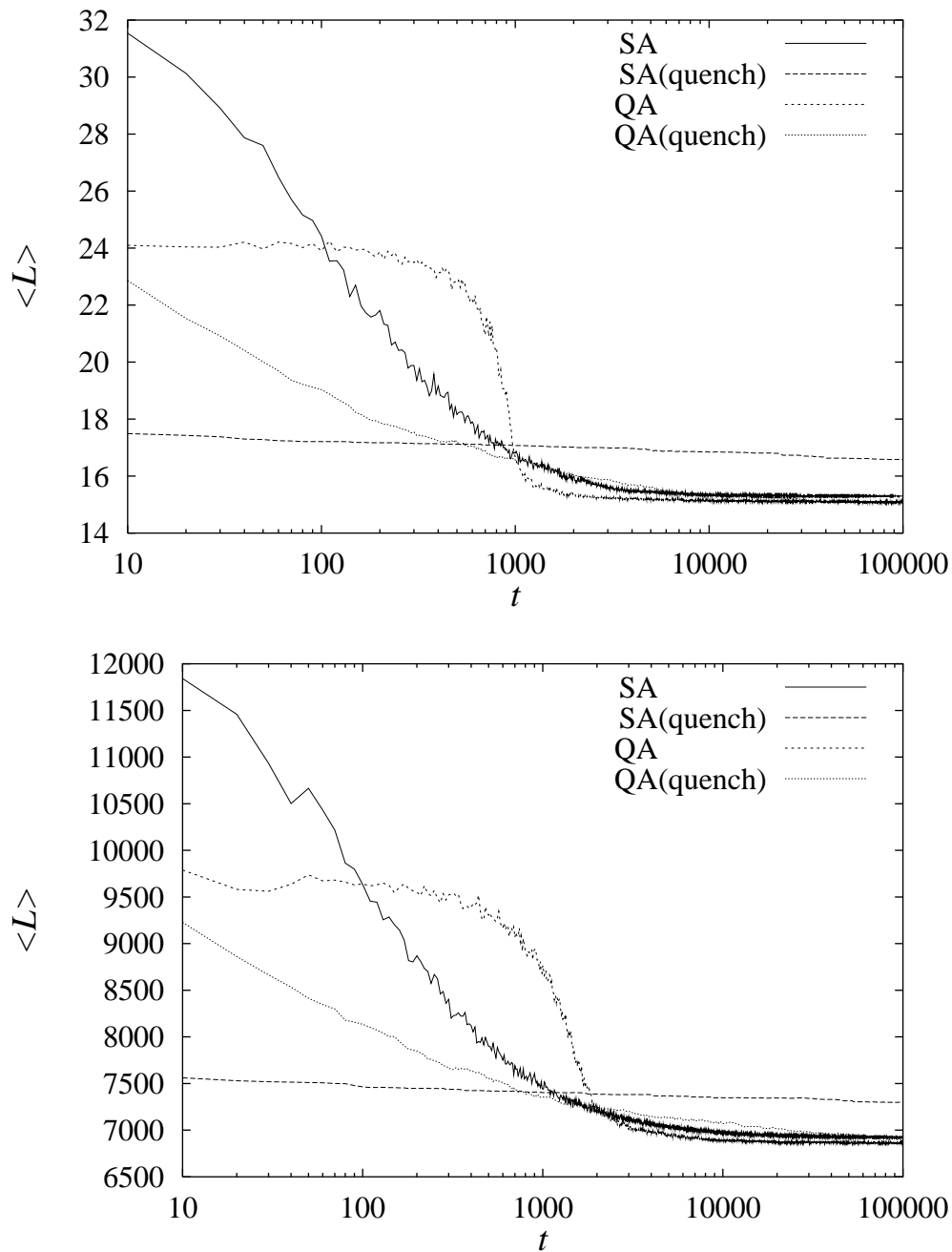


Figure 4.15: Difference in the average energy between annealed and quenched systems. Top and bottom figures are the results of “random” and “ulysses16” respectively.

Chapter 5

Summary

We have proposed a new idea on the general method to solve combinatorial optimization problems. The idea is quantum annealing (QA) in which quantum tunneling effects cause transitions between states, in contrast to the usual thermal transitions in simulated annealing (SA). First, we studied QA by the time-dependent Schrödinger equation for small-size systems. Next, we extended QA to the stochastic process, the quantum Monte Carlo method. The two dynamics, the Schrödinger equation and the quantum Monte Carlo dynamics, are not equivalent to each other. However, for the purpose of finding the ground state, both of them work and the performance is improved in comparison with SA. Finally, we presented the possibility of the implementation of QA for the general combinatorial optimization problems. The test-bed was the traveling salesman problem (TSP). The chance of finding the optimal solution by QA was larger than by SA.

The idea of QA is based on SA which was proposed by Kirkpatrick *et al.* to find the optimal state of the optimization problems by introducing the annealing process [21]. Annealing is performed by decreasing the temperature of the system from a high temperature to a low temperature. For instance, let us consider the silicon oxide SiO_2 . If the decreasing rate is slow enough, the system is in crystalline state. If the rate is fast, the glass state appears. SA imitates this process by the Monte Carlo simulation. We consider QA by replacing thermal fluctuations in SA with quantum fluctuations.

First, we adopt the transverse field as the quantum effect of the Ising

spin systems. The task is to find the ground state of the system without the transverse field. The transverse field term is controlled and vanishes in the infinite-time limit so that the system approaches the ground state. The dynamics of this system is not described by the Monte Carlo simulation used for SA. The natural dynamics of the present system is provided by the Schrödinger equation. We checked the performance of QA in finding the ground state in comparison with SA by numerical calculations. In these calculations, we applied the same function to the time-dependent schedules of the temperature T and the amplitude of the transverse field Γ . For the c/\sqrt{t} schedule, the behaviors of QA and SA were quite different. By QA we find the ground state with probability one, while we do not find the ground state by SA. We also found the remarkable property that the probability to find the ground state converges to one asymptotically as $1/t$. This property suggests that the system follows the stationary (or almost stationary) state, because the probability to find the system in the ground state is expressed using the perturbation in terms of $\Gamma(\ll 1)$ as

$$P_{\text{QA}}(\Gamma) \sim 1 - \Gamma^2 \sum_{i \neq 0} \frac{1}{(E_0^{(0)} - E_i^{(0)})^2},$$

where $E_i^{(0)}$ is the energy of the i th state of the non-perturbed (classical) system and $E_0^{(0)}$ is the ground-state energy. When we put $\Gamma = c/\sqrt{t}$, the $1/t$ -law appears.

Secondly, we have considered the calculation for the large-size systems. The calculation of the Schrödinger equation faces difficulties for larger N because the number of states increases exponentially as 2^N and the size of the storage for the Hamiltonian reaches the storage limit of the computer. The Monte Carlo method can be used to avoid this difficulty. There are two ideas to replace the dynamics of the Schrödinger equation with the Monte Carlo method. One is the path-integral Monte Carlo [49, 50] which regards the Trotter direction as the time (more precisely, the imaginary time). The other is the quantum Monte Carlo with “the Monte Carlo step”-dependent interaction between Trotter slices. We regard the Monte Carlo step as the time in the Schrödinger equation. From the similarity to SA, we adopted the

quantum Monte Carlo for large-size systems of QA.

We found that QA improves a performance in finding the ground state even if we take into account that QA needs M times more calculations than SA. The Trotter number we adopt is $M = 100$, which is large enough for our calculations (for the two-dimensional EA model with $N = 625$). The $1/t$ convergence of the probability to find the ground state still appears in the Monte Carlo calculation of QA. We also found that the relaxation of the quantum system is faster than the classical system, if the amplitude of the transverse field Γ in the quantum system and the temperature in the classical system have the same value. This implies that the quantum effect accelerates relaxations. We consider that this fact is the reason for the better performance of QA than SA.

Lastly, we have applied QA to TSP by expressing the problem in terms of the Ising system. Numerical results show that QA has a better performance than SA in the probability to find the minimum-length of the closed tour and the average of the tour length at the same Monte Carlo step. Moreover, the $1/t$ convergence of the probability to find the optimal tour still appears in TSP by QA. These results imply that the QA works also in TSP. However, we did not check the actual performance of QA. QA needs the computational power Trotter-number times in comparison with SA, but we did not take into account this disadvantage. We only calculated the quantities as a function of the Monte Carlo step, not the real computational time. In other words, we can not conclude which method finds the minimum-length tour of TSP with smaller computer power, SA or QA, and only conclude so far that QA can be applied to TSP and QA improves in terms of Monte Carlo steps, not in the real computational time.

The findings in our study are summarized briefly as follows: QA provides a general and faster algorithm to find the ground state of the Ising system whose energy landscape is complicated. If we adopt the schedule of the transverse field as $\Gamma = c/\sqrt{t}$, the asymptotic form of the probability to miss the ground state is proportional to $1/t$. The relaxation of the quantum system is faster than the classical system under the condition of the control parameter $\Gamma = T$. From the application side, the optimal schedule is not

known in general. If the relaxation is fast, we do not have to take into account the possibility to be stuck in local minima more seriously in QA than SA. QA may also work for the combinatorial optimization problems which can be mapped to the Ising spin system.

The future problems are the followings: The analytical foundations of the better performance of QA than SA and the critical rate of the decreasing the transverse field are needed. (The same method of the analysis of SA by Geman and Geman [22] may be applied to the analysis of the Trotter decomposed system of QA.) The application to the study of the ground state property of the Ising spin systems, especially the three-dimensional EA model, is attractive. Whether the same picture as the SK model, the Parisi picture [13, 18], can be applied to the three-dimensional EA model or not is an open problem. For some problems in SA the multi-spin flip is performed and the corresponding interaction term representing quantum effect in QA is the multi-spin interaction term. For instance, SA for TSP needs four-spin flip, but we adopt only a single-spin interaction term (the transverse field). To study the effect of the multi-spin interaction term is needed. It is not clear whether the multi-spin interaction makes the system converge to the optimal state faster or not. On the other hand, the transverse field is mapped to the interaction between the Trotter slices and the strength of the interaction is controlled by the strength of the field. This interaction forces neighbor Trotter slices to be in the same configuration in the representation of Suzuki-Trotter decomposition. Assuming that this effect is the essence of QA, we can import such an effect to a wide class of non-Ising systems. For example, it is possible to extend our method to the problems represented in terms of Potts spins. This is one possible way to apply QA to general problems which can not be expressed in terms of the Ising spin.

Appendix A

Single-spin problem

In this Appendix we explain some technical aspects to derive the exact solution of the time-dependent Schrödinger equation for the transverse Ising model with a single spin. The three cases of $\Gamma(t) = -ct, c/t$ and c/\sqrt{t} will be discussed.

A.1 Case of $\Gamma(t) = -ct$ (Landau-Zener model) [33, 34, 35, 36, 37]

Let us express the solution of the Schrödinger equation at time t by the parameters $a = \langle +|\psi(t)\rangle$ and $b = \langle -|\psi(t)\rangle$. The Schrödinger equation (2.3) with $\mathcal{H} = -h\sigma^z - \Gamma\sigma^x$ is expressed as a set of first order differential equations for a and b . It is convenient to change the variables as

$$\tilde{a} = \frac{1}{\sqrt{2}}(a + b), \quad \tilde{b} = \frac{1}{\sqrt{2}}(a - b), \quad (\text{A.1})$$

by which the Schrödinger equation is now

$$\frac{d^2\tilde{b}(t)}{dt^2} + (-ic + h^2 + c^2t^2)\tilde{b}(t) = 0. \quad (\text{A.2})$$

By using the notation

$$z = \sqrt{2c}e^{-\pi i/4}t, \quad (\text{A.3})$$

$$\lambda = \frac{ih^2}{2c}, \quad (\text{A.4})$$

we find

$$\frac{d^2\tilde{b}(t)}{dz^2} + \left(\lambda + \frac{1}{2} - \frac{1}{4}z^2\right)\tilde{b}(t) = 0. \quad (\text{A.5})$$

The initial state is specified as $a = b = 1/\sqrt{2}$ or $\tilde{b} = 0$ as $t \rightarrow -\infty$. The solution of (A.5) satisfying this condition is the parabolic cylinder function $D_{-\lambda-1}(-iz)$ [51]. Thus, we obtain the solution as

$$\tilde{a}(t) = \frac{1}{h} \left(-ct\tilde{b}(t) - i\frac{d\tilde{b}(t)}{dt} \right), \quad (\text{A.6})$$

$$\tilde{b}(t) = C_1 D_{-\lambda-1}(iz), \quad (\text{A.7})$$

where C_1 is a constant. To fix C_1 , we use the condition

$$|\tilde{a}(-\infty)| = \frac{2C_1 c e^{\pi h^2/8c}}{h\sqrt{2c}} = 1. \quad (\text{A.8})$$

Then we have

$$C_1 = \frac{h}{\sqrt{2c}} e^{-\pi h^2/8c}. \quad (\text{A.9})$$

The wave function of this system is given in Eq. (2.6).

A.2 Case of $\Gamma(t) = c/t$

We next consider the case of $\Gamma(t) = c/t$. By eliminating a from the Schrödinger equation, we obtain

$$\begin{aligned} \frac{d^2b(t)}{dt^2} - \frac{1}{\Gamma(t)} \frac{d\Gamma(t)}{dt} \frac{db(t)}{dt} \\ + \left(h^2 + \Gamma^2(t) - \frac{ih}{\Gamma(t)} \frac{d\Gamma(t)}{dt} \right) b(t) = 0. \end{aligned} \quad (\text{A.10})$$

Substituting $\Gamma(t) = c/t$, we have

$$\frac{d^2b(t)}{dt^2} - \frac{1}{t} \frac{db(t)}{dt} + \left(h^2 + \frac{ih}{t} + \frac{c^2}{t^2} \right) b(t) = 0. \quad (\text{A.11})$$

The solutions of this equation are expressed by the confluent P function [51]

$$\begin{aligned} \tilde{P} \left\{ \begin{array}{c} \infty \\ \overbrace{ih \ 1} \\ -ih \ 0 \end{array} \begin{array}{c} 0 \\ ic \ t \\ -ic \end{array} \right\} \\ = e^{iht} t^{ic} \tilde{P} \left\{ \begin{array}{c} \infty \\ \overbrace{0 \ 1+ic} \\ 1 \ ic \end{array} \begin{array}{c} 0 \\ 0 \ -2iht \\ -2ic \end{array} \right\}, \end{aligned} \quad (\text{A.12})$$

the right-hand side of which has two independent expressions in terms of the confluent hypergeometric function

$$f(t) = e^{iht} t^{ic} F(1 + ic, 1 + 2ic; -2iht), \quad (\text{A.13})$$

$$\begin{aligned} g(t) &= e^{iht} t^{ic} (-2iht)^{-2ic} \\ &\times F(1 - ic, 1 - 2ic; -2iht). \end{aligned} \quad (\text{A.14})$$

The general solution is $b(t) = C_1 f(t) + C_2 g(t)$. Using the initial condition

$$b(0) = C_1 + C_2 = \frac{1}{\sqrt{2}}, \quad (\text{A.15})$$

$$a(0) = C_1 - C_2 = \frac{1}{\sqrt{2}}, \quad (\text{A.16})$$

we find

$$b(t) = \frac{1}{\sqrt{2}} e^{iht} t^{ic} F(1 + ic, 1 + 2ic; -2iht). \quad (\text{A.17})$$

The asymptotic forms of $b(t)$ and $|b(t)|^2$ are then given as

$$\begin{aligned} b(t) &\sim \frac{\sqrt{2}(2h)^{-ic} \Gamma(2ic)}{\Gamma(ic)} \\ &\times \{e^{-iht - \pi c/2} + ce^{iht + \pi c/2} (2ht)^{-1}\}, \end{aligned} \quad (\text{A.18})$$

$$|b(t)|^2 \sim \frac{\sinh(\pi c)}{\sinh(2\pi c)} \left\{ e^{-\pi c} + \frac{c \cos(2ht)}{ht} + \frac{c^2 e^{\pi c}}{4h^2 t^2} \right\}. \quad (\text{A.19})$$

A.3 Case of $\Gamma(t) = c/\sqrt{t}$

The final solvable model has $\Gamma(t) = c/\sqrt{t}$. The Schrödinger equation (A.10) is then expressed as

$$\frac{d^2b(t)}{dt^2} - \frac{1}{2t} \frac{db(t)}{dt} + \left(h^2 + \frac{2c^2 + ih}{2t} \right) b(t) = 0. \quad (\text{A.20})$$

The solution is the confluent P function [51]

$$\begin{aligned} \tilde{P} & \left\{ \begin{array}{c} \infty \quad 0 \\ ih \quad \frac{1}{2} - i\gamma \quad 0 \quad t \\ -ih \quad i\gamma \quad \frac{1}{2} \end{array} \right\} \\ & = e^{iht} \tilde{P} \left\{ \begin{array}{c} \infty \quad 0 \\ 0 \quad \frac{1}{2} - i\gamma \quad 0 \quad -2iht \\ 1 \quad i\gamma \quad \frac{1}{2} \end{array} \right\}, \end{aligned} \quad (\text{A.21})$$

where $\gamma = c^2/2h$. The two independent solutions are thus [51]

$$f(t) = e^{iht} F\left(\frac{1}{2} - i\gamma, \frac{1}{2}; -2iht\right), \quad (\text{A.22})$$

$$g(t) = e^{iht} (-2iht)^{1/2} F\left(1 - i\gamma, \frac{3}{2}; -2iht\right). \quad (\text{A.23})$$

The general solution of (A.20) is therefore the linear combination of the above two functions

$$b(t) = C_1 f(t) + C_2 g(t). \quad (\text{A.24})$$

The constants C_1 and C_2 are fixed by the requirement

$$b(0) = C_1 = \frac{1}{\sqrt{2}}, \quad (\text{A.25})$$

$$a(0) = \frac{\sqrt{h}}{\sqrt{2}c} e^{(5/4)\pi i} C_2 = \frac{1}{\sqrt{2}}. \quad (\text{A.26})$$

Substituting C_1 and C_2 into Eq. (A.24), we find

$$\begin{aligned} b(t) & = \frac{1}{\sqrt{2}} e^{iht} F\left(\frac{1}{2} - i\gamma, \frac{1}{2}; -2iht\right) \\ & \quad + \frac{c}{\sqrt{h}} e^{(3/4)\pi i} e^{iht} (-2iht)^{1/2} F\left(1 - i\gamma, \frac{3}{2}; -2iht\right). \end{aligned} \quad (\text{A.27})$$

The asymptotic form is

$$b(t) \sim \sqrt{\pi} e^{-\pi c^2/4h} \left[e^{-iht} (2ht)^{-i\gamma} \left\{ \frac{1}{\sqrt{2}\Gamma(\frac{1}{2} - i\gamma)} + \frac{\sqrt{h} e^{(5/4)\pi i}}{c\Gamma(-i\gamma)} \right\} + e^{iht} (2ht)^{-1/2+i\gamma} \left\{ \frac{e^{-(1/4)\pi i}}{\sqrt{2}\Gamma(i\gamma)} + \frac{c}{2\sqrt{h}\Gamma(\frac{1}{2} + i\gamma)} \right\} \right]. \quad (\text{A.28})$$

The probability $|b(\infty)|^2$ that the system remains in the excited state can be calculated as the asymptotic form of (A.28) with the condition $c^2/h \gg 1$

$$|b(\infty)|^2 = \frac{\pi e^{-\gamma\pi}}{2} \left| \frac{1}{\Gamma(\frac{1}{2} - i\gamma)} + \frac{\gamma^{-1/2} e^{(5/4)\pi i}}{\Gamma(-i\gamma)} \right|^2 \quad (\text{A.29})$$

$$\sim \frac{e^{-\gamma\pi}}{4} \left| e^{1/2} \left(\frac{1}{2} - i\gamma \right)^{i\gamma} + \gamma^{-1/2} e^{(5/4)\pi i} (-i\gamma)^{i\gamma+1/2} \right|^2 \quad (\text{A.30})$$

$$\sim \frac{e^{-\gamma\pi}}{4} \left| (-i\gamma)^{i\gamma} \frac{i}{8\gamma} \right|^2 = \frac{1}{256\gamma} = \frac{h^2}{64c^4}. \quad (\text{A.31})$$

A.4 Dependence of the final value on the initial condition

We show that we can choose the initial condition so that the final state is the ground state when $\Gamma = c/\sqrt{t}$. This is not possible for $\Gamma = -ct$ or c/t . From Eq. (A.24), the asymptotic form of the solution as $t \rightarrow \infty$ is

$$b(t) \sim C_1 \frac{\sqrt{\pi} e^{-\pi c^2/4h - iht} (2ht)^{-ic^2/2h}}{\Gamma(1/2 - ic^2/2h)} + C_2 \frac{i\sqrt{\pi} h e^{-\pi c^2/4h - iht} (2ht)^{-ic^2/2h}}{c^2 \Gamma(-ic^2/2h)}. \quad (\text{A.32})$$

The coefficients C_1 and C_2 are fixed under the conditions $b(\infty) = 0$ and $|a(0)|^2 + |b(0)|^2 = 1$ as

$$C_1 = \left\{ 1 + \frac{\sinh(\pi c^2/h)}{2 \sinh^2(\pi c^2/2h)} \right\}^{-1/2}, \quad (\text{A.33})$$

$$C_2 = \frac{ic^2 \Gamma(-ic^2/2h)}{h \Gamma(1/2 - ic^2/2h)} C_1. \quad (\text{A.34})$$

This solution is not the ground state of the Hamiltonian $\mathcal{H}(0)$.

The reason why one cannot obtain such a solution for the other schedules ($\Gamma = c/t, -ct$) is the following: The general solution for $\Gamma = c/t$ also has two coefficients, and the initial state is represented as the linear combination of two terms whose phases are indefinite:

$$a(0) = C_1 t^{ic} \Big|_{t \rightarrow 0} - C_2 t^{-ic} \Big|_{t \rightarrow 0}, \quad (\text{A.35})$$

$$b(0) = C_1 t^{ic} \Big|_{t \rightarrow 0} + C_2 t^{-ic} \Big|_{t \rightarrow 0}. \quad (\text{A.36})$$

The lowest-energy state at $t = 0$ corresponds to $a(0) = b(0) = 1/\sqrt{2}$ (times an arbitrary phase factor), which is realized by choosing $C_2 = 0$ in Eqs. (A.35) and (A.36). The indefiniteness of t^{ic} as $t \rightarrow 0$ is irrelevant because this is only the overall phase factor. Such a situation does not happen for other values of $a(0)$ and $b(0)$, leading to a serious difficulty to determine the wave function at $t = 0$. Thus we cannot choose an initial condition other than $a(0) = b(0) = 1/\sqrt{2}$. A similar fact exists in the case of $\Gamma = -ct$.

Bibliography

- [1] E. L. Lawler and J. K. Lenstra and A. H. G. Rinnooy Kan and D. B. Shmoys, *The Traveling Salesman Problem: A guided Tuor of Combinatorial Optimization* (John Wiley & Sons, 1985).
- [2] M. R. Garey and D. S. Johnson, *Computers and Intractability: A Guide to the Theory of NP-Completeness* (Freeman, San Fransisco, 1979).
- [3] A. V. Aho, J. E. Hopcroft and J. D. Ullman, *The design and analysis of computer algorithms* (Addison-Wesley, 1974).
- [4] V. Cannella and J. A. Mydosh, Phys. Rev. B **6** (1972) 4220.
- [5] M. A. Ruderman and C. Kittel, Phys. Rev. **96** (1954) 99.
- [6] T. Kasuya, Progr. Theoret. Phys. **16** (1954) 45.
- [7] K. Yoshida, Phys. Rev **106** (1957) 893.
- [8] S. F. Edwards and P. W. Anderson, J. Phys. F **5** (1975) 965.
- [9] D. Sherrington and S. Kirkpatrick, Phys. Rev. Lett. **35** (1975) 1792.
- [10] J. R. L. de Almeida and D. J. Thouless, J. Phys. A **11** (1978) 983.
- [11] G. Parisi, Phys. Lett. **73** A (1979) 203.
- [12] G. Parisi, J. Phys. A **13** (1980) L115, 1101 and 1187.
- [13] G. Parisi, Phys. Rev. Lett. **50** (1983) 1946.
- [14] D. J. Thouless, P. W. Anderson and R. G. Palmer, Phil. Mag. **35** (1977) 593.

- [15] F. Tanaka and S. F. Edwards, *J. Phys. F* **10** (1980) 2769.
- [16] N. D. Mackenzie and A. P. Yong, *J. Phys. C* **16** (1983) 5321.
- [17] K. Nemoto and H. Takayama, *J. Phys. C* **18** (1985) L529.
- [18] C. De Dominicis and A. P. Yong, *J. Phys. A* **16** (1983) 2063.
- [19] J. Hertz, A. Krogh and R. G. Palmer, *Introduction to the Theory of Neural Computation* (Addison-Wesley, 1995).
- [20] S. Shinomoto, *Statistical mechanics in information theory* (Maruzen, 1992) (in Japanese)
- [21] S. Kirkpatrick, C. D. Gelett and M. P. Vecchi, *Science* **220** (1983) 671.
- [22] S. Geman and D. Geman, *IEEE Trans. PAMI* **6** (1984) 721.
- [23] C. Tsallis and D. A. Stariolo, *Physica A* **233** (1996) 395.
- [24] T. J. P. Penna, *Phys. Rev. E* **51** (1995) R1.
- [25] I. Andricioaei and J. E. Straub, *Phys. Rev. E* **53** (1996) R3055.
- [26] H. Nishimori and J. Inoue, *J. Phys. A* **31** (1998) 5661.
- [27] H. Nishimori and Y. Nonomura, *J. Phys. Soc. Jpn.* **65** (1996) 3780.
- [28] K. Tanaka and T Horoguchi, *IEICE A* **J80-A** (1997) 2117 (in Japanese)
- [29] B. K. Chakrabarti, A. Dutta and P. Sen, *Quantum Ising Phases and Transitions in Transverse Ising Models* (Springer, Berlin, 1996).
- [30] D. Lancaster and F. Ritort, *J. Phys. A* **30** (1997) L41.
- [31] J. V. Alvarez and F. Ritort, *J. Phys A* **29** (1996) 7355.
- [32] T. Sato, N. Hatano, M. Suzuki and H. Takayama (unpublished).
- [33] S. Miyashita, *Prog. Theor. Phys.* **69** (1983) 714.
- [34] C. Zener, *Proc. R. Soc. London, Ser A* **137** (1932) 696.

- [35] S. Miyashita, J. Phys. Soc. Jpn. **64** (1995) 3207.
- [36] S. Miyashita, J. Phys. Soc. Jpn. **65** (1996) 2734.
- [37] H. De Raedt, S. Miyashita, K. Saito, D. Gracia-Pablos and N. Gracia, Phys. Rev. B **56** (1997) 11761.
- [38] H. F. Trotter, Proc. Am. Math. Soc. **10** (1959) 545.
- [39] M. Suzuki, Commum. Math. Phys. **51** (1976) 183.
- [40] A. C. C. Coolen, S. N. Laughton and D. Sherrington, Phys. Rev. B **53** (1996) 8184.
- [41] S. N. Laughton, A. C. C. Coolen and D. Sherrington, J. Phys. A **29** (1996) 763.
- [42] H. Nishimori and M. Ymamna, J. Phys. Soc. Jpn. **65** (1996) 3.
- [43] M. Yamana, H. Nishimori, T. Kadowaki and D. Sherrington, J. Phys. Soc. Jpn. **66** (1997) 1962.
- [44] Wenhao Wu, *et. al.*, Phys. Rev. Lett. **67** (1991) 2076.
- [45] J. J. Hopfield and D. W. Tank, Biological Cybernetics **52**(1985) 141.
- [46] J. J. Hopfield and D. W. Tank, Science **233** (1986) 625.
- [47] M. Suzuki, Porg. Theor. Phys. **56** (1976) 1454.
- [48] TSPLIB is a library of sample instances for the TSP (and related problems) from various sources and of various types. TSPLIB is available on the Internet. <http://www.iwr.uni-heidelberg.de/iwr/comopt/soft/TSPLIB95/TSPLIB.html>.
- [49] M. Creutz and B. Freedman, Ann. Phys **132** (1981) 427.
- [50] J. Bonča and J. E. Gubernatis, Phys. Rev. E **53** (1996) 6504.
- [51] A. Erdélyi *et al.*, *Higher Transcendental Functions* (MaGraw-Hill, New York, 1953).